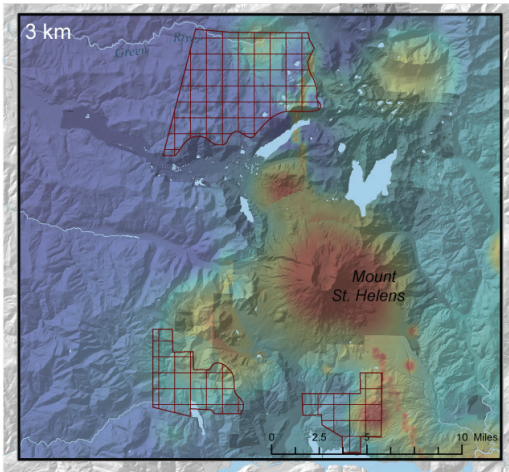
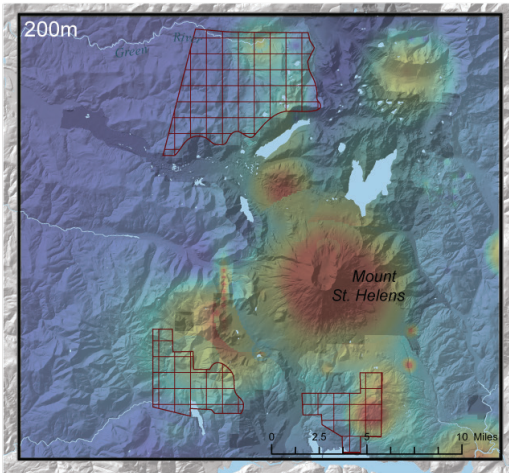
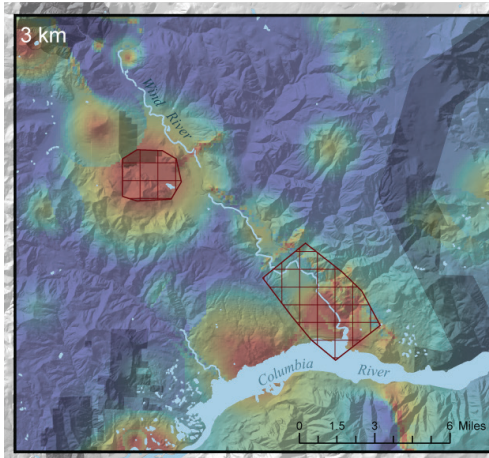
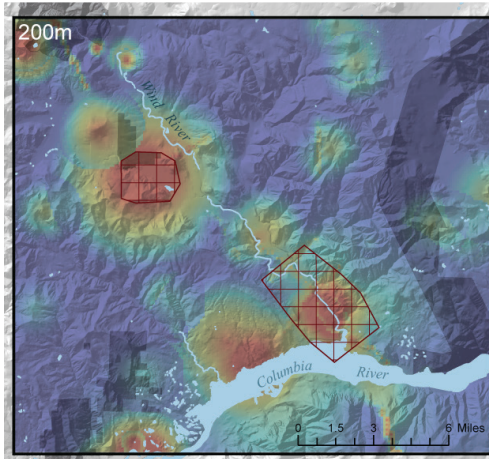


GEOHERMAL PLAY-FAIRWAY ANALYSIS OF WASHINGTON STATE PROSPECTS: PHASE 1 TECHNICAL REPORT

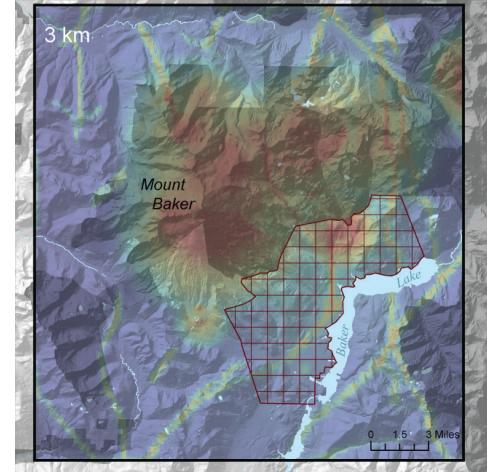
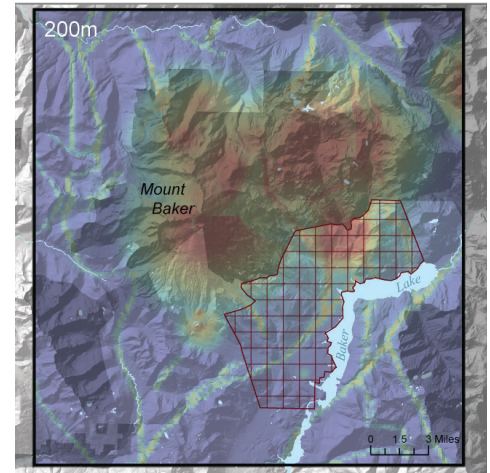
MOUNT ST. HELENS SEISMIC ZONE



WIND RIVER VALLEY



MOUNT BAKER



WASHINGTON STATE DEPARTMENT OF
Natural Resources
Peter Goldmark - Commissioner of Public Lands



ALTA ROCK



by David K. Norman¹, Corina Forson¹, Jessica L. Czajkowski¹,
Michael W. Swyer², Trenton T. Cladouhos²,
Gima M. Shcmalzle³, and Nicholas, Davatzes⁴

from
¹Washington State Department of Natural Resources
Geology and Earth Resources Division,
²AltaRock Energy, Inc., ³BOS Technologies, LLC,
and ⁴Temple University

under contract to
U.S. Department of Energy Geothermal Technologies Program
Award no. DE-EE0006728

Phase 1 Technical Report and Phase 2 Proposal

Federal Agency and Organization: DOE EERE – Geothermal Technologies Program

Recipient Organization: Washington Division of Geology and Earth Resources

DUNS Number: [808883474]

Recipient Address: 1111 Washington Street SE, MS 47007, Olympia, WA 98504

Award Number: DE-EE0006728

Project Title: Geothermal Play-Fairway Analysis of Washington State Prospects

Project Period: 10/1/2014-10/31/2015

Principal Investigator: David K. Norman

State Geologist/ Manager

Dave.Norman@dnr.wa.gov

(360) 902-1439

Report written and submitted by: Corina Forson

Natural Resource Scientist 2

Corina.Forson@dnr.wa.gov

(360) 902-1455

Date of Report Submission: October 16, 2015

Project Partners: David K. Norman¹, Corina Forson¹, Jessica L. Czajkowski¹, Michael W. Swyer², Trenton T. Cladouhos², Gina M. Schmalzle³, Nicholas Davatzes⁴

1) Washington Division of Geology and Earth Resources*

2) AltaRock Energy, Inc.*

3) BOS Technologies, LLC

4) Temple University

* Indicates cost sharing partner

DOE Project Team: DOE Contracting Officer – Laura Merrick

DOE Project Officer – Eric Hass

Project Monitor – Not Assigned

Signature David K Norman Date 10/16/2015

*The Prime Recipient certifies that the information provided in this report is accurate and complete as of the date shown.

Table of contents:

Executive Summary	1
Project Overview	3
1.1. Objectives and Downselect Criteria	4
1.2. Summary of Project Activities	5
2. Geologic Background	6
2.1. Site Geologic Settings	7
2.1.1. Mount St. Helens Seismic Zone (MSHSZ)	7
2.1.2. Wind River Valley (WRV)	8
2.1.3. Mount Baker (MB)	9
2.2. Conceptual Resource Models	11
2.2.1. MSHSZ	12
2.2.2. MB	12
2.2.3. WRV	12
3. Methodology	14
3.1. Play-Fairway Methodology and Assumptions	14
3.2. The Analytical Hierarchy Process	15
3.3. Heat Potential Modeling Methodology	16
3.4. Permeability Potential Modeling Methodology	17
3.5. Combining the Heat and Permeability Potential Models	21
3.6. Utility of Methods for Applications at Other Sites	21
3.7. Uncertainty and Sensitivity Modeling Methodology	21
4. Results	25
4.1. Geothermal Favorability Modeling	26
4.1.1. Geothermal Favorability Models of MSHSZ	26
4.1.2. Geothermal Favorability Models of WRV	27
4.1.3. Geothermal Favorability Models of MB	28
4.2. Uncertainty and Risk Modeling	29
4.2.1. Uncertainty Model of MSHSZ	29
4.2.2. Uncertainty Model of WRV	30
4.2.3. Uncertainty Model of MB	31
5. Areas of Interest for Future Exploration Based on Risk Mapping	33
5.1. Risk Maps	34
5.1.1. Risk Maps for MSHSZ	34
5.1.2. Risk Maps for WRV	35
5.1.3. Risk Maps for MB	36
6. Commercial Viability of the Play-Fairways	37
6.1. Presence of a Resource	37
6.2. Local Factors Supporting Development	37
6.3. Land Status	37
6.4. Potential Industry Partners	38
7. Conclusions	39
8. Recommendations for Future Exploration	39
8.1. Description of Phase 2 Objectives and Outcomes	39

Washington Division of Geology and Earth Resources

Phase 1 Technical Report

8.2. Summary of Proposed Activities for Phase 2	40
8.3. Description of Planned Activities (SOPO Tasks)	45
8.4. Partners Identified and Roles.....	46
8.5. Preliminary Timeline	46
8.6. Preliminary Phase 2 Budget Information	47
8.6.1. High-Cost Proposal Budget Sheets and Justification.....	47
8.6.2. Low-Cost Proposal Budget Sheets and Justification	50
8.7. Anticipated Permitting Requirements and Barriers to Address.....	52
9. Catalog of Supporting Files Used in the Analysis	53
10. Technology Transfer Activities	56
11. References Cited	57
12. Appendix A: Data Processing for the Heat Potential Models	61
13. Appendix B: Data Processing for the Permeability Potential Models	66
14. Appendix C: Analytical Hierarchy Process	84
15. Appendix D: Analysis of High Precision GPS Time Series and Strain Rates	86
16. Appendix E: Data Processing for the Uncertainty and Risk Models	87
17. Appendix F: Preliminary USGS Work Plan and Budget for Proposed Phase 2 Collaboration	93

Figures:

1. Statewide resource model.....	3
2. MSHSZ Regional setting.....	7
3. WRV Regional setting.....	9
4. MB Regional setting.....	10
5. Conceptual resource models	11
6. WRV structural setting.....	13
7. Model workflow diagram.....	15
8. Combined heat potential models for three plays	17
9. Combined permeability potential models for three plays.....	20
10. Heat uncertainty	22
11. GPS velocity uncertainty.....	23
12. Permeability uncertainty.....	24
13. Permeability sensitivity	25
14. MSHSZ heat and permeability combined at 200m and 3km.....	27
15. WRV heat and permeability combined at 200m and 3km.....	28
16. MB heat and permeability combined at 200m and 3km.....	29
17. MSHSZ heat and permeability uncertainty combined at 200m and 3km.....	30
18. WRV heat and permeability uncertainty combined at 200m and 3km.....	31
19. MB heat and permeability uncertainty combined at 200m and 3km.....	32
20. MSHSZ risk maps at 200m and 3km with AOI	34
21. WRV risk maps at 200m and 3km with AOI	35
22. MB risk maps at 200m and 3km with AOI	36
23. MSHSZ proposed activities for Phase 2.....	42
24. WRV proposed activities for Phase 2.....	43
25. MB proposed activities for Phase 2.....	44
A1. Vent proximity workflow.....	61
A2. Individual heat parameter heat potential maps for MSHSZ.....	64

A3. Individual heat parameter heat potential maps for WRV.....	65
A4. Individual heat parameter heat potential maps for MB.....	65
B1. Fault geometry in relation to hot springs.....	66
B2. Failure potential model at the Desert Peak geothermal field.....	67
B3. Workflow for constructing fault geometry using LOWESS	69
B4. Strain rate from GPS velocities	70
B5. Crustal block boundaries.....	71
B6. Block rotational velocities.....	71
B7. Strain rate tensors not removed near the crustal block boundaries	72
B8. Strain rate tensors with crustal block boundaries removed for MSHSZ.....	73
B9. Strain rate tensors with crustal block boundaries removed for WRV	74
B10. Strain rate tensors with crustal block boundaries removed for MB	75
B11. Geometry of the MSH magma chamber.....	76
B12. Displacement on fault surface in north MSHSZ	77
B13. Displacement gradient on fault surface north of MSHSZ	78
B14. Mohr circle illustrating equations defining Max Coulomb shear stress and Σ_3	79
B15. Individual permeability potential rasters for MSHSZ.....	81
B16. Individual permeability potential rasters for WRV	82
B17. Individual permeability potential rasters for MB	83
C1. AHP worksheet sample.....	84

Tables:

1. Summary of SOPO tasks	5
2. Heat potential parameters and assumptions	16
3. Permeability potential parameters and assumptions	18
4. Fault data quality values	23
5. Summary of low cost estimate proposed activities for Phase 2.....	40
6. Summary of high cost estimate proposed activities for Phase 2.....	41
7. Description of Phase 2 planned activities	45
8. Description of partners identified and roles.....	46
9. Preliminary project timeline.....	46
10. High-cost budget estimate.....	47
11. Low-cost budget estimate	50
12. Catalog of supporting files.....	53
A1. Weighting schema for temperature-gradient wells	63
C1. AHP derived weights for the three study areas.....	85
E1. Spring data quality and spatial accuracy weights.....	87
E2. Geothermometry data quality and spatial accuracy weights	88
E3. Volcanic vent data quality weights	89
E4. Intrusive rock data quality weights	90
E5. Temperature gradient data quality weights	91
E6. Radii of influence for temperature-gradient wells.....	91

Executive Summary

Analysis of a previous statewide geothermal resource assessment (Boschmann and others, 2014) revealed areas with elevated heat and permeability, within close proximity to transmission lines, and at elevations reasonable for development, defining three promising plays along the central axis of the Cascade magmatic arc in Washington State: Mount St. Helens seismic zone (MSHSZ), Wind River valley (WRV), and Mount Baker (MB).

The play-fairway is constituted by the collocation of heat, permeability, and saturated porosity in sufficient volume that provide adequate heat exchange at depths accessible by modern drilling technologies. Three sites showed regional scale characteristics consistent with these attributes and sufficient data exists to support more detailed analysis. In addition, these three sites span the two key play types in the Cascades magmatic arc: (1) magmatic systems penetrated by faults on near active stratovolcanoes such as at Mount St. Helens and Mount Baker, and (2) geothermal fluid circulation supported by active faulting at Wind River valley.

The focus of Phase 1 of this play-fairway project is to develop and apply a methodology to integrate detailed models of heat and permeability potential for each play type. The goal is to minimize risk associated with investments in geothermal exploration of greenfield projects by rigorously analyzing available data, applying favorability modeling concepts that have been successfully used at known geothermal systems, and addressing data quality and model sensitivity. The integrated results indicate locations where commercial geothermal potential is highest. These results also reveal where new data is needed to increase resolution and reduce uncertainty to minimize risk (steps proposed for Phase 2), and thus successfully identify sites for exploration wells (in Phase 3).

This project goes beyond the existing statewide model by explicitly improving assessment of the heat and permeability necessary to support commercial geothermal operations. Potential permeability is assessed through geomechanical modeling of the deformation that can generate and maintain reservoir porosity and permeability. Metrics to inform permeability potential include (1) slip and (2) dilation tendency on mapped and seismic faults (3) maximum shear strain, and (4) dilational strain at the surface, (5) modeled fault displacement distribution, and (6) displacement gradient, (7) shear, and (8) tensile fracture density. Metrics to inform heat potential include (1) temperature-gradients, (2) Quaternary volcanic vents, (3) Quaternary intrusive rocks, (4) spring temperature, and (5) reservoir temperature inferred from geothermometry. These results are then weighted and combined to generate geothermal favorability maps for each of the three play areas.

This information is vital for: (1) revealing the detailed variability in heat and permeability potential of each study area that can distinguish successful from unsuccessful wells, (2) locating areas of undiscovered or untapped resource potential, and (3) reducing the risk and cost of greenfield exploration and development.

Quantifying input parameter uncertainty and assessing the sensitivity of model predictions to available constraints revealed areas where new data can provide critical information to improve model resolution and distinguish competing hypotheses. Combining the geothermal potential maps with these uncertainty analyses provides a guide for future exploration efforts.

Phase 1 results highlight areas with collocated heat and permeability at 200 m and 3 km depth slices at each of the three sites and identify favorable locations within developable land for more detailed research. The work in this phase resulted in three distinct products; (1) maps of heat and permeability potential; (2) maps of uncertainty in these models; and (3) maps of development risk. The construction of these maps and the integration of (1) and (2) into (3) use new methodologies specifically developed for the Cascades play-fairway project, fulfilling the goals of Phase 1.

Phase 2 focuses on specific geothermal areas of interest (AOI) identified from the favorability and risk maps from Phase 1, at each of the three sites. The AOI are located on land that, to the best of our knowledge, can be permitted for geophysical exploration, and developed for geothermal production if future exploration proves promising. The AOI at each of the three areas are the focus of Phase 2 exploration. The Phase 2 activities proposed at all three sites are primarily geophysical surveys (magnetotelluric, aeromagnetic, magnetic, gravity, electrical resistivity, passive seismic) that have been tested and used extensively in oil and gas, mineral, and geothermal exploration, as well as geological and geochemical analysis that will add critical data to the areas where data are sparse (geologic mapping, LiDAR analysis and field surveys, geochronology, temperature-gradient well drilling). Each of these methods is designed to address a specific issue influencing resource potential or uncertainty identified in the Phase 1 analysis; thus the data types vary by site reflecting both differences in existing data and analysis sensitivities. In general, these geophysical and geological methods focus on refining the geometry of known faults, testing for hidden faults, better understanding the local geology, and detecting areas with low resistivity that may be associated with hydrothermal alteration and geothermal fluids.

Each of these three maps contributes to the work proposed in Phase 2, to gather relatively low-cost data that resolves uncertainty, improves the geothermal potential models, and in turn reduces development risk to guide exploratory drilling. In addition, Phase 2 will provide a basis for validation and continued development of the Cascades play-fairway methodology with specific exploration targets to be identified for Phase 3. Already in Phase 1, potential industry partners, interested in and capable of supporting geothermal developments at the plays have been identified. We anticipate further engagement with potential partners in Phase 2 and continued search for additional funding opportunities. Continued progress on this project will provide a strong basis for handoff to industry development at specific sites and deployment of the methodology more broadly by industry partners.

1 Project Overview

A pivotal step in development of a potential geothermal resource is the ability to successfully identify sites for exploration wells. The high-cost and high-risk associated with drilling wells require that all factors influencing well productivity/injectivity are considered and that uncertainty is minimized. A comprehensive analysis of the geologic, geochemical, structural, and geophysical properties of the study area are crucial when addressing this challenge. Not only must these data be collected, but they must be assembled using a methodology that distinguishes the resource potential, sources of uncertainty, and thus the risk of development in regard to a specific play type. The goal of this study is to provide both the tools and the quantitative analysis of the geothermal potential that delineates profitable areas for further exploration in three plays along the Cascade magmatic arc: Mount St. Helens seismic zone (MSHSZ), Wind River valley (WRV), and Mount Baker (MB) (Figs. 1–4). The goals of the project are to use detailed modeling of these three areas to provide better definition of geothermal resources at depth, identify areas warranting further exploration and thus targeting of resources that minimizes risk, to eventually promote commercial development.

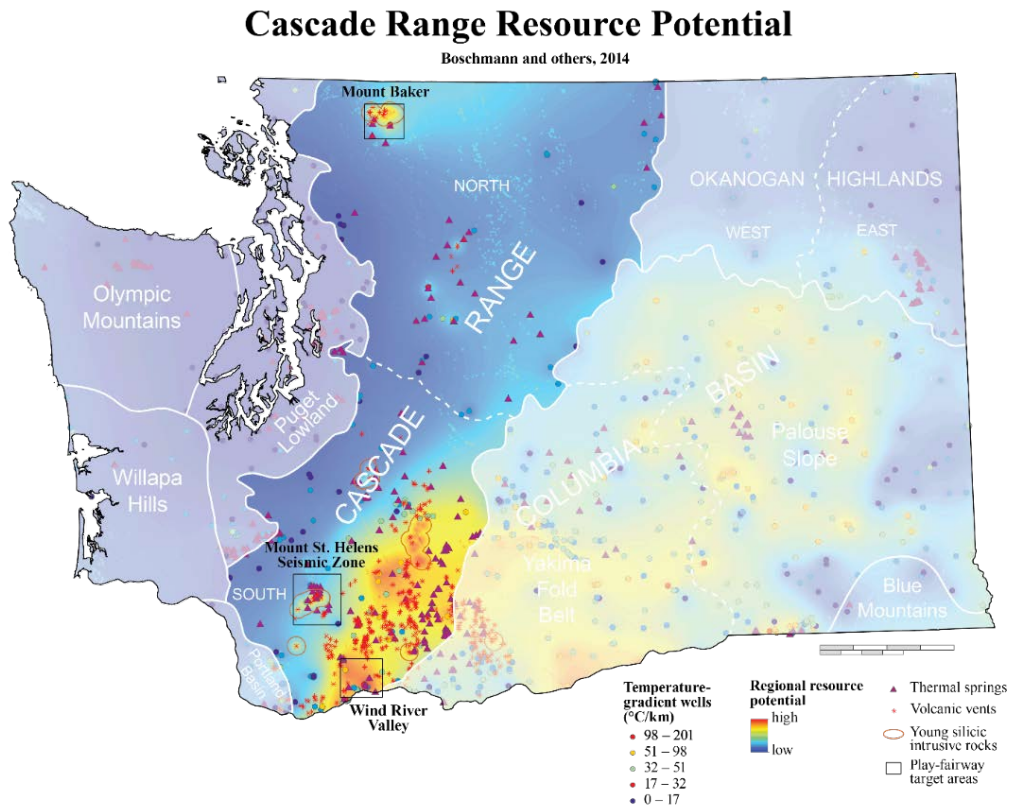


Figure 1: Statewide geothermal resource potential model (Boschmann and others, 2014) with the three study areas outlined in black.

The Cascade Range in Washington State hosts some of the most active volcanic centers in the United States. Geothermal activity associated with the magmatic arc is typically expressed as hot springs and fumaroles. The region is tectonically dynamic and structurally complex demonstrated by frequent seismicity, historic volcanic eruptions, ongoing subduction, and active faults. However, the massive amount of precipitation, dense vegetation, and high relief in the western part of the state can mask surface manifestations as well as dampen the thermal signature of magmatic heat sources, conventionally detected through remote sensing, and thus act as a barrier to geothermal development. Despite the high geothermal favorability in Washington (Fig. 1; Boschmann and others, 2014), there are no current geothermal energy development projects in the state, making it impossible to test modeling parameters against known resources in the northern Cascades volcanic arc.

Geothermal energy development is a promising option for Washington State to meet the Renewable Portfolio Standards (RPS) set forth in the Energy Independence Act (EIA or I-937). The EIA requires that utilities in Washington use renewable energy and energy conservation in serving their customers. The RPS renewable energy targets increase over time, from 3% in 2012 to 15% in 2020. Hydro-electric power generation, the state's primary source of energy, is not included as a renewable resource under the EIA. If this project continues through Phase 2, the results will provide both the methodology and initial assessments of developable lands placing industry partners in a position to develop geothermal energy to meet these RPS requirements.

1.1 Objectives and Down-select Criteria

The objectives of Phase 1 were to develop a methodology that can assess the geothermal potential of an area, determine where data are lacking (or of poor quality) and further exploration is warranted, and to evaluate project risk based on the combined favorability and uncertainty of the areas. A measure of uncertainty was determined from both the quantity and quality of input datasets and features. Relative risk within each play is highest where high uncertainty is collocated with low favorability.

While this methodology is tuned to the plays encountered in the Cascades magmatic arc in which volcanism is the key source of heat and faults provide the necessary conduits for transporting and hosting geothermal fluids, it is intended to be applicable for any fault-controlled geothermal system. This study builds off of methodologies that have been deployed successfully in oil and gas, geothermal, and mineral resource exploration studies. Data used and created as well as custom codes and scripts developed during this project will be readily available through the Geothermal Data Repository (GDR) and can be used to re-run the analyses with the addition of new data.

Phase 1 project criteria necessitated the use of existing public data. Careful analysis of each model's sensitivity to uncertain parameters provides a basis for determining what data is needed to improve predictions of resource potential during Phases 2 and 3. Key new data sets will include LiDAR analysis (no LiDAR acquisition is proposed for Phase 2 because new LiDAR was recently flown in our study areas and will be available for use in spring 2016) and magnetotellurics (MT) as appropriate to each play.

LiDAR is very useful for identifying detailed structures, but use of this data requires field validation to confirm the initial interpretations. Both incomplete LiDAR coverage and an inability to conduct field validation during Phase 1 make this an excellent candidate for many sites in Phase 2. To support access to this data, we are currently engaging collaborators to provide LiDAR and related mapping at no additional cost. MT can improve resolution of fault geometry at depth, detect hidden faults, and detect geothermal fluids or alteration. This will be particularly advantageous where complementary passive seismic, gravity, magnetics, and other techniques are integrated to resolve non-uniqueness in MT data.

With consideration of land-use availability, proximity to economic markets, interested industry partners and local agencies with renewable energy quotas, this project has identified areas of interest with commercial viability.

1.2 Summary of Project Activities

Each performance period successfully resulted in the necessary key data products, as well as development of methods to organize, integrate, and use these data. Although tasks are assigned to discrete performance periods, development of methods and data sets has continued throughout the project. Project partners were successfully coordinated through email correspondence, twice-monthly as well as ad hoc web conferencing, and cloud-based data sharing. The project progressed according to the Statement of Project Objectives (SOPO), all reports were submitted on time, and the project adhered to the proposed budget. There were no major variations from proposed activities.

The Phase 1 play-fairway project was subdivided into four main performance periods as outlined in the SOPO, all of which were successfully completed:

Performance period/ Task	Activity	Result
1	Data collection	Gathering of existing public and partner data and metadata, determination of suitability for modeling, and data distribution to partners.
2	Model input development	Model inputs prepared for all three play areas
3	Geothermal resource modeling, methodology development, and risk analysis	Favorability, uncertainty, and risk modeling for the three target areas (MSHSZ, WRV, and MB).
4	Reporting and data delivery	Final technical report and data to NGDS. Methodology for geothermal favorability modeling, uncertainty, and risk as deliverables in the report. Phase 2 decision point: Define a targetable zone within accessible land, or identify zone(s) where more data is needed.

Table 1: Summary of SOPO tasks.

Performance period 1, data collection went smoothly because much of the data used in this analysis was already gathered for use in the statewide favorability model and submitted to the National Geothermal Data System. Data was gathered from numerous sources and was then stored in geodatabases, folders, and on cloud services. Supplemental data gathered for this project includes: water wells with bottom-hole temperature measurements, updated earthquake catalog with focal mechanisms where available, fault data from all available mapping, geologic cross sections, hydrothermal alteration, geothermometry for hot springs, strain rate, local stress orientations and magnitudes, as well as supplemental geomechanical data from a literature review.

Performance period 2, data preparation for each of the three plays consisted of: refining the data gathered in period one; clipping the data to each study area; removing data that was not suitable for our analysis; determining data quality and spatial accuracy; building three-dimensional fault models from faults mapped at the surface, cross sections, and fit to seismicity at depth (described in detail below); and generating the strain rate maps from the GPS velocity data at each site.

Performance period 3 incorporated the data gathered in periods 1 and 2 into the respective geothermal resource models for each target area. This period included reducing the three-dimensional permeability model to two-dimensional potential maps, use of MATLAB, Poly3D and GIS processing to produce final geothermal favorability models for each area. Uncertainty and risk models for each of the three plays were also generated in this period.

The final *performance period 4* (reporting, data delivery, and Phase 2 decision point) included: the generation of this final technical report, data and metadata organization and submission to NGDS, and analysis of the favorability and uncertainty models for the three plays to determine areas of interest within developable land.

2 Geologic Background

The Cascade magmatic arc is the result of oblique (northeast directed) subduction of the Juan de Fuca plate beneath the North American plate. GPS-derived secular velocity estimates of the Pacific Northwest show the Oregon Coast Range Block is rotating clockwise with respect to stable North America, causing crustal extension in the backarc and contraction in central Washington (Wells and others, 1998; McCaffrey and others, 2000b; McCaffrey and others, 2007). Voluminous—albeit discontinuous—volcanism has accompanied subduction and is expressed as a chain of active volcanoes along the crest of the Cascades. Additionally, the Cascade Range in Washington State is host to active faulting and abundant seismicity in the upper crust, likely related to complex subduction, block rotation, and active volcanism. The three study areas (Fig. 1) are all located within the Cascade magmatic arc; however, each occupy different geologic and tectonic settings.

2.1 Site Geologic Settings

2.1.1 Mount St. Helens (MSH) is located along the western front of the Cascade Range in southwest Washington (Figs. 1 and 2). The frequency and scale of the eruptions at MSH over the last few thousand years make it currently the most active volcano in the Cascades (Sherrod and others, 2008). MSH lies along a 100-km-long zone of moderate (up to 5.5) magnitude earthquakes with predominantly strike-slip focal mechanisms along north-to-northwest-striking fault planes (Weaver and Smith, 1983; Weaver and others, 1987), which we refer to as the MSHSZ. Although MSH itself lies within a national monument and is thus off-limits to geothermal development, this project focuses on the extensive potential resources on accessible lands in the larger MSHSZ outside of the protected monument both north and south of MSH.

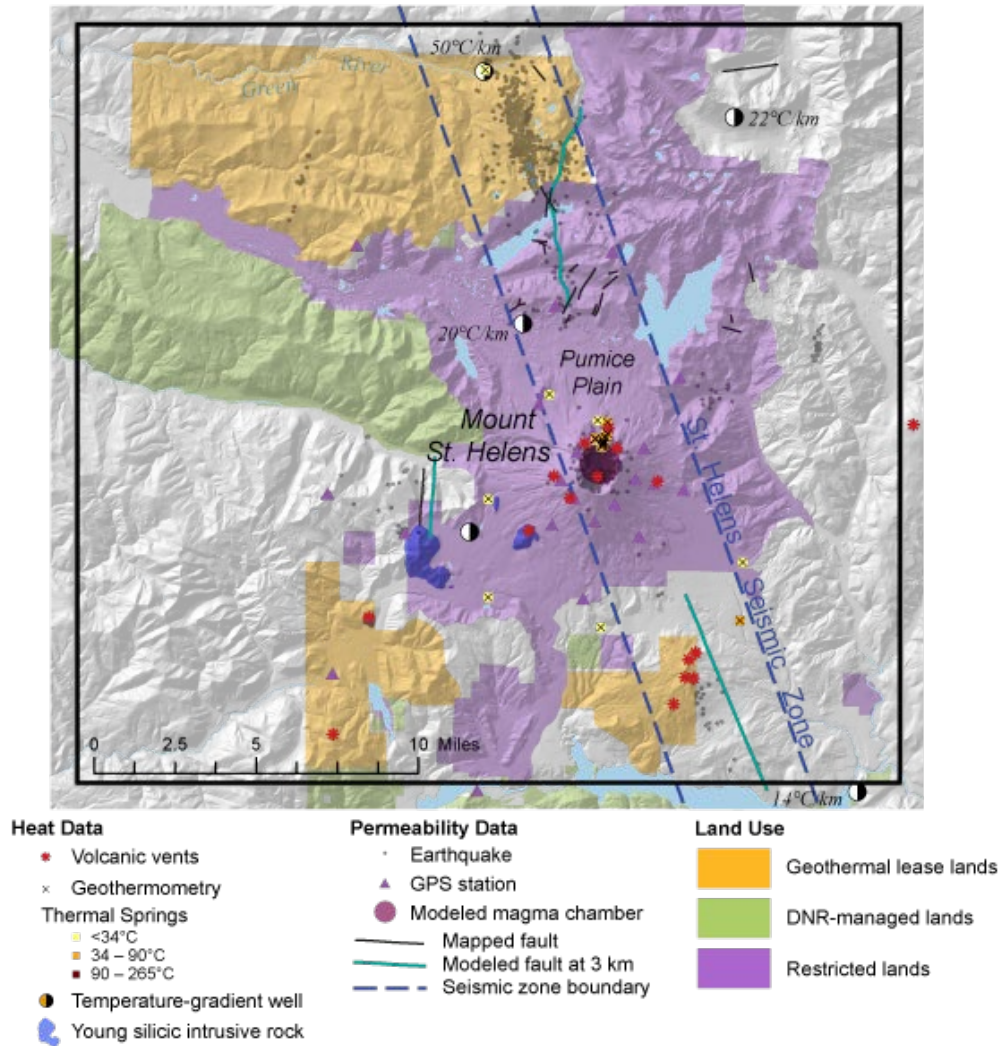


Figure 2: MSHSZ regional setting showing the heat input data, permeability input data, land use restrictions, and geothermal lease lands (colored in gold) (note that the land north of MSH is owned by Weyerhaeuser and geothermal rights are leased by our project partner AltaRock Energy, Inc.).

Interestingly, no surface trace has been identified along the trend of the MSHSZ (Evarts and others, 1987). The focal mechanism-determined motion along the MSHSZ is right-lateral strike-slip. A right step in the MSHSZ beneath the volcanic center generates a zone of extension between the offset faults. MSH is centered on this dextral offset, and the earthquake swarms there are likely related to volcanic eruptions (Weaver and others, 1987). Weaver and others (1987) mapped faults from the seismicity surrounding MSH—the permeability modeling employed in this study expands on this premise and also uses seismicity to map fault planes at depth in this area.

The MSH volcano is the site of ongoing geothermal activity, expressed in part by numerous hot springs and fumaroles located in the central crater, along the northern flank, and on the debris flow and the pyroclastic deposits north of the 1980 flank collapse (henceforth referred to as “the Pumice Plain”). The fumaroles and springs located within the crater are likely connected directly to a magmatic heat source, while Pumice Plain springs are “rootless”, meaning they are not connected directly to the magmatic source of heat or gas. Spring chemistry trends and alteration mineralogy from this area support this idea (Keith and others, 1981, Shevenell and Goff, 1995). For this reason, the Pumice Plain springs were excluded from this analysis. Four temperature-gradient wells were drilled in the MSHSZ study area; the highest recorded gradient is 50°C/km.

2.1.2 The *Wind River valley*, located in southwestern Washington, is a northwest-trending valley draining southeastward into the Columbia River near Washington’s southern border (Figs. 1 and 3). There are numerous thermal and mineral springs and seeps along and adjacent to this valley, several of which are developed into resorts. Several temperature-gradient wells drilled in the early 1980s yielded gradients as high as 160°C/km (Czajkowski and others, 2014c), and some water wells at the southern end of the valley, near the town of Carson, contain warm water. Detailed investigations with emphasis on the geothermal resources of the Wind River valley include Berri and Korosec (1983) and Czajkowski and others (2014a). There are numerous minor vents in the area, the youngest is Trout Creek Hill with a reported K-Ar age of 0.34 ± 0.07 Ma (Korosec, 1984, Berri and Korosec, 1983). Czajkowski and others (2014a) identified two dominant sets of faults in the area; northwest-striking faults (such as the Wind River fault), and northeast-striking faults (such as the Shiphards fault zone). Based upon the presence of thermal and mineral springs, high temperature gradients, and warmer water along the valley’s axis, it is proposed that intersections of the northeast and northwest faults channel geothermal fluids from depth to the near surface within and along the length of this valley.

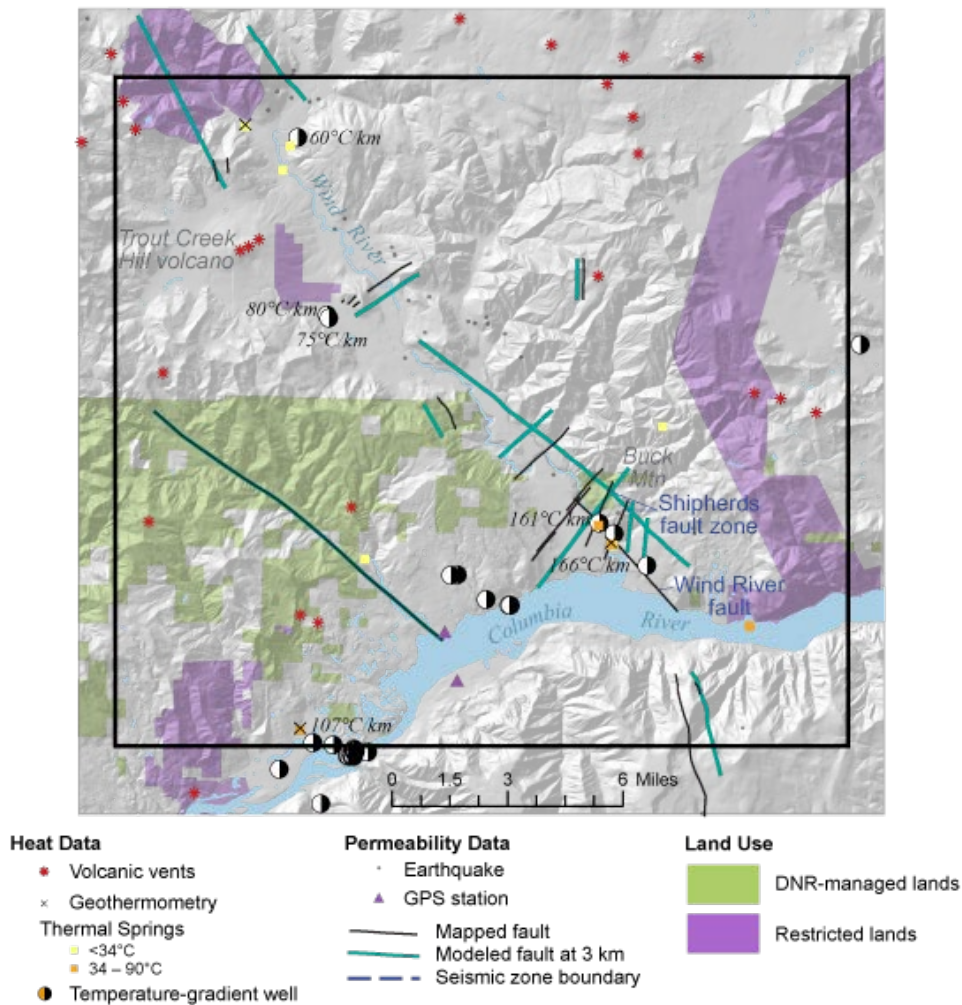


Figure 3: WRV regional map showing heat input data, permeability input data, and land use.

2.1.3 The *Mount Baker* study area is located in northwestern Washington, east of Bellingham in the North Cascades (Fig. 1). Like MSH, Mount Baker is also a Quaternary stratovolcano on the western front of the North Cascades. It is located within the Mount Baker–Snoqualmie National Forest, much of which is designated a national wilderness area (Fig. 4). However, the Mount Baker study area was chosen to include existing Bureau of Land Management (BLM) geothermal leases and lands that the U.S. Forest Service has recently given consent-to-lease to the BLM.

The Mount Baker volcano and surrounding area have received attention from the geothermal community due to the presence of thermal features and young volcanic centers. Exploration activities have included some detailed geologic mapping, spring sampling, geophysical surveys, soil mercury measurements, and limited temperature-gradient drilling (Korosec, 1984). Chemical geothermometry of Baker Hot Springs suggests that reservoir equilibrium temperature of this

system may reach as high as 150° to 170°C (Korosec, 1984). In 1983, a 140-m deep (460 ft) temperature-gradient well was drilled near Baker Hot Springs. It had a bottomhole temperature of 48°C and a geothermal gradient between 200° and 309°C/km (Czajkowski and others, 2014c). However, this gradient is likely affected by hot spring circulation and may not represent a typical background value for the area. Proposed exploration activities include additional temperature-gradient drilling to better constrain the heat at depth in the area.

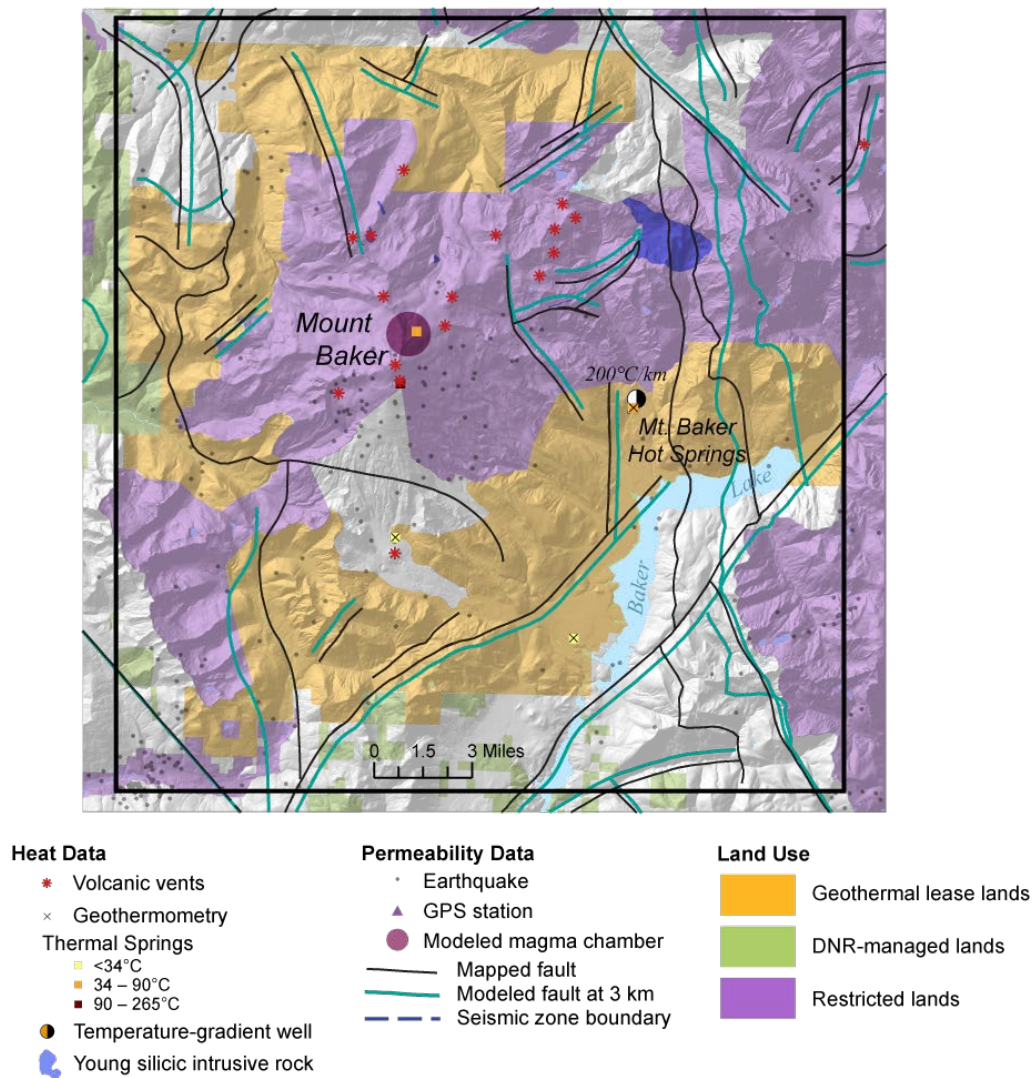


Figure 4: MB regional setting showing the heat input data, permeability input data, land use restrictions and geothermal lease lands.

The incomplete, yet promising data at MB creates an interesting contrast to MSHSZ and WRV. In this case, MSHSZ and WRV provide a case study of each play type, with more complete data to develop methodology. MB provides a third site where we can mimic a more

complete play-fairway characterization from early sparse data in Phase 1, applying lessons learned from MSH to characterization, and then gathering of targeted data in Phase 2 to enrich the assessment which will have the ancillary benefit of motivating commercial exploration.

2.2 Conceptual Resource Models

Assessment of geothermal resource potential must explicitly identify potential play types in the fairway and use these as the basis for characterizing the key attributes of commerciality and related risks due to uncertain, low quality, or incomplete data sets. In addition, in the early development of the fairway, explicit definition and then refinement of play-type models as data is assembled and analyzed is essential (as reflected in method development in Phase 1 and planning for Phase 2).

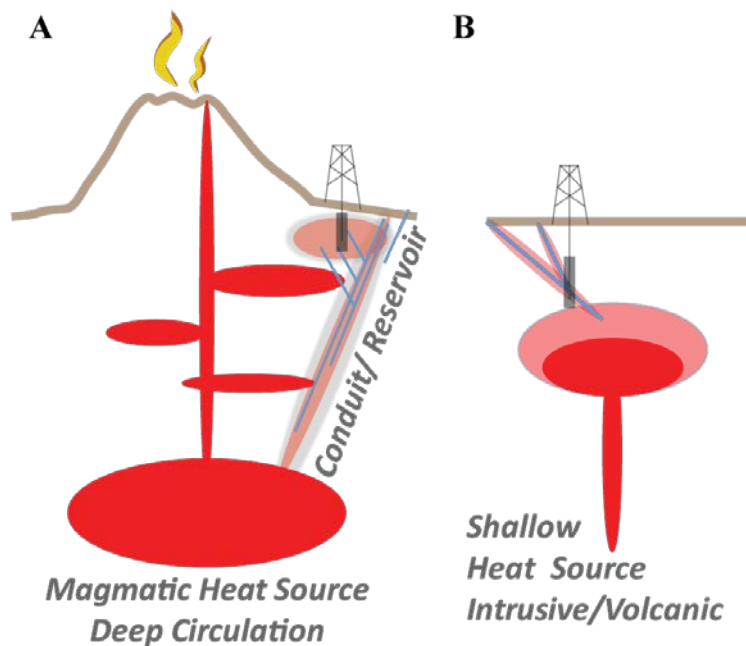


Figure 5: Schematic diagram of the three play-fairway targets in the Cascade magmatic arc. **A)** Magmatic heat source with deep circulation, the MSHSZ and MB are associated with active volcanism and a magmatic heat source although in both cases there is also significant horizontal separation between the magmatic heat source and the potential drill sites, that are not depicted on the vertical cross section. **B)** Heat source from a stalled or shallowly implaced intrusion, such as the WRV study area. Dark red regions indicate primary heat sources supporting the reservoir, whereas paler red areas indicate porous permeable rock heated by this heat source.

The underlying assumption in these conceptual models is that there is high potential for a geothermal reservoir where heat from active magmatism is coincident with permeability generated along faults and associated fractures. Deep crustal structures and fracture networks can provide permeable pathways for cool meteoric water to percolate downward and reach magmatic and intrusive heat sources and then convectively rise to transfer heat toward the surface (Fig. 5).

This behavior, combined with damage surrounding such structures—locally influenced by the interaction of the detailed fault geometry and the stresses driving slip—provide connected porosity to host a reservoir.

2.2.1 MSHSZ: The conceptual resource model for the MSHSZ area is a convection dominated system, with an active magmatic heat source, and a combination of magmatic hydrothermal fluid circulation as well as fault controlled fluid circulation (schematic example in Fig. 5A). Mount St. Helens is an active volcano (it erupted in 1980 with subsequent intermittent volcanic activity continuing through 2006) and is the assumed heat source for the hot springs, fumaroles, and warm temperature gradients in the area. The working assumption is that areas with high fracture density and active deformation (as evidenced from seismicity) provide a percolating fracture network and porosity to store fluids. The steeply dipping faults modeled along the MSHSZ—and the volume of rock surrounding these faults—are the most likely volumes of high permeability and heat transport in the MSHSZ study area. Segmentation and other complexities in fault geometry can promote concentrations of stress that both extend to depth and could fracture large volumes to potentially support economically viable geothermal reservoirs. These favorable areas are highlighted in the permeability potential modeling results section below.

2.2.2 MB: The conceptual resource model for the MB area is also a convection dominated system, with an active magmatic heat source, and a combination of magmatic hydrothermal fluid circulation as well as fault-controlled fluid circulation (schematic example in Fig. 5A). Mount Baker is an active volcano, with the most recent eruption in 1880 along with signs of unrest and fumarole activity in 1975. Steam and gas still issue from both Sherman Crater and the Dorr fumarole field on the northeast flank of the volcano, further evidence that it remains an active heat source. Elevated gas and heat fluxes cause localized extensional strain two orders of magnitude greater than tectonic strains. The faults in the MB study area were mapped at 1:100,000 scale and generally have not been studied in detail. According to Tabor and others (2003), the faults were last active in the Eocene. However, preliminary analysis of available LiDAR data suggests there may be multiple unmapped northeast-trending faults in the area near Baker Hot Spring. If these lineaments are indeed active faults, they may be responsible for geothermal fluid circulation. Future plans include field analysis of the lineaments and geophysical modeling to aid in constraining fault locations and identifying zones of alteration.

2.2.3 WRV: The conceptual resource model for the WRV area more uncertain than MSHSZ or MB because it is not situated near an active stratovolcano. However, the WRV study area is located in the heart of the Cascade magmatic arc and is surrounded by Mount Hood, Mount Adams, and Mount St. Helens. Many small Quaternary volcanic vents are present in the valley but are not close enough to the hot springs and warm temperature-gradient wells—or large enough volumetrically—to be considered a viable heat source. One working hypothesis is that there is a stalled or shallowly emplaced silicic intrusion below the surface (schematic example in Fig. 5B), possibly related to the diorite intrusion on Buck Mountain (age of emplacement

unknown), located near the intersection of the Shipherd fault zone and Wind River fault zone. Another hypothesis is that there is a magma chamber at depth and the Trout Creek Hill basalt flow was the most recent eruption from that system (0.34 ± 0.07 Ma). While the heat source is not certain, a critical element is that the faults and fault intersections in the WRV area act as conduits for meteoric water to travel to depth where they are heated (either by a deeper intrusion or the magma chamber). Subsequently, these fluids cycle back up through a percolating network of fractures proximal to the faults where the hot water eventually makes it to the surface as hot springs or in the volume of rock around temperature-gradient wells. This hypothesis is supported by the spring geochemistry, which does not suggest a magmatic fluid source.

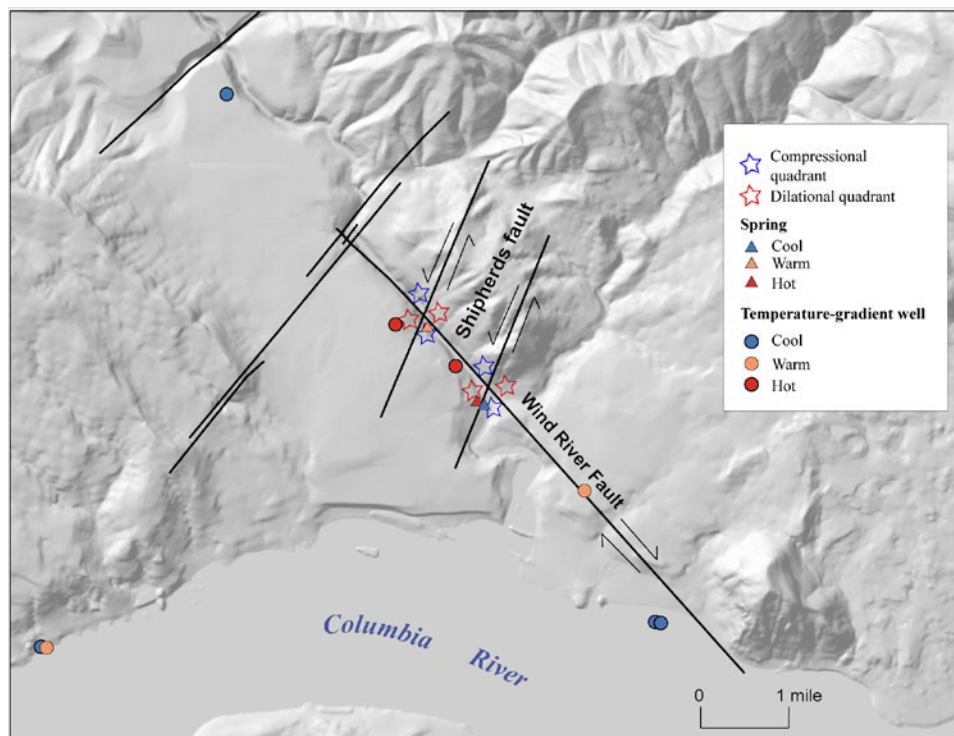


Figure 6: Structural controls of the WRV hot springs and temperature-gradient wells. This figure is a close up view of southern WRV.

The WRV geothermal area's structural setting associated with a system intersections among faults. The northwest-striking, right-lateral Wind River fault is intersected by the Shipperds fault zone, which is mapped as a series of north-northeast-striking en echelon left-lateral faults (Figs. 3 and 6). The intersections between these two opposing fault systems generates quadrants of compression and dilation. Interestingly, the hot springs and high temperature gradients (colored in red in Fig. 6) are found in the dilational quadrants, while slightly cooler springs are found in the compressional quadrants (colored in blue in Fig. 6). This is because the dilational quadrants are zones of upwelling where geothermal fluids travel from depth to the surface, whereas the compressional quadrants are less conducive to deep circulation.

3 Methodology

3.1 Play-Fairway Favorability Modeling Methodology and Assumptions

A geothermal reservoir requires that heat, permeability, and saturated porosity are present to provide adequate heat exchange, and are collocated at depths accessible by modern drilling technologies. Significant reservoir permeability enables thermal fluids to migrate freely through a reservoir and into a wellbore. The volume of enhanced permeability and the intensity of fracturing in combination with the temperature of the volume determine the commerciality by defining the in place heat and the recovery factor. This study generated maps of the most favorable combinations of heat and structural permeability, and identifies uncertainties within these categories for the three plays. An underlying assumption in this study is that there is abundant fluid present (from meteoric water, stored ground water, and in saturated rocks) in the Cascade Range to saturate fractures and provide the heat transport mechanism from depth to the near surface. This situation is consistent with the massive precipitation in the Cascades fairway (~180 in. of annual precipitation).

In this section, we summarize the play-fairway favorability modeling methodology that we developed for the Washington Cascades (Fig. 7). Heat potential maps were generated by compiling data on hot springs, geothermometry, temperature-gradient, volcanic vents, and intrusions. Permeability potential maps were generated by compiling data on faults, earthquake and crustal movements, and modeling the permeability field using geomechanical modeling software. The results of the heat and permeability potential maps are combined into geothermal favorability maps using weighting developed by a quantitative expert opinion approach. Uncertainty is quantified by determining data quality, spatial accuracy, and quantity of data at each of the sites (Fig. 7). As alluded to below, the detailed analysis steps and justifications are presented in separate appendices, allowing the focus to remain on the overall integrative methodology and results.

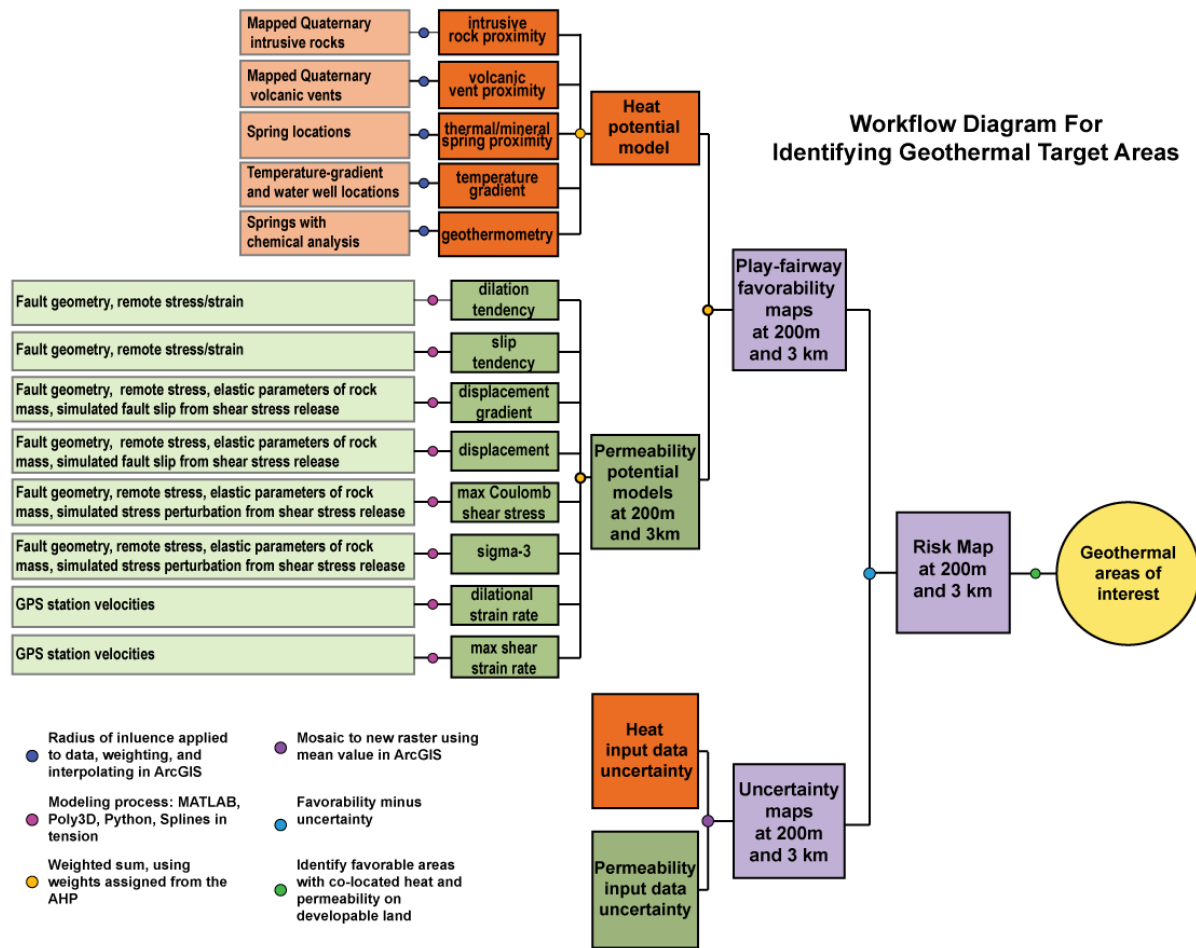


Figure 7: Model workflow illustrating input data, data processing techniques, heat and permeability potential model outputs and the end result of play-fairway favorability maps. This process was used at each of the three study areas.

3.2 The Analytical Hierarchy Process

All of the heat and permeability data are combined for favorability mapping in ArcGIS by normalizing each of the input layers, and assigning them weights according to expert opinion from partners on the project using the Analytical Hierarchy Process (AHP) (Saaty, 2008; Goepel, 2013). The AHP is a valuable tool for complex decision making by completing a series of pairwise comparisons. The AHP automatically tests the consistency of the decision maker’s evaluations, which is useful for reducing bias in the decision making process. The AHP was used in this project as a way to compare, and ultimately weight the value of the many heat and permeability input parameters to produce a fully integrated prediction of resource potentially. This analysis also provides a complimentary evaluation of the value of data for assessing the potentials of the play types in the Cascades to the sensitivity and uncertainty modeling individually conducted in the heat and permeability mapping tasks. An example of an AHP sheet for permeability potential is shown in Appendix C. Each of the experts involved in this project completed the AHP process for the heat and permeability input parameters for each of the study

areas in order to weight the parameters in order of importance to the favorability model (see Appendix C for AHP weights for all three study areas). The individual expert opinions/weights are combined in the excel sheet to generate the overall weights for each of the parameters, the software lets the users know if the expert opinions are inconsistent with each other and team members are strongly disagreeing on the various weights.

3.3 Heat Potential Modeling Methodology

The heat potential model is relatively straightforward; it models heat potential at the surface based on Quaternary volcanic vents, hot springs, geothermometry, Quaternary intrusive rocks, and temperature gradient data (Figs. 2–4). The heat model does not account for differences in heat at 200 m vs. 3 km, due to the lack of temperature-gradient data at depths greater than 200 m and a general lack of reliable heat flow data. The underlying assumptions in the heat potential modeling are shown below in Table 2.

Heat Potential Parameter	Where/radius of influence	Assumptions
Temperature gradient	Regional	Temperature gradient (measured in TG wells and water wells) is indicative of heat flow at depth
Proximity to Quaternary volcanic vents	Stratovolcanoes= 5 miles	Active or recently erupted volcanoes provide a source of heat from magma chambers at depth
	Calderas= 3 miles	
	Minor vents= 1.5 miles	
Proximity to Quaternary silicic intrusive rocks	3 miles from the edge of the intrusion	Young silicic intrusions have a tendency to stall in the upper crust and can remain a heat source for some time
Proximity to hot springs and fumaroles	0.5 miles from the spring	Hot springs and fumaroles are direct surface expressions of hot fluid upwelling
Proximity to geothermometry from hot springs	0.5 miles from the spring	spring geothermometry, when chemistry is reliable, can indicate the reservoir fluid temperature

Table 2: Heat potential parameters with assumptions.

Temperature-gradient wells were compiled from the Washington Division of Geology and Earth Resources (WADGER) geothermal well database (Czajkowski, 2014), published data (Huang and Pollack, 1998; Fairbank and Faulkner, 1992; Jessop and others, 2005), and Southern Methodist University's Western Geothermal Areas Database (Blackwell, 2010). In large areas where no temperature gradients have been measured, a WADGER database of bottomhole-

temperature data from water wells (Czajkowski, 2014c) was combined with average surface temperature (Gass, 1982) to calculate synthetic temperature gradients. The areal surficial extents of young silicic intrusive rock bodies were obtained from WADGER 1:100,000-scale digital geologic map data (WADGER, 2010a) and geologic mapping by Hildreth and others (2003). Spatial and attribute data for volcanic vents and springs were obtained from recent compilations from WADGER (Czajkowski and others, 2014b; Czajkowski and Bowman, 2014). Much of the data cited above was submitted to the National Geothermal Data System. Geothermometry temperatures for springs were calculated using the liquid geothermometer spreadsheets of Powell and Cumming (2010).

The five heat inputs were weighted based on the Analytical Hierarchy Process (AHP) results (Appendix C) and then combined using the weighted sum tool in ArcGIS for the heat potential models for each of the three plays (Fig. 8).

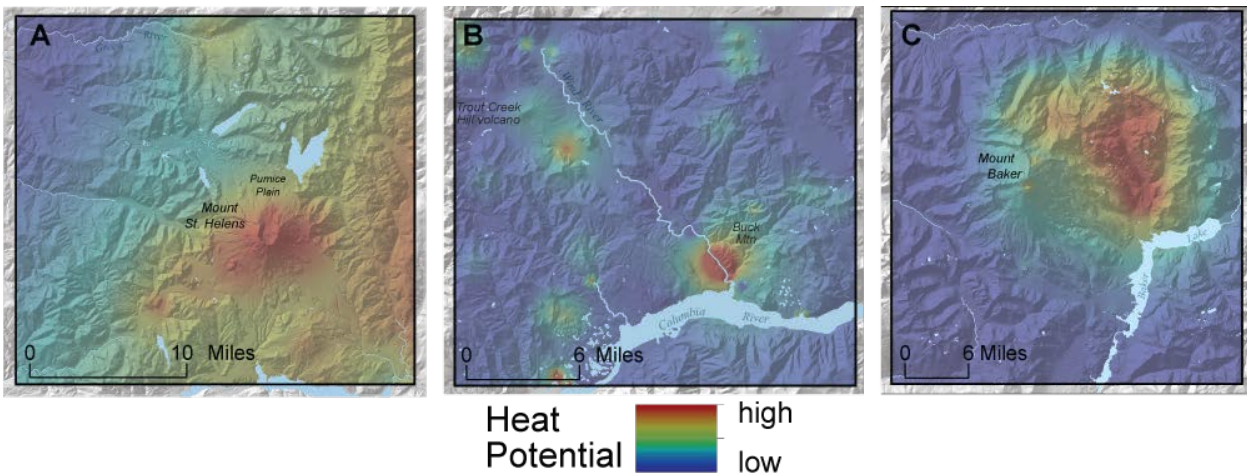


Figure 8: Combined heat potential models for the three play-fairway areas **A)** MSHSZ, **B)** WRV, **C)** MB. See Appendix C for AHP weights.

3.4 Permeability Potential Modeling Methodology

The permeability potential model takes into account many criteria that are related to fault and tectonically controlled permeability. The abundantly available seismic monitoring and geodetic data, as well as the body of literature on tectonic and volcanic models in this region has been utilized to develop a methodology for permeability potential modeling that accounts for the complex nature of crustal deformation and advances the understanding of geothermal resources in the Pacific Northwest. The permeability modeling methodology is summarized here. The reader is referred to Appendices B and D for detailed descriptions of derivations, workflow and lessons-learned for the methodology. The permeability potential models in this study focus on two depths within the crust, 200 m (typical temperature gradient well depth), and 3 km (likely production well depth for this region). The permeability can change drastically between these two depths because mapped faults may not correlate to active faults delineated by seismicity at depth (Figs. 2, 3, and 4), which often have no surface expression. Similarly, there is variability in the available constraints on model inputs that influences the uncertainty and therefore risk

associated with the permeability model. Existing data sets provide reasonably strong constraints where geologic mapping and seismicity are available; elsewhere, new data is identified in Phase 2 to improve Phase 1 results and fill data gaps.

The multi-criteria permeability potential model for each of the three plays is comprised of the weighted sum of eight intermediate rasters: (1) slip and (2) dilation tendency on mapped and seismically inferred faults (3) maximum shear strain rate, and (4) dilational strain rate at the surface, (5) fault displacement distribution, and (6) displacement gradient, (7) maximum Coulomb shear stress, and (8) tensile fracture density (Σ_3). Parameters 1–6 are modeled from faults mapped at the surface, seismicity, and GPS derived strain rate data; parameters 7 and 8 are derived from GPS velocity data. The underlying assumptions in the permeability potential modeling are that (a) geothermal fluids travel along faults and in the damage zone surrounding the fault, that (b) high fracture density promotes a percolating fracture network with porosity to store fluids and a heat exchange area, and (c) active or episodic brittle deformation is necessary to maintain the permeability and porosity that would otherwise be lost to mineral alteration and precipitation. See Table 3 for a description of the permeability layers, where they influence the permeability model, and what assumptions are being made.

Permeability Layer	Where	Implication	Assumption
displacement/slip tendency	along fault	fault hosted flow	active faulting promotes fault permeability
dilation potential	along fault	fault hosted flow	low normal stress enables dilation during slip
displacement gradient	along fault	localized fault hosted flow	dU/dx indicates high local strain and intense fracturing
Coulomb Stress/ σ_3	volume around fault	fractured reservoir extent	favorable stress change = high fracture density
shear and dilational strain	larger scales of earths crust	regional position of reservoir	active crustal deformation promotes fractures and permeability

Table 3: Permeability potential parameters with implications and assumptions.

The premise of critically-stressed fracture flow theory (for example, Barton and others, 1995; Heffer, 2002) is that fluid flow preferentially occurs along fractures and faults that are favorably oriented for slip. In addition, slip on large faults induces a zone of damage characterized by connected fracture porosity (Caine and others, 1996; Curewitz and Karson, 1997; Hickman and others, 2000; Eichubl and others, 2009; Hickman and Davatzes, 2010).

Consequently, by modeling the stress conditions and slip tendency of fractures and faults, as well as localized elastic strains or stresses resulting from this slip that promote damage, we provide constraints on the potential permeability of a fractured rock mass. The resulting model addresses key aspects of commerciality including the position and relative intensity of fractured volumes, their potential connectivity to each other (or to a potential heat source), and the relative volume associated with intense fracturing. In Poly3D faults, fractures, and cavities are modelled as displacement discontinuities discretized into triangular elements in an elastic half-space to simulate fault slip and surrounding rock deformation. Local elastic deformations have a strong dependence on detailed fault geometry and the regional strain field driving slip on a fault. As a result, the method provides a sound mechanical means for predicting the local variability in fracturing that often frustrates drilling.

Regional strain rates and remote stresses used in Poly3D for each of the three plays were derived from the publically available GPS time series from the National Science Foundation (NSF) Earthscope's Plate Boundary Observatory (PBO) and Central Washington University's Pacific Northwest Geodetic Array (PANGA). GPS station velocities (Fig. 8) were used to infer strain rates using the 'splines in tension' method (Wessel and Bercovici, 1998). Strain rates were derived separately for subduction zone locking at depth and block rotation near the surface (Appendix D) within crustal block boundaries. The crustal block boundaries used were modeled by McCaffrey and others (2007) from GPS velocities, as well known or suspected mapped faults, seismicity, and paleomagnetic rotations. This approach is vital to modeling the stress/strain for the complex tectonics in this region, which consists of highly localized areas of extension, rotation, compression and shearing. Fault data were compiled from the DGER 1:100,000- and 24,000-scale digital surface geology, and active faults data within the digital seismogenic features database (WADGER, 2010a,b; Bowman and Czajkowski, 2014). Earthquake hypocenter locations were taken from the DGER seismogenic features database (Bowman and Czajkowski, 2014), originally obtained from the Pacific Northwest Seismic Network (PNSN), along with available earthquake focal mechanisms.

This approach has been successfully used in the oil and gas sector to prospect and characterize reservoirs as well as improve flow simulations used to define drilling targets and pumping plans. Maerten and others (2001) successfully used similar approaches to predict the attitude and density distribution of small faults from the geometry of larger faults and strain boundary conditions. Bourne and others (2000) and Bourne and Willemse (2001) successfully predicted detailed fault and joint patterns due to slip on larger faults (verified by detailed mapping) as inputs to a reservoir flow model. More recently Tamagawa and Pollard (2008) used related techniques to explain short wavelength variations in stress documented in wells that impacted productivity of an oil reservoir. Heffer (2002) has illustrated that even in fractured as well as "traditional un-fractured" oil fields, stress and its relationship to active structures is a key predictor of sweep efficiency and breakthrough during water floods. Work by Micklethwaite and Cox (2004) further demonstrates that these approaches predict ore bodies that are necessarily the result of long-term sustained flow of large fluid volumes.

Workflows and scripts were developed in MATLAB to model fault geometries from earthquake data and to calculate slip and dilation tendency which are highly dependent on fault

geometry. *Poly3D* is used to model fault displacement and stress perturbation in larger volumes surrounding faults. This analysis requires knowledge of the orientation and magnitude of the current stress/strain rates at each play area. The GPS strain rates derived at the surface (data acquired from the Plate Boundary Observatory) are used as an initial constraint to derive the 3D, quasi-static, strain tensors at depth. In addition to constraining the boundary conditions for *Poly3D*, the strain rate was used to map maximum shear strain rate and dilational strain rate at the surface.

The eight permeability inputs were weighted using the AHP results (Appendix C) and then combined using the sum tool in ArcGIS. The individual permeability output rasters for each of the three play areas are shown in Appendix B. The weights of each individual permeability input are shown in Appendix C as percentages. Figure 9 shows the combined permeability potential rasters at 200 m and 3 km depth slices for each of the three plays.

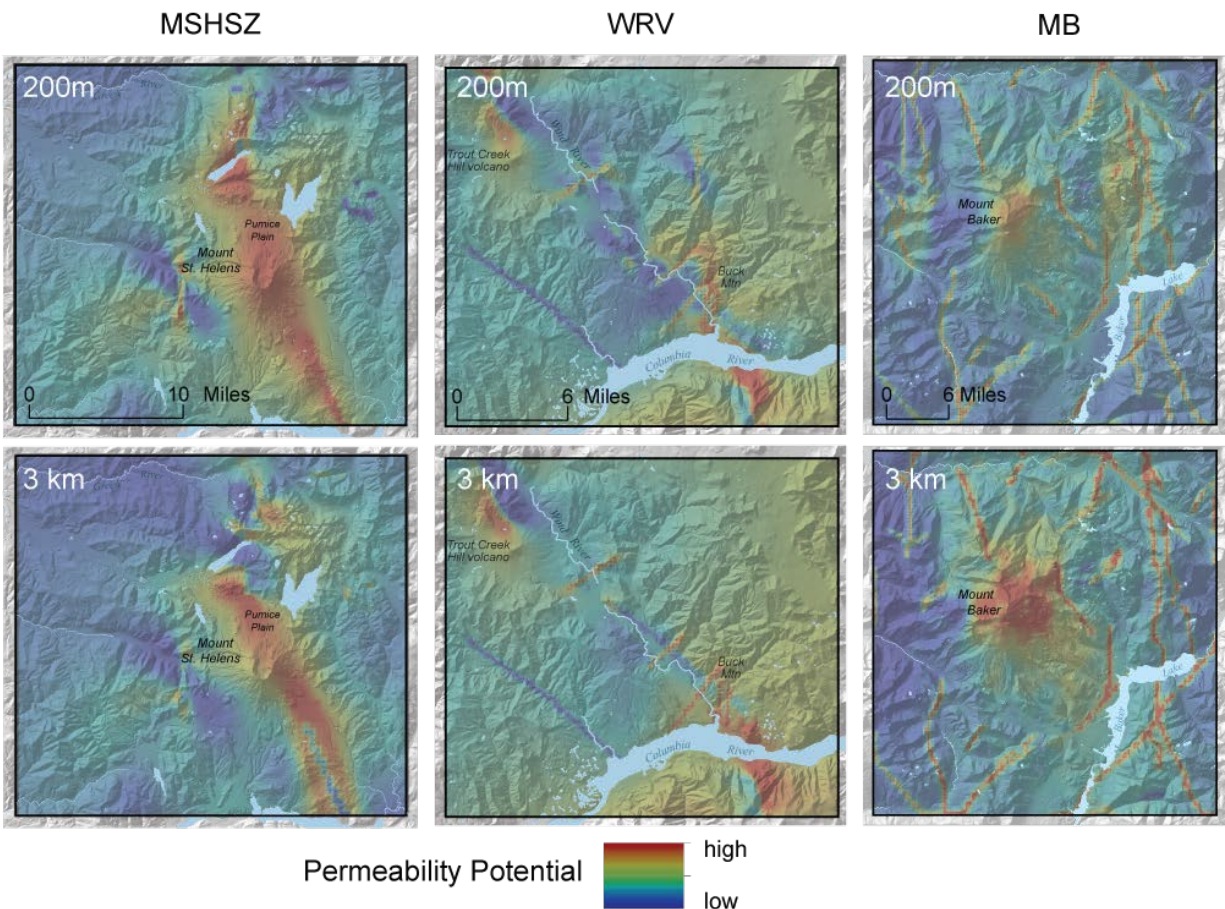


Figure 9: Combined permeability potential for 200 m and 3 km depth slices at each of the three play-fairway areas (from left to right: MSHSZ, WRV, MB).

3.5 Combining the Heat and Permeability Potential Models

The innovative permeability modeling approach combined with conventional techniques for heat potential mapping were used to improve the resolution of the statewide geothermal assessment, and attempts to provide metrics for the dimensions of the potential reservoir based on favorable areas of heat and permeability. Maps at two depths, 200 m and 3 km, have been produced for each play to illustrate the potential for a geothermal resource at the play (Please see the Results section for the combined heat and permeability potential maps).

The geothermal play-fairway resource potential models represent the relative geothermal potential at each of the three plays based on the weighted sum of the permeability and heat potential models. These models characterize geothermal resource potential without consideration of regulatory restrictions, land-management restrictions, or economic viability. In addition to the assumptions inherent in the permeability potential and heat potential models, the resource potential model assumes that areas with coincident elevated permeability and heat will have higher favorability for future exploration. The final combined heat and permeability layers for all three study areas are shown below in the results section.

3.6 Utility of Methods for Applications at other Sites

The methods employed in this study were designed for our purposes (a magmatic system with little or no developed geothermal resources for model validation). However these methods could easily be used on a known geothermal system and it would be very interesting to test this methodology in an area with existing production wells to see how the model predicts areas of co-located heat and permeability.

The GIS-based heat modeling approach employed in this project draws from and builds upon methods from previous GIS-based models of geothermal favorability applied to regional studies in Japan (Noorollahi and others, 2007), Iran (Noorollahi and others, 2008), Oregon (Poux and Suemnicht, 2012), Washington (Boschmann and others, 2014), and elsewhere.

The permeability modeling method used in this study is widely applicable to any fault controlled geothermal resource. In addition to the examples from oil and gas and mineral exploration cited in the sections above, this methodology has been used for understanding the permeability structure at the Desert Peak geothermal field in Nevada, and accurately predicted areas of favorable stress at the location of the most successful injection and production wells, as well as helps explain the barrier between distinctly produced reservoir volumes. (Fig. B1) (Swyer and Davatzes, 2013).

3.7 Uncertainty and Sensitivity Modeling Methodology

In order to validate the geothermal favorability modeling and locate areas where further investigation and data collection would improve the favorability model, the data quality and spatial certainty of the existing data points must be addressed.

Data quality is a proxy for the uncertainty or reliability of the data used. Each of the heat data inputs (hot spring locations, temperature-gradient wells, etc.) were assigned data quality

values specific to the type of data that was modeled (example: springs were ranked on the year sampled, the completeness of the water chemistry analysis, if the spring was located using GPS, etc.) detailed data quality information can be found in Appendix E. Data quality is a proxy for the uncertainty or reliability of the data used. Each heat parameter input has a radius of influence (ROI), where the data-quality value (1 to 5, with 5 = highest data quality) decreases radially within the ROI. The individual heat uncertainty rasters were combined and values were averaged to generate the final heat uncertainty models for all three play areas (Fig. 10).

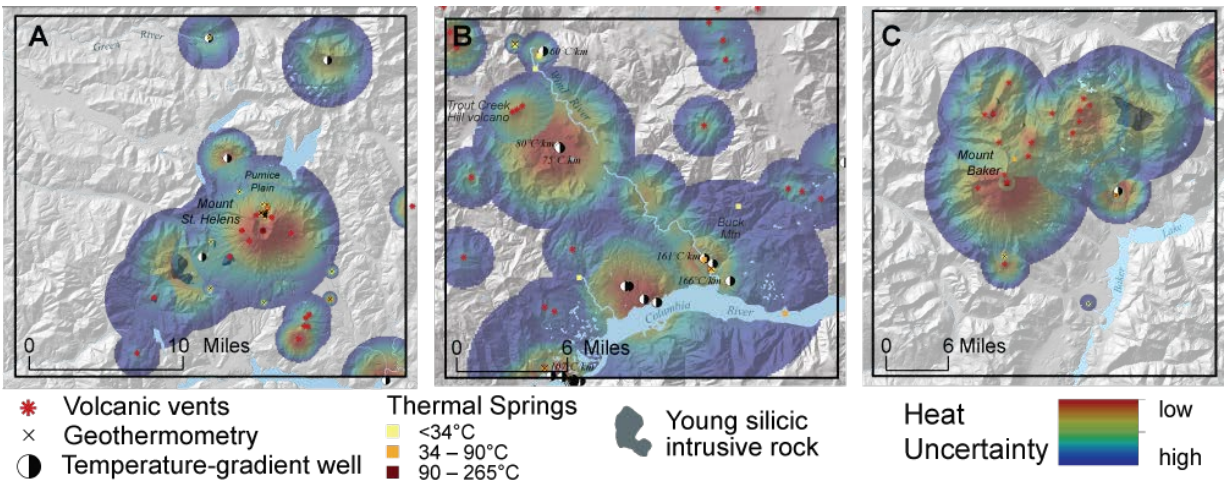


Figure 10: Combined heat uncertainty models for the three play-fairway areas **A)** MSHSZ **B)** WRV **C)** MB. See Appendix E for the individual heat uncertainty maps and detailed data processing descriptions.

The method employed to derive the uncertainty of the GPS data in modeling the strain rate and remote stress for the three plays is detailed in Appendix D. This is commonly depicted as maps of the GPS station locations with velocity vectors and *confidence ellipses* that define the uncertainty of the station velocities. Figures 11A and B map the rotational and subduction locking velocity/uncertainty. Sensitivity was quantified and mapped at each play by finding the absolute difference between the strain rate layers (d and ϵ_{max_shear}) modeled from \pm one standard deviation of the station velocities. Because the data comes from long-term monitoring of GPS benchmarks, and there is adequate coverage in this region, there are no proposed plans to improve this dataset.

Washington Division of Geology and Earth Resources
Phase 1 Technical Report

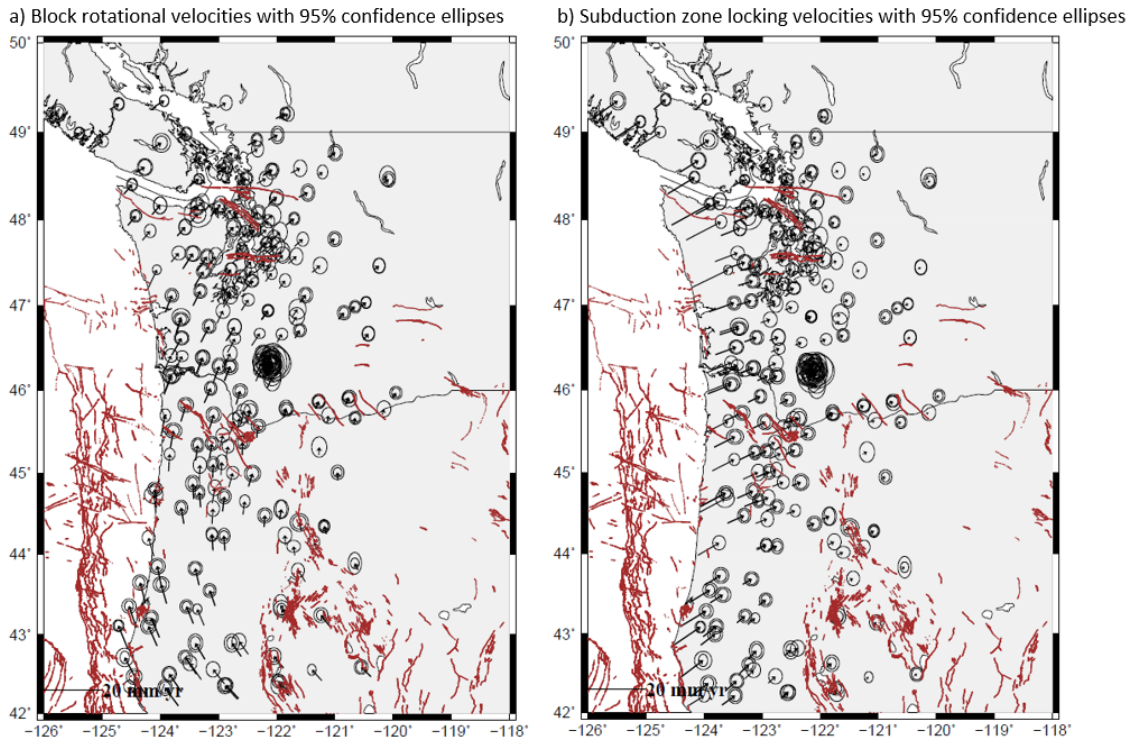


Figure 11: GPS velocity uncertainty **a)** Block rotational velocities and **b)** Subduction zone velocities with 95% confidence ellipses.

The uncertainty modeling for the permeability potential is based on (1) the reliability of the fault mapping, (2) the density of micro-seismicity used to construct fault planes at depth and (3) the residuals derived from fitting of planes to earthquake and fault trace. Items 2 and 3 utilize Inverse Distance Weighting (IDW) by taking the sum of the inverse distances from points along the fault to all the micro-seismic events used to construct the fault plane for Item 2, and taking the inverse distance between the upper/lower residual fault geometry for Item 3. Item 1 was assigned a data quality value from 1 to 5 according to quality of fault mapping, whether or not seismicity was used, and whether or not the fault was modeled in 3D (Table 4). Items 2 and 3 were normalized from 0 to 5 on a log scale for each fault across all three sites. Items 1 through 3 were averaged for the final permeability uncertainty (Fig. 12).

Fault Data Quality Value	Data Quality Criteria
5	Mapped at surface and fit to seismicity at depth
4	Fit to seismicity and not mapped
3	Mapped at 24k and modeled in 3D (dip assumed)
2	Mapped at >24k and modeled in 3D (dip assumed)
1	Mapped fault, mapping quality suspect, not modeled in 3D

Table 4: Fault data quality values.

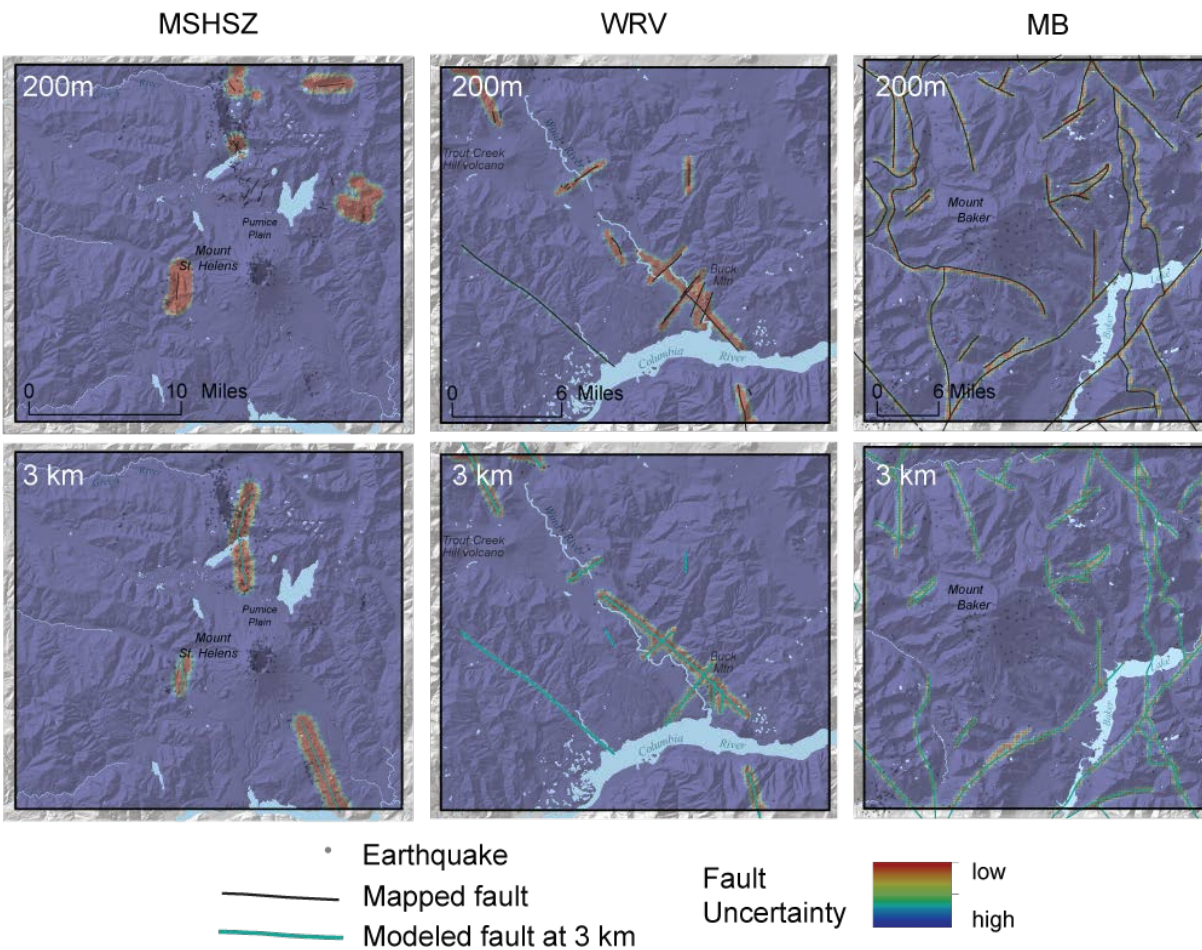


Figure 12: Combined permeability/fault uncertainty models for the three play-fairway areas at 200 m and 3 km depth slices (from left to right: MSHSZ, WRV, MB). See Appendix E for the individual heat uncertainty maps and detailed data processing.

The sensitivity of the predicted permeability potential was assessed by adjusting parameters with significant uncertainty within ranges of error. The model prediction relies heavily on the fault geometry, so it was varied within the residual boundaries of the fit to the micro-seismicity used to construct fault geometry at depth. Faults that were not fit to micro-seismicity were assumed to have a dip uncertainty of $\pm 10^\circ$. The most significant parameter uncertainties in the magma chamber models were varied as well. At MSH, the mapped location and geometry of the magma chamber is very well constrained from seismic data but has a depth uncertainty of ± 1000 m. The strain rate magnitude and uncertainty used for the MB magma chamber is extremely high (420 ± 140 nanostrain/yr) compared to background tectonic strain. The resulting set of models are compared to quantify variability in the predictions. The sensitivity maps (Fig. 13) reveal robust features in the model, as well as features that significantly change due to uncertainty in an input parameter. Such parameters become the focus for new data acquisition to resolve this uncertainty (and ultimately reduce the risk of exploratory drilling and site development). In general, fault tips, intersections and bends, which have a large impact on local stressing, become critical

features to confirm due to their strong influence on predicted permeability potential. At MSHSZ, the model is very sensitive near the fault system to the north of MSH, where the seismicity indicates a bifurcation at depth (Weaver and others, 1987); the model is also sensitive to the magma chamber depth, and the unknown geometry of the Goat Mountain fault to the west of MSH. At WRV, the model is sensitive in the southeast along the Wind River fault where there are multiple fault intersections at shallow depths, and further northwest along the Wind River fault where there is uncertainty of where the fault terminates at depth. The MB model is the most sensitive to the magma chamber deformation, which could be improved by more geophysical surveys. The model can also be improved by gathering more recent (last survey in 2007) line-length changes in the field from the remote GPS benchmarks placed on the summit (Crider and others, 2011).

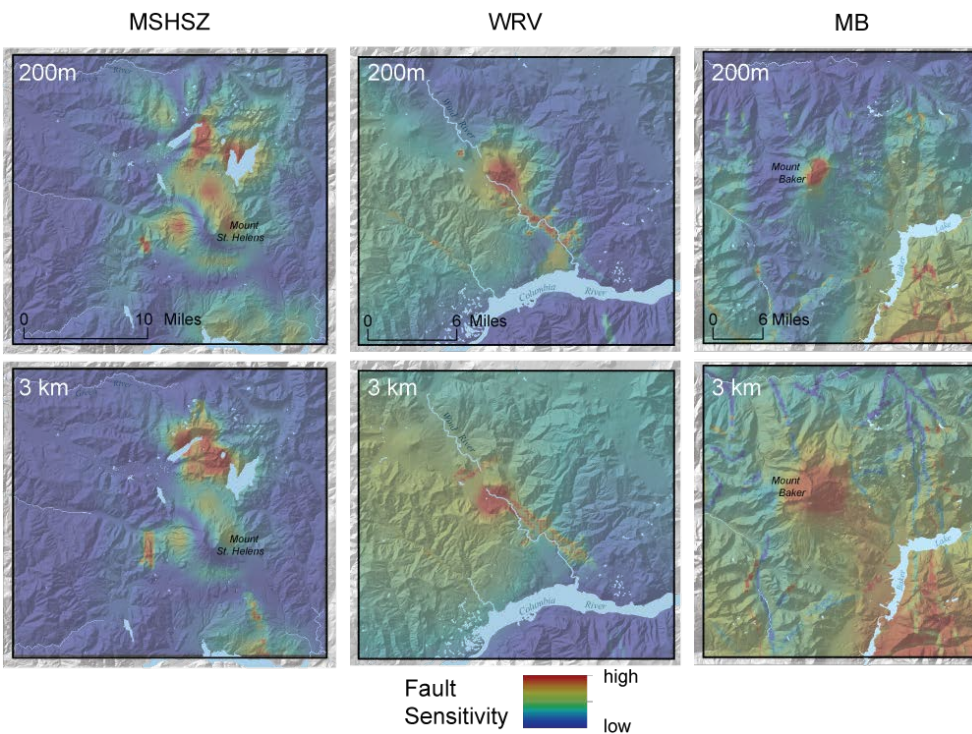


Figure 13: Permeability model sensitivity to fault geometry for MSHSZ, WRV and MB

4 Results

This project was successful in generating detailed favorability, uncertainty, sensitivity, and risk maps for the MSHSZ, WRV, and MB. The favorability maps are the result of the combined heat and permeability potential models, and will be addressed first in this section. The uncertainty maps address the uncertainty in both the heat and permeability input parameters, and will be discussed after the favorability models. Lastly this project addresses development risk by combining the favorability and uncertainty maps. The results of the risk maps can be

significantly changed by gathering new data that either removes uncertainty, thus reducing risk, or actually changes the resource potential in favorability modeling.

4.1 Geothermal Favorability Modeling Results

The geothermal resource potential models for all three play-fairway areas successfully distinguish zones with high favorability for geothermal resource based on heat and permeability potential models at depths of 200 m and 3 km. One important difference in the 200 m and 3 km depth slices for all three areas is that at 3 km depth, the permeability was weighted much higher than the heat (permeability potential = 70% and heat potential = 30%), whereas at 200 m depths, heat and permeability potential were weighted evenly. The reason for this difference in weighting is based on the assumption that at 3 km depth, there is a higher chance that heat will be present in most places, but that localized zones of enhanced permeability are less likely. The favorability maps at 3 km depth are modeled at a typical depth for production drilling and therefore focus on optimally oriented structures that would be the targets for geothermal fluid circulation. The heat and permeability are weighted evenly in the shallow subsurface (200 m) model because the goal of favorability modeling at this depth slice is siting a temperature-gradient well, which requires knowledge of the background heat signature as well as where there are structures that channel upwelling fluids. Detailed analyses of the favorable locations in each of the three study areas are presented below. The areas of interest (AOI) for future exploration are determined from the combination of the favorability and uncertainty models and are outlined and discussed in more detail in Section 5.

4.1.1 MSHSZ: As expected, the MSH volcano shows the highest favorability, in large part due to the high weight assigned to volcanic vents and intrusive rock in the heat potential model (see Appendix C for weights), along with the high weight assigned to dilational strain rate and maximum Coulomb shear stress in the permeability model (all are favorable directly centered on MSH). Additionally, the SHZ is located along the axis of MSH and contributes to the permeability potential in that area. It should be mentioned that some areas, particularly the northwest part of the study area, data are sparse and therefore impart a low favorability based on lack of data (as seen by the distribution of input data points in Fig. 2).

Although there is not a drastic difference between the 200 m and 3 km combined heat and permeability maps (Fig. 14), there are subtle differences. The main contrast is in areas where seismicity-defined faults cross the 3 km observation plane but not the 200 m plane (Figs. 9 and 14). Because the heat potential is only modeled at 200 m the heat input for the combined favorability does not change and this causes some of the similarities seen in each of the resource potential maps.

Outside of the MSH National Volcanic Monument (restricted lands in Figure 14) the most favorable areas are along the trend of the MSHSZ to the north and south of the volcano, within lands that have geothermal leases and are potentially developable.

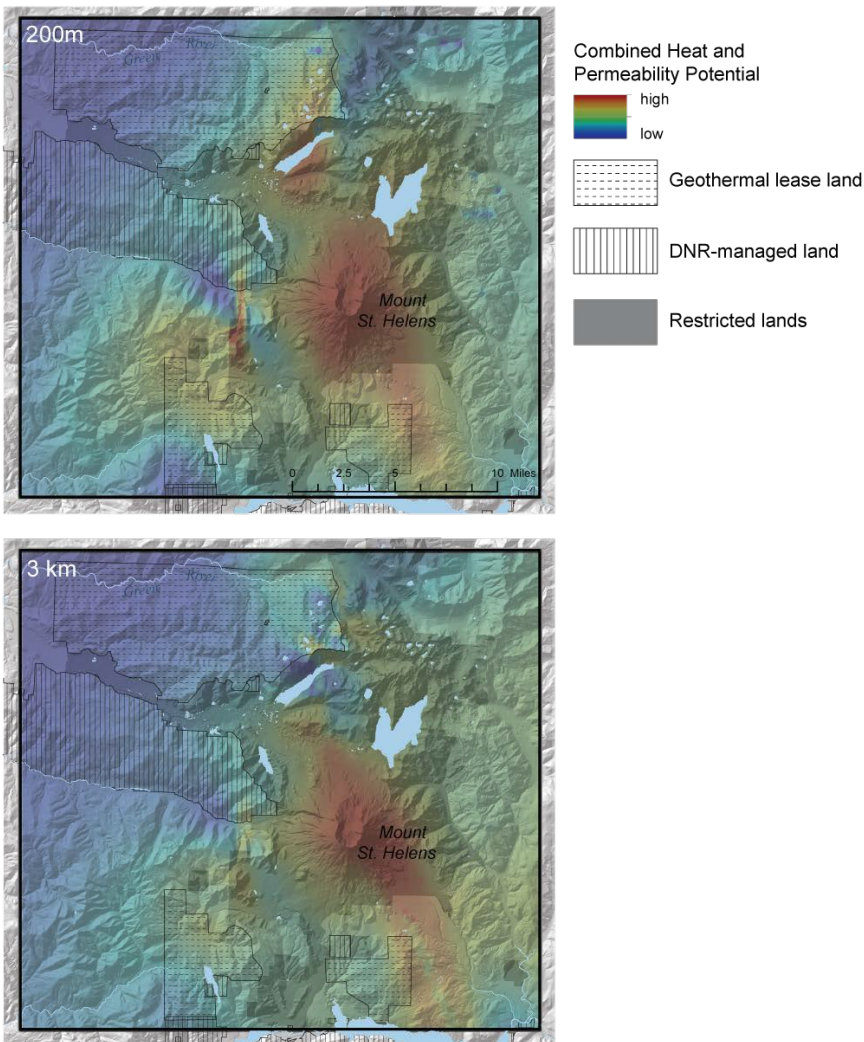


Figure 14: MSHSZ Heat and permeability potential combined at 200 m and 3 km. The 200 m combined heat and permeability potential map is the sum of the heat potential map (Fig. 8A) and the 200 m permeability potential map (Fig. 9A), with equal weights assigned to both maps. The 3 km combined heat and permeability potential map is a weighted sum of the heat potential map (Fig. 8A) and the 3 km permeability potential map (Fig. 9A) with 30% weight assigned to the heat potential map and 70% weight assigned to the 3 km permeability potential map.

4.1.2 WRV: The WRV geothermal favorability maps at both 200 m and 3 km show localized zones of enhanced heat and permeability, primarily in the south end of the Wind River valley. The south WRV area is the most favorable in both the heat potential map (Fig. 8B) and the permeability potential map (Fig. 9B). The high favorability in this area is due to: high temperature gradient values (two wells in the south end of the valley with gradients of $161^{\circ}\text{C}/\text{km}$ and $166^{\circ}\text{C}/\text{km}$ [Fig. 3]), hot springs (with measured temperatures of 50°C and 53°C), numerous faults (Shipherds fault zone, Wind River fault, and Brush Creek fault (Fig. 3), as well as a high density of fault intersections. Complex fault geometry such as fault terminations, dilational fault intersections, and step overs are proven to be the most favorable structural settings for hosting geothermal systems worldwide (Curewitz and Karson, 1997; Faulds and others, 2004). The major differences in the 200 m and 3 km favorability maps (Fig. 15) are due to the location of the fault at 200 m vs. 3 km (due to fault dip), and the higher weight assigned to permeability at the 3 km depth slice (70%) compared to the equal weights assigned to heat and permeability at 200 m.

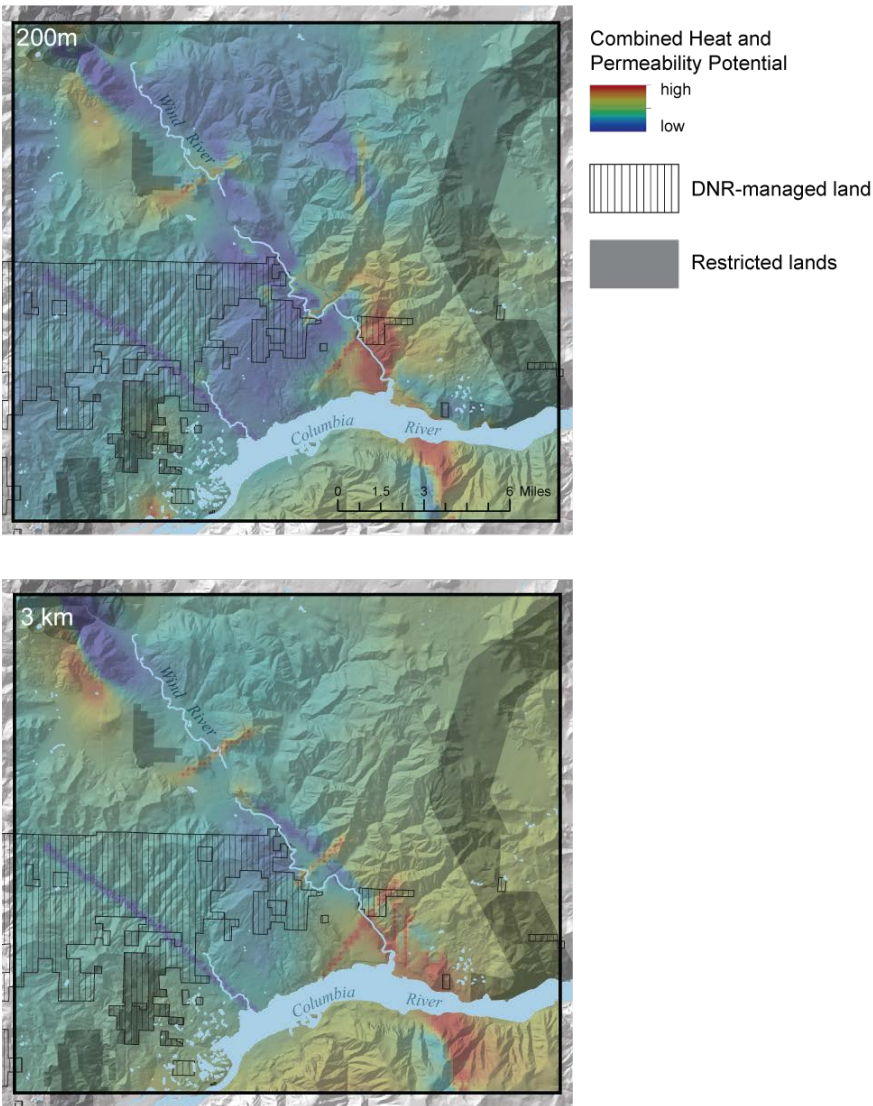


Figure 15: WRV Heat and permeability potential combined at 200 m and 3 km. The 200 m combined heat and permeability potential map is the sum of the heat potential map (Fig. 8B) and the 200 m permeability potential map (Fig. 9B), with equal weights assigned to both maps. The 3 km combined heat and permeability potential map is a weighted sum of the heat potential map (Fig. 8B) and the 3 km permeability potential map (Fig. 9B) with 30% weight assigned to the heat potential map and 70% weight assigned to the 3 km permeability potential map.

4.1.3 MB: The MB combined heat and permeability potential map at 200 m shows the highest geothermal favorability in the shallow subsurface to the east of Mount Baker volcano and north of Baker Lake (Fig. 16). This is due to: the high weight assigned to the temperature-gradient well raster for this study area (53.9%), the temperature gradient well has the highest gradient in the state (200°C/km), numerous Quaternary volcanic vents with high favorability scores, the location of Baker Hot Spring (44°C) which has high geothermometry (equilibrium temperature of 148°C), and the termination and intersection of faults near the hot spring. The 3 km heat and permeability potential map differs from the 200 m map due to the high weight assigned to the permeability potential raster (70%) (Fig. 16). This causes the volcano (the magma chamber) and the fault traces to show up with higher favorability in the 3 km layer and the heat signature associated with the temperature-gradient well and the hot spring to have less of an effect on the model.

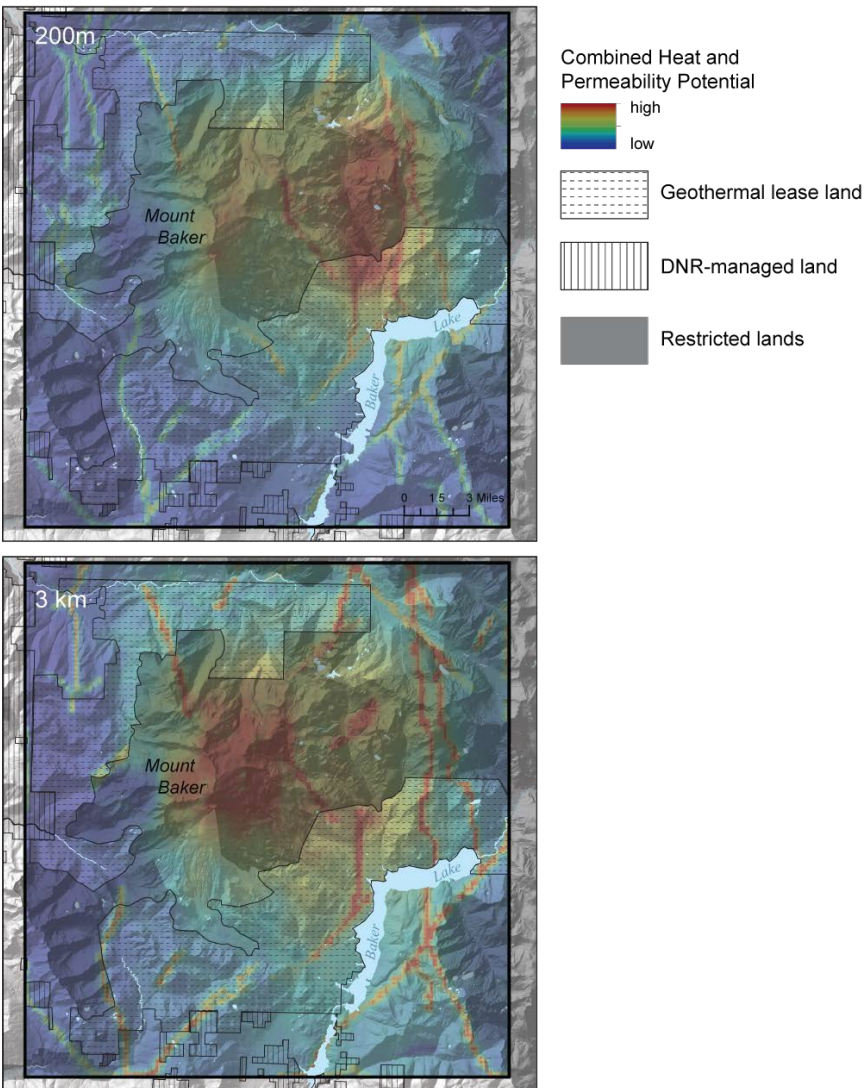


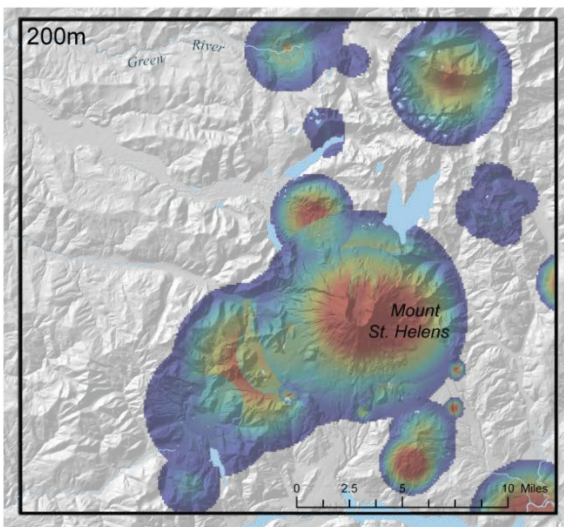
Figure 16: MB Heat and permeability potential combined at 200 m and 3 km. The 200 m combined heat and permeability potential map is the sum of the heat potential map (Fig. 8C) and the 200 m permeability potential map (Fig. 9C) with equal weights assigned to both maps. The 3 km combined heat and permeability potential map is a weighted sum of the heat potential map (Fig. 8C) and the 200 m permeability potential map (Fig. 9C) with 30% weight assigned to the heat potential map and 70% weight assigned to the 3 km permeability potential map.

4.2 Uncertainty Modeling Results

Uncertainty modeling illustrates where data to constrain models is lacking (areas without color), where there is abundant high quality data (warm colors) and where the data quality or spatial accuracy is lacking (cool colors). The uncertainty modeling helps to identify where there are uncertainties in the data and guides plans for Phase 2 by determining where better data quality or quantity could improve the model.

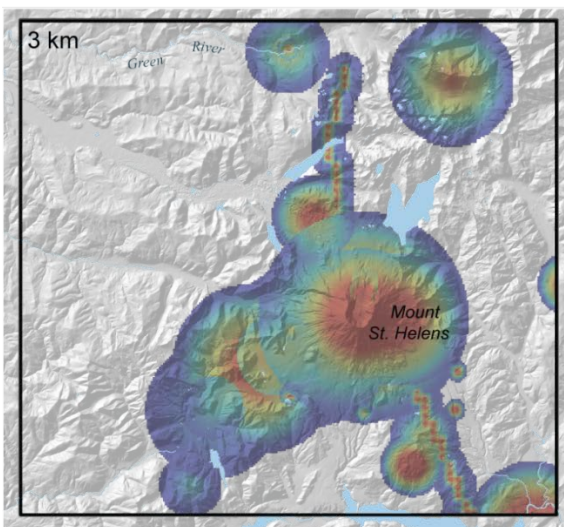
4.2.1 The MSHSZ uncertainty models at 200 m and 3 km depth slices illustrate that there is a significant lack of data in the western part of the study area, this contributes to the low favorability in this area (Fig. 17). This model shows that there is high certainty of the presence of collocated heat and permeability near the volcano, and high fault certainty at 3 km along the seismic zone. The fault geometry is well constrained at depth in the MSHSZ, due to the abundant seismicity in the area, however most of the seismicity in the area is deeper than 3 km and so the

fault geometry is poorly constrained at the 200 m depth slice. The uncertainty modeling shows that better constraints on temperature gradient are needed, particularly to the west. In addition, detailed geologic mapping is needed to either confirm the absence of structures to the north and the south of the volcano, or to identify previously unmapped structures and update the favorability modeling. Consequently, geophysical techniques are proposed to aid in refining the geometry of the seismic zone, locate offset lithologies and structures, and identify subsurface alteration that may be associated with geothermal fluid upwelling.



Heat and
Permeability
Uncertainty
low
high

Figure 17: MSHSZ Heat and permeability uncertainty combined at 200 m (top) and 3 km (bottom). Areas that are not colored (gray shaded relief map) are areas where there are no input data, and therefore are not modeled in the uncertainty maps. Warmer colors indicate areas with higher data quality and spatial accuracy (low uncertainty) and cooler colors are areas with low spatial accuracy (on the periphery of the ROIs for the input data) and (or) poor data quality.



4.2.2 The WRV uncertainty models at 200 m and 3 km depth slices illustrate that there is high certainty of co-located heat and permeability near the southern end of Wind River valley, and in the central Wind River valley (Fig. 18). These locations of high certainty are centered on areas with high quality temperature-gradient wells (see Table E5 for more details), and coincident faults, vents, springs, and high quality geothermometry. The fault certainty in the WRV study

area is high because the area has been mapped at 1:24,000 (Czajkowski and others, 2014), and there are a few earthquakes guide projection of the surface structures to depth. The uncertainty modeling shows that the geometry of the north-northeast-trending faults (Shipherds fault zone and Brush Creek fault) are poorly constrained (see Fig. 3 for locations of faults). Geophysical techniques are proposed to better constrain the geometry of known faults, identifying offset lithologies and structures, and identifying subsurface alteration that may be associated with geothermal fluid upwelling. The uncertainty is highest in the northeast part of the study area where there are little data, and the data that are present are low quality.

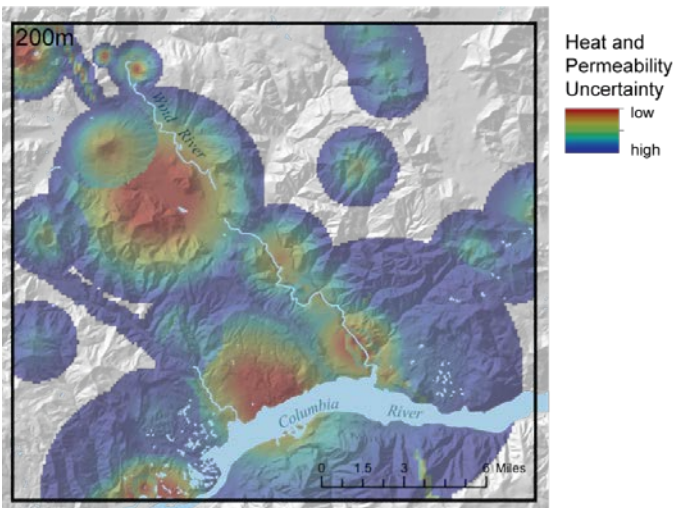
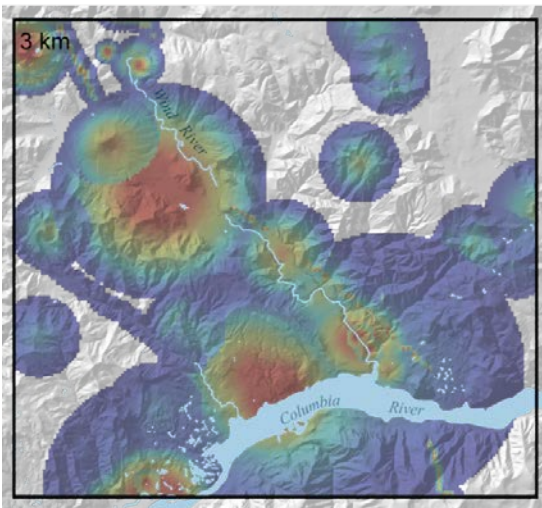


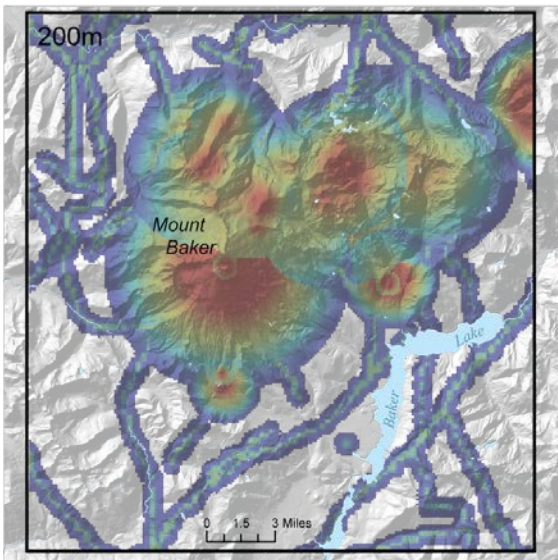
Figure 18: WRV Heat and permeability uncertainty combined at 200 m (top) and 3 km (bottom). Areas that are not colored (gray shaded relief map) are areas where there are no input data, and therefore are not modeled in the uncertainty maps. Warmer colors indicate areas with higher data quality and spatial accuracy (low uncertainty) and cooler colors are areas with low spatial accuracy (on the periphery of the ROIs for the input data) and (or) poor data quality.



4.2.3 The **MB** uncertainty models at 200 m and 3 km depth slices (Fig. 19) illustrate that there is high certainty of collocated heat and permeability near the edifice of the Mount Baker volcano, to the southeast near the location of Baker Hot Spring and the warm temperature-gradient well and at the locations of volcanic vents and intrusions (Figs. 4 and 8C). These areas of high certainty are primarily centered on areas with high quality heat data (see Table E5 for more

details). The fault geometry at MB is the least well constrained of all three study areas, this is due to very dense vegetation, the large scale at which the faults were mapped (1:100,000 scale at MB compared to 1:24,000 at WRV), the lack of seismicity associated with crustal faults, and the lack of fault information (no measured fault dips).

The uncertainty modeling shows that more data are needed to better constrain the location and geometry of the faults (Fig. 19). Geophysical techniques are proposed to aid in refining the geometry of known and inferred faults, identifying offset lithologies and structures, and identifying subsurface alteration that may be associated with geothermal fluid upwelling.



Heat and
Permeability
Uncertainty

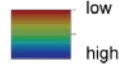
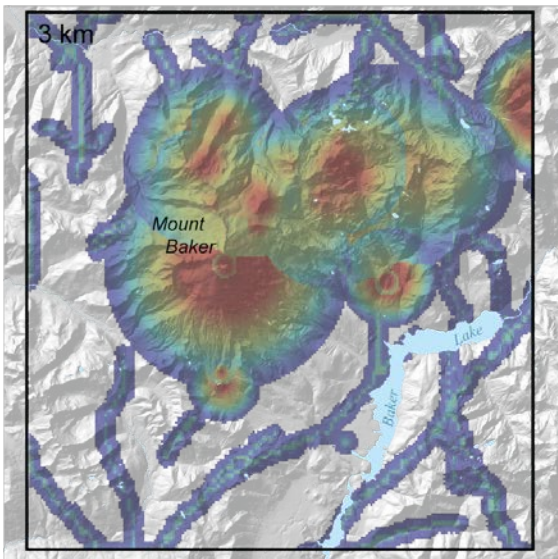


Figure 19: MB Heat and permeability uncertainty combined at 200 m (top) and 3 km (bottom). Areas that are not colored (gray shaded relief map) are areas where there are no input data, and therefore are not modeled in the uncertainty maps. Warmer colors indicate areas with higher data quality and spatial accuracy (low uncertainty) and cooler colors are areas with low spatial accuracy (on the periphery of the ROIs for the input data) and (or) poor data quality.



5 Areas of Interest for Future Exploration Based on Risk Mapping

Risk maps were made for the three play-fairway study areas at 200 m and 3 km depth (Figs 20–22). The goal of these maps is to combine the favorability and uncertainty models to determine the best locations to conduct future exploration with the ultimate goal of drilling a well to test the viability of a geothermal resource. The risk maps were made by subtracting the normalized uncertainty maps from the normalized favorability maps. These risk maps show where there are areas with high favorability and low uncertainty = low risk (warm colors), and where there is low favorability and high uncertainty = high risk (cool colors). Based on these risk maps we have identified areas with low risk that are located within developable land (existing geothermal lease lands, lands available for geothermal lease bids in the near future, DNR-managed lands, and land privately owned by parties interested in geothermal development). These low-risk, high-favorability areas are the geothermal areas of interest (AOI) which are outlined in Figures 20–22. These AOIs are also the focus of our Phase 2 exploration, which is discussed in detail in Section 6.

The MSHSZ AOIs are located outside the National Volcanic Monument, along the trend of the MSHSZ, in areas with high-moderate favorability, low-intermediate risk, and on land with geothermal lease held by AltaRock Energy. These AOIs cover an area slightly larger than the low-risk zones (warm colors) because we are interested in collecting data in areas with sparse or no data (Figs. 2 and 17) that are preferentially located along the MSHSZ (such as the northern AOI in Fig. 20).

The two WRV AOIs (Fig. 21) are located in the south of the valley, where the two hottest temperature-gradient wells and a high density of faults are located, and in the center of the valley (near Trout Creek hill), where two warm temperature-gradient wells were drilled (see Fig. 3 for more information). While some locations in the south of the study area—on the north bank of the Columbia River—show up as low risk, they are located in an area that has been inundated by massive landslides (such as the Bonneville slide) and are not suited for development.

The MB AOI is centered along the southeast flank of the volcano within existing geothermal lease lands. This AOI is defined by a hot temperature-gradient well, a hot spring with high geothermometry, and a fault termination. The AOI also includes the land to the southwest of the lowest risk area, with the goal of collecting more data in an area that is high risk simply because data are sparse (Fig. 19).

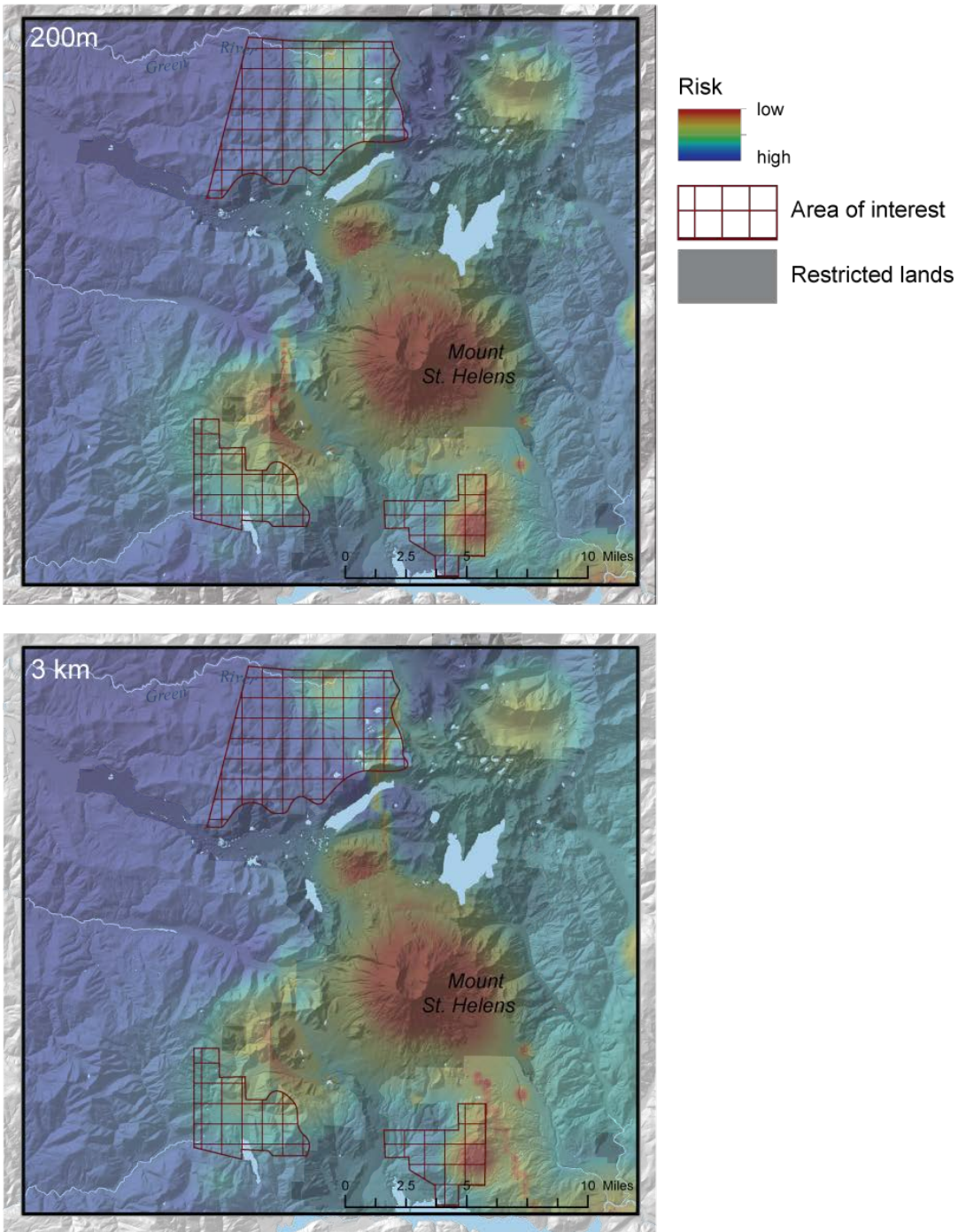


Figure 20: MSHSZ risk maps at 200 m and 3 km with AOI areas outlined in red.

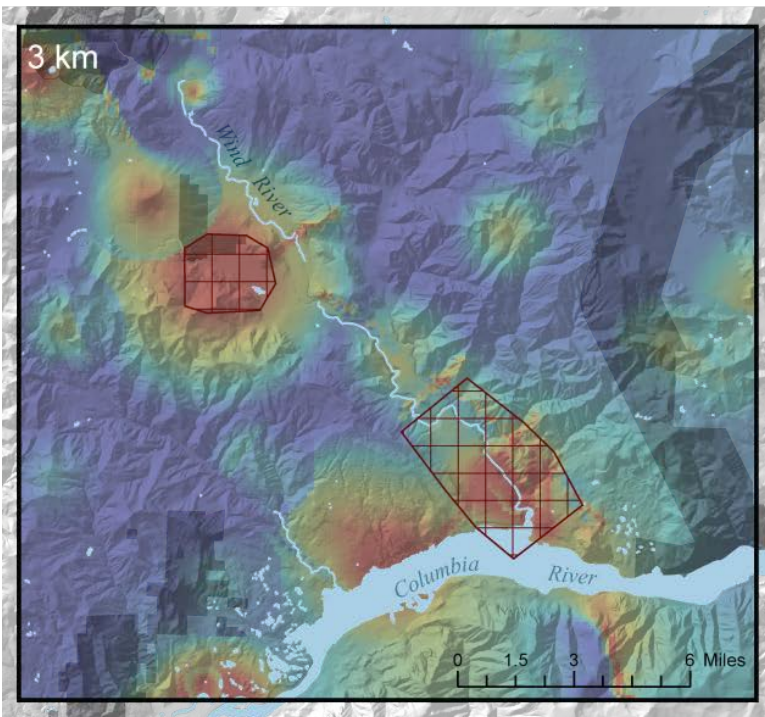
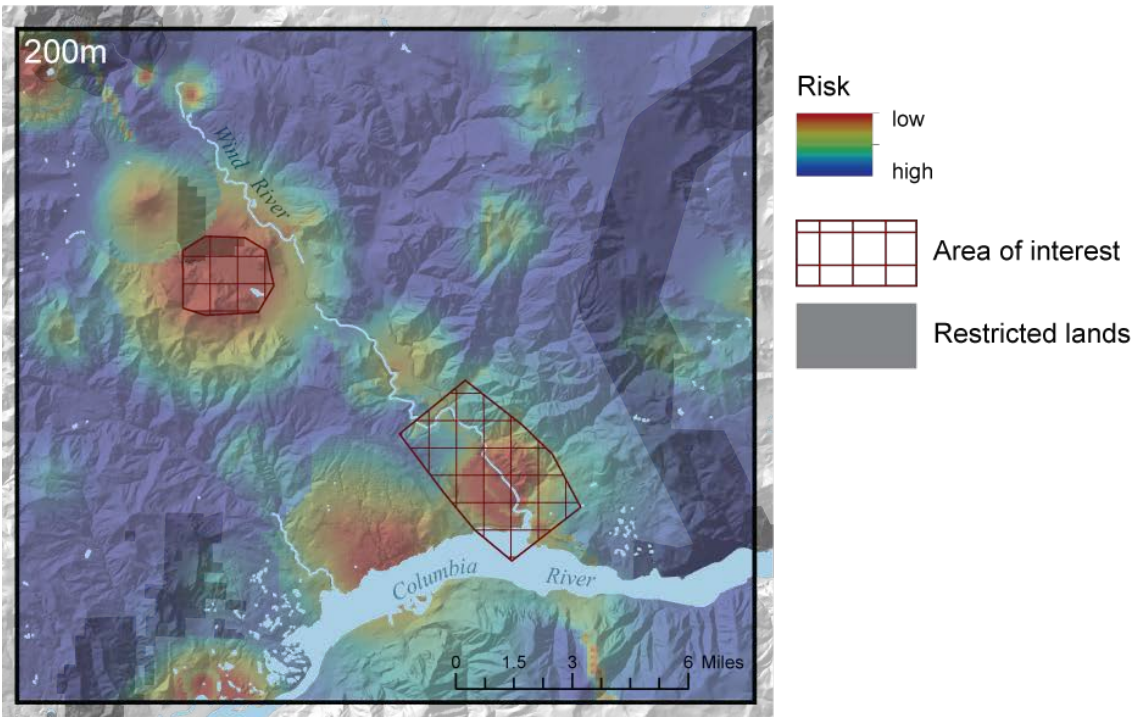


Figure 21: WRV risk maps uncertainty at 200 m and 3 km with AOI areas outlined in red.

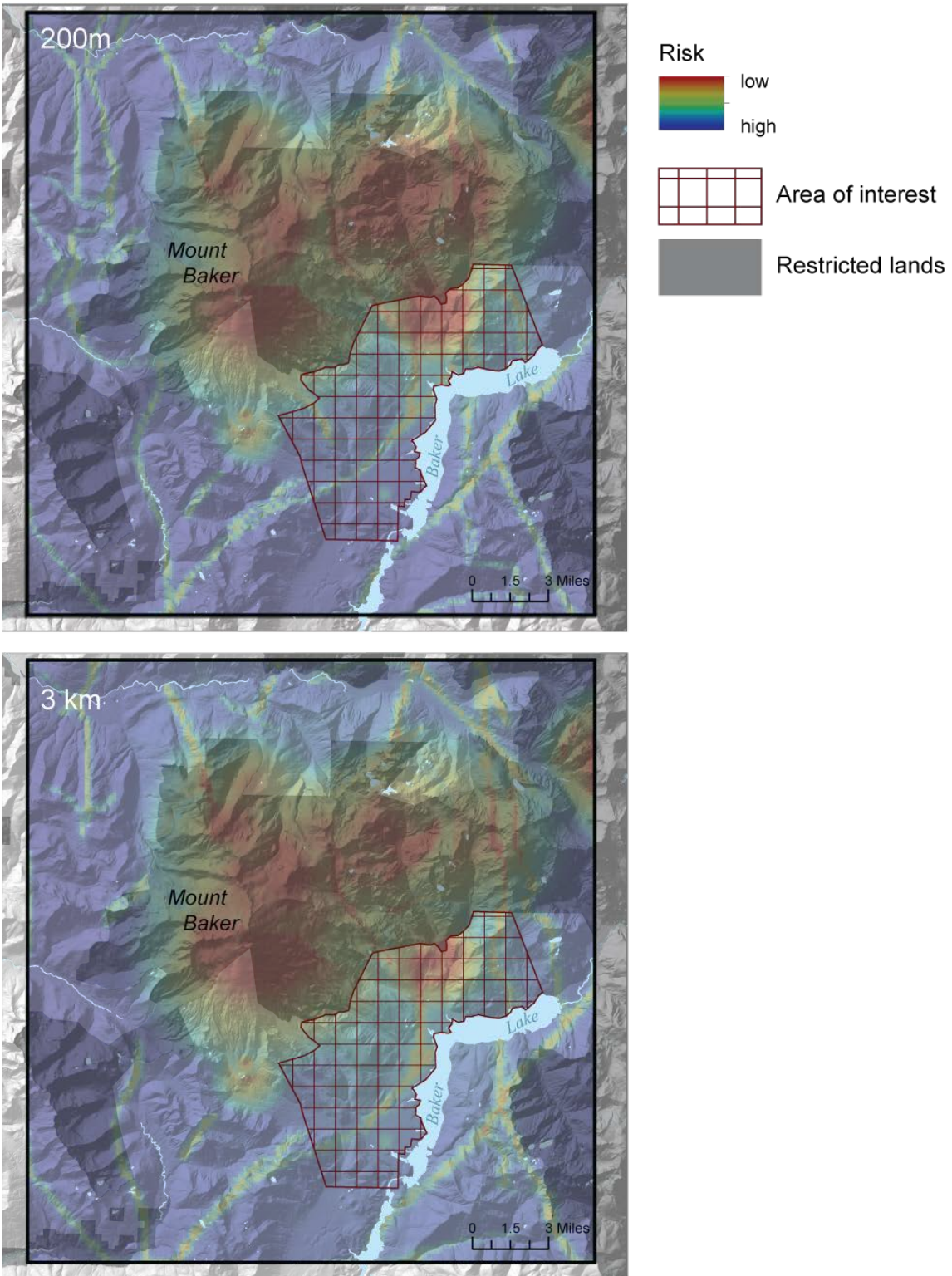


Figure 22: MB risk maps at 200 m and 3 km with the AOI area outlined in red.

6 Commercial Viability of the Three Play-Fairways

6.1 Presence of a Resource

Each of the three play-fairway areas show promise for a viable commercial resource within developable land, but further exploration activities are needed to better delineate fault geometry and heat sources in the areas of interest (AOI) (Figs 20-22). The presence of a resource for this study is defined as areas that have high favorability based on both the heat potential model and the permeability potential model.

6.2 Local Factors Supporting Development

MSHSZ: The dam, substation, and transmission line at Mossyrock Dam (located to the north of MSH) owned by Tacoma Public Utilities, is roughly 20 km from the existing geothermal leases.

WRV: The WRV play-fairway area is located 20 km east of the Bonneville dam, owned and operated by the Bonneville Power Administration. This dam is connected to more dams upstream by an extensive transmission line that transmits power to Washington and Oregon. A geothermal power plant in this area could easily connect to the grid.

MB: The dam, substation, and transmission line at Upper Baker Lake, owned by Puget Sound Energy, is just 3–14 km from the existing geothermal leases. This nearby infrastructure makes the Mount Baker leases attractive from a development perspective because the building of these assets can be an expensive part of any geothermal development. Lastly, it should be noted that Mount Baker is the only identified geothermal resource listed in the USGS assessment of Washington (USGS, 2008) which estimates a generation potential of 23 MWe.

6.3 Land Status

MSHSZ: The Mount St. Helens North AOI is located on land that is owned by Weyerhaeuser Company and Weyerhaeuser Real Estate Development Company. Of those lands, 19,284 acres of geothermal leases are held by AltaRock Energy. Because the surface is privately owned on the Mount St Helens North AOI and the geothermal rights are leased by AltaRock Energy, further exploration of land and any required permitting will be the most straightforward of any of the play-fairway sites. AltaRock Energy also holds geothermal rights in part of the Mount St. Helens South AOI; however, the lease block is much smaller and does not include the central portion of the MSHSZ.

WRV: The Wind River play-fairway AOI is located on privately owned land. In the southern AOI, the land is a combination of residential and commercial (the Beacon Rock Golf Course owned by Bonneville Hot Spring Resort, and the High Cascade Timber Company) land. We have talked with some of the land owners in the AOI and have received positive feedback.

MB: The Mount Baker play-fairway area includes 8,350 acres of BLM geothermal leases currently held by Cyrq Energy. In 2011, 5,500 acres around the existing leases were nominated for geothermal leasing by an anonymous company. In 2013, an additional 14,260 acres north of Mount Baker were nominated. In 2014, the U.S. Forest Service (USFS), the agency that controls the surface rights to these lands, consented to lease the all nominated acres and self-nominated an additional 81,820 acres (USFS, 2014). The U.S. Bureau of Land Management (BLM), the agency that controls the geothermal resources, is currently planning to auction the geothermal leases in October, 2016 (personal comm., Steve Storo, BLM, 2015).

6.4 Potential Industry Partners

MSHSZ: In 2008, AltaRock Energy made an agreement with Weyerhaeuser Company to explore the potential for developing geothermal projects on 667,000 acres of land in California, Oregon, and Washington. After 3 years of exploration and evaluation, AltaRock Energy exercised its option to lease the geothermal rights to approximately 45,000 acres of the land with the best potential for geothermal development. Almost half of the lands AltaRock leased from Weyerhaeuser are the Mount St Helens North AOI. Weyerhaeuser is very supportive of developing geothermal resources on their land in order to earn the royalties that would be produced. Weyerhaeuser has also been aggressive developing wind resources on their land.

Another potential industry partner on this AOI is TransAlta USA, owner of the Centralia Coal plant, 60 km northwest of the leases. The coal plant will be closed down in stages between 2020 and 2025. To support education and retraining; energy efficiency measures for low-income residents; and new technologies geared to improving the environment, TransAlta has agreed to fund grants worth \$55 million (<http://cctgrants.com/>). AltaRock has already submitted a proposal to this program to evaluate the feasibility of replacing the electricity from the Centralia Coal plant with geothermal electricity.

WRV: No industry partners have yet been identified for WRV.

MB: AltaRock has previous working relationships with two potential partners interested in geothermal development at Mount Baker: Cyrq Energy and Snohomish Public Utilities (SnoPUD). AltaRock has worked with Cyrq since 2011 on geothermal well stimulations, exploration, and development. Cyrq recently acquired the geothermal leases at Mount Baker when they purchased the assets of Gradient Resources. SnoPUD and AltaRock have worked together since 2008, when SnoPUD asked AltaRock to evaluate geothermal resources in Snohomish and adjacent counties. This led to a program of spring sampling, drilling of five temperature-gradient wells along U.S. Highway 2, and a deep (5,000 ft) exploration slimhole at Garland Mineral springs, a project on which WADGER also participated. Unfortunately, despite a 110° C/km gradient in the first 230 m, the Garland slimhole failed to find higher temperatures than background or a geothermal resource. Since then, SnoPUD has turned attention to Mount Baker, as there is excess transmission capacity from the north into Snohomish County. SnoPUD had negotiated with Gradient Resources, LLC regarding the Mount Baker leases but came to no

agreement. Since Cyrq acquired the leases, AltaRock has facilitated the introduction to SnoPUD, who is still interested in partnering with geothermal developers in the Mount Baker area.

7 Conclusions

The three Washington State geothermal play-fairway study areas all have areas with high potential for collocated heat and permeability at 200 m (a typical depth to drill a temperature-gradient well) and 3 km (a typical geothermal production well depth) depth slices, based on the geothermal favorability modeling, uncertainty modeling, and risk mapping. Geothermal favorability modeling is the product of heat potential mapping and innovative three dimensional permeability potential mapping. Uncertainty models illustrate where the data used in the favorability models are high quality and spatially accurate, and where there is a lack of data and the favorability mapping is based on interpolation. The risk maps are calculated by taking the difference between the favorability maps and the uncertainty maps, this illustrates where there is high favorability and low uncertainty areas (low risk) and vice versa. The geothermal areas of interest (AOI) at each of the three sites were identified from the risk maps. The AOI are located on land that, to the best of our knowledge, can be permitted for geophysical exploration, and can potentially be developed for geothermal production if future exploration proves promising. The AOI at each of the three areas are the focus of Phase 2 exploration. The activities proposed at all three sites for Phase 2 are primarily geophysical surveys that have been tested and used extensively in oil and gas, mineral, and geothermal exploration, as well as geological and geochemical analysis that will add critical data to the areas where data are sparse. These geophysical and geological methods focus on refining the geometry of known faults, better understanding the local geology and hopefully identifying new faults, locating subsurface discontinuities, and detecting areas with low resistivity that may be associated with hydrothermal alteration and geothermal fluids.

8 Recommendations for Future Exploration

8.1 Description of Phase 2 Objectives and Outcomes

Phase 2 focuses on acquiring data to help refine fault geometry on the surface through geologic mapping, LiDAR analysis, and geophysical surveys (MT, seismic, and resistivity). Geophysical methods are proposed to aid in constraining subsurface geology, fault geometry, and alteration and potential fluid pathways. In addition one temperature-gradient well is proposed at the MB study area to help constrain the temperature at depth in the region. It should be noted that no LiDAR is proposed for Phase 2, this is because new LiDAR was recently flown in the MB and

WRV study areas and will be available for use for Phase 2, and LiDAR in MSHSZ is recently available through Weyerhaeuser and can be used for Phase 2. The preliminary Phase 2 proposals of specific methods planned for each site are listed in the tables below, and are also broken out in further detail in the preliminary budget sheets. The timeline and description of the planned activities assumes a 16 month performance period for Phase 2 and a January 2016 start date.

8.2 Summary of Proposed Activities for Phase 2

Low-cost (Table 5) and high-cost (Table 6) estimates for activities proposed at all three play-fairway areas. Figures 23–25 show the locations of the proposed Phase 2 activities for each of the three study areas. We have been in contact with the USGS for potential for collaboration in Phase 2 activities. They have been very helpful and have provided us with preliminary cost estimates and a preliminary work plan which are provided in Appendix E.

Low-cost estimate proposed activities		
MSHSZ	WRV	MB
Geologic mapping in north MSHSZ	Radiometric age dating of the Buck Mountain intrusion	Geologic field survey (Lidar analysis, mapping, trenching?)
Passive seismic survey		Magnetotelluric survey
Magnetotelluric survey (at no cost to project)		Electrical resistivity survey
Electrical resistivity survey		

Table 5: Low-cost estimate for the activities proposed for Phase 2.

High-cost estimate proposed activities		
MSHSZ	WRV	MB
Geologic mapping	Radiometric age dating of the Buck Mountain intrusion	Geologic field survey (Lidar analysis, mapping, trenching?)
Passive seismic survey	Aeromagnetic survey	Passive seismic survey
Magnetotelluric survey (at no cost to project)	Gravity survey	Magnetotelluric survey
Gravity survey		Electrical resistivity survey
Electrical resistivity survey		Temperature-gradient well

Table 6: High-cost estimate for the activities proposed for Phase 2.

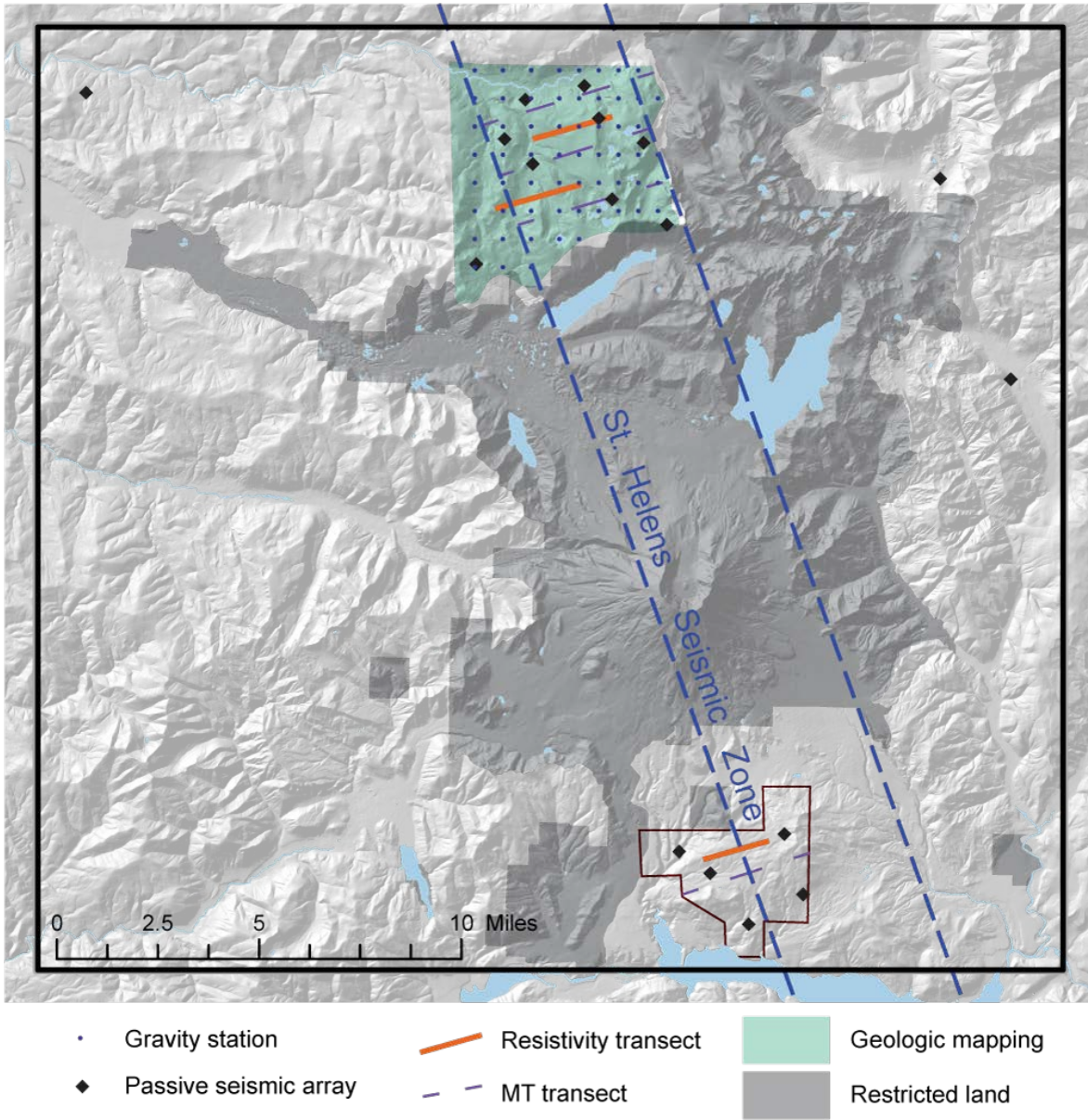
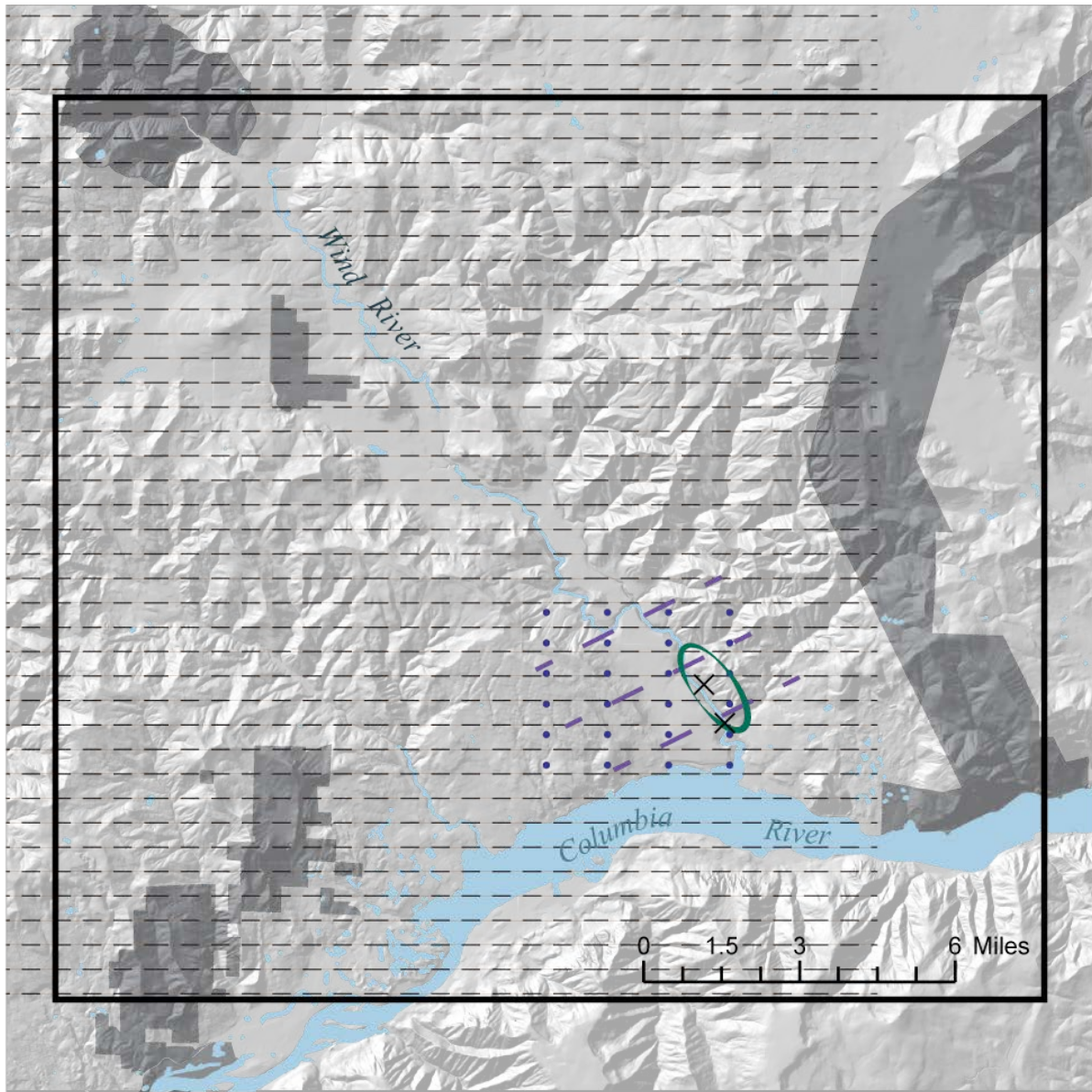
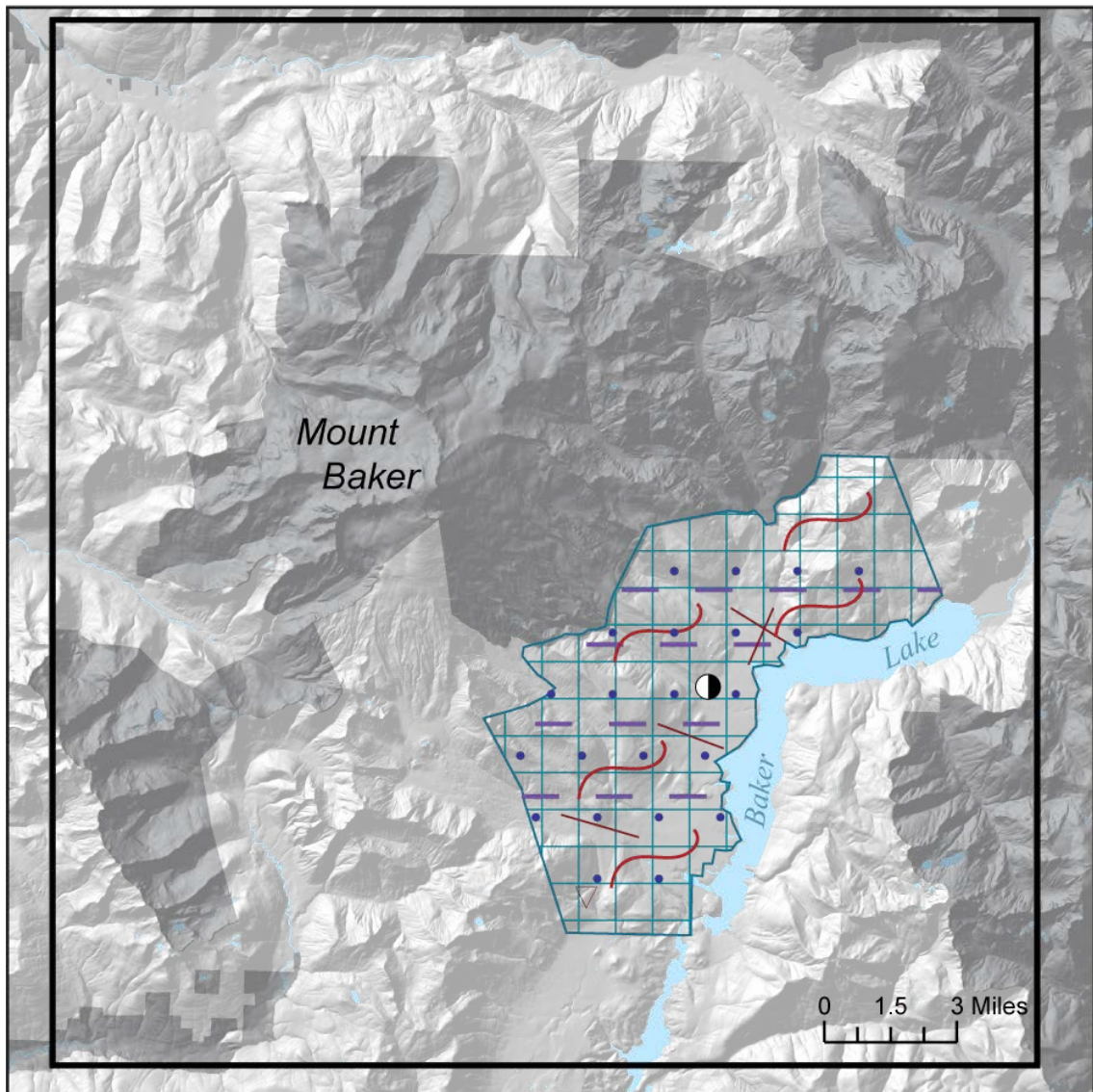


Figure 23: MSHSZ proposed activities for Phase 2.



- × Geothermometry
- Gravity station
- Radiometric dating
- - - MT transect
- - - Aeromagnetic survey
- Restricted land

Figure 24: WRV proposed activities for Phase 2.



- Gravity station
- Temperature-gradient well
- Electrical resistivity survey
- Ground-based magnetics
- MT transect
- Field survey
- Restricted land

Figure 25: MB proposed activities for Phase 2.

8.3 Description of Planned Activities (SOPO tasks)

Preliminary Milestone Summary Table				
Recipient: Washington Division of Geology and Earth Resources				
Project Title: Geothermal Play-Fairway Analysis of Three Washington State Prospects				
Task Number	Task Title	Milestone Description	Milestone Verification Process	Anticipated Month of Completion
1	Negotiation and Planning	Award negotiation, contract negotiation and geophysical survey planning, permit negotiation for all exploration activities, data organization	Permits approved, contracts awarded, funding implemented, surveys planned	March 2016
2	Field Work	Geologic mapping, geophysical surveys, TG well drilling	Successful completion of field surveys, data collection complete	October 2016
3	Data Interpretation	Data analysis and interpretation	Contractors deliver data and work with partners on data interpretation	December 2017
4	Update Favorability Modeling	Incorporate new data into favorability models for all three plays	New favorability models generated for all three plays	March 2017
5	Reporting and Data Submission	Final technical reporting and data submission	Report submitted and data uploaded to NGDS	April 2017

Table 7: Description of planned activities for Phase 2.

8.4 Partners Identified and Roles

Organization	Role
Washington Division of Geology and Earth Resources (WADGER)	Project PI, geologic mapping, geophysical field survey help, well logging, LiDAR analysis and field checking, geologic age dating, integration of new data into the existing model, report writing, and partner collaboration and organization
AltaRock Energy Inc.	Geophysical field survey equipment owners and contractors, well logging, expert advice and data interpretation, integration of new data into a new and improved permeability model
Temple University	Expert advice, data interpretation, Poly3D license holder, integration of new data into a new and improved permeability model
USGS (?) or other Geophysical Contractors	Passive seismic tomography at MSHSZ, WRV, and MB, magnetotelluric survey at MSHSZ, WRV and MB, aeromagnetic survey over WRV, drilling TG well at MB, gravity survey at MSHSZ, assistance in geologic mapping and LiDAR scarp examination

Table 8: Description of project partners and their roles in Phase 2

8.5 Preliminary Timeline

Month(s)	Planned Activities
January-March 2016	Award negotiation, contract negotiation and survey planning for the geophysical surveys, permit negotiation for all exploration activities, data organization and dispersion to project partners
March-October 2016	Geologic mapping, LiDAR scarp examination and field checking, geophysical field surveys (MT, seismic tomography, resistivity, aeromag), TG well drilling, send samples to lab to get age dates
November 2016-January 2017	Data collection from geophysical stations that were deployed in the field, data interpolation and analysis
January-March 2017	Integration of new data into favorability models
March-April 2017	Reporting, Phase 3 planning, data submission

Table 9: Preliminary project timeline. This timeline assumes Phase 2 is 16 months, and funds become available in January 2016.

8.6 Preliminary Phase 2 Budget Information:

The preliminary budget information shows the proposed high (Table 7) and low (Table 8) budget activities for each of the three play-fairway areas. These tables also describe what the logistical site advantages are for each area, what the favorable factors for each site are, and what the main uncertainties are at each site, in addition we have listed what we hope to learn from each of the proposed activities.

High-Cost Budget Estimate

MSHSZ		
Logistical Site Advantages	Site Favorables	Site Uncertainties
Surface Ownership, road access, geothermal rights, low public visibility, TransAlta and Weyerhaeuser as partners, Centralia coal mine replacement funding	Existence of large, active fault zone, moderate gradient, active stratovolcano	Details of fault geometry that would affect fault permeability and reservoir extent
Activity	What we hope to learn from activity and cost	
Geologic Mapping	Look for surface expression of young faults (alteration, fluid leaks, etc.) to complete 3D model of MSHSZ. Use Weyerhaeuser LiDAR	
Mapping Total	\$4,000	
Passive Seismic Survey	Image details of shear zone including permeability anomalies, magma chamber	
Seismic Survey Total	\$100,000	
Magnetotelluric Survey	Further confirmation of 3D fault structure, hydrothermal alteration, fluid conduit, in order to recommend slimhole sites.	
MT Survey Total	\$28,500	
Gravity Survey	Further confirmation of 3D geology and fault structure, in order to recommend slimhole sites.	
Gravity Survey Total	\$28,500	
Electrical Resistivity Survey	Check LiDAR lineaments and mapped faults for resistivity anomalies indicative of leaky structures	
Electrical Resistivity Survey Total	\$2,500	
MSHSZ High-Cost Estimate (not including staff time)	\$163,500	

Washington Division of Geology and Earth Resources

Phase 1 Technical Report

WRV		
Logistical Site Advantages	Site Favorables	Site Uncertainties
Close proximity to transmission lines, road access, highest data quality and quantity	Very high gradient. Clear geomorphic expression of faulting.	Depth and extent of heat source, extent and geometry of faults.
Activity	What we hope to learn from activity and	
Gravity Survey	Further confirmation of 3D fault geometry, image intrusive heat source, in order to recommend slimhole sites.	
Gravity Survey Total	\$28,500	
Aeromagnetic Survey	Further confirmation of 3D fault geometry, image intrusive heat source, in order to recommend slimhole sites.	
Aeromagnetic Survey Total	\$126,000	
Geochronology of Buck Mountain diorite	Is Buck Mountain a heat source?	
Age Analysis Total	\$5,000	
WRV High-Cost Estimate (not including staff time)	\$159,500	
MB		
Logistical Site Advantages	Site Favorables	Site Uncertainties
Cyrq and SnoPUD as potential partners, close proximity to transmission lines, road access, existing geothermal leases	Very high shallow gradient, Quaternary stratovolcano	Fault locations, are LiDAR lineaments active structures?, what are the fluid pathways, deep structures
Activity	What we hope to learn from activity and cost	
Geologic Field Survey	New LiDAR recently flown. Check LiDAR lineaments, if faults are found, then trench faults to determine timing of deformation	

Washington Division of Geology and Earth Resources

Phase 1 Technical Report

Geologic Field Survey Total	\$14,000
Temperature-Gradient Drilling	Confirm high gradient from one existing well in this area
Drilling Total	\$100,000
Electrical Resistivity Survey	Check LiDAR lineaments and mapped faults for resistivity anomaly indicative of leaky structures
Resistivity Survey Total	\$2,500
Magnetotelluric Survey	Further confirmation of 3D fault structure, hydrothermal alteration, fluid conduit, in order to recommend slimhole sites.
MT Survey Total	\$28,500
Gravity and Ground-Based Magnetic Survey	Further confirmation of 3D geology and fault structure, in order to recommend slimhole sites.
Gravity and Magnetic Total	\$45,000
MB High-Cost Estimate (not including staff time)	\$190,000
Staffing Costs	
Activity: staff salary, indirect, supplies, travel, software	Cost
WADGER total: Staff time, indirect costs, travel (per diem, driving, hotel), supplies	\$279,560
AltaRock	\$70,000
Temple University	\$20,000
USGS: Indirect (~25%), meetings, workshops, supplies, and software	\$111,758
Staff Cost Total	\$481,318
High-Cost Budget Total	\$994,318

Table 10: High-cost estimate proposal for Phase 2.

Low-Cost Budget Estimate

MSHSZ		
Logistical Site Advantages	Site Favorables	Site Uncertainties
Surface Ownership, road access, geothermal rights, low public visibility, TransAlta and Weyerhaeuser as partners, Centralia coal mine replacement funding	Existence of large, active fault zone, moderate gradient, active stratovolcano	Details of fault geometry that would affect fault permeability and reservoir extent
Activity	What we hope to learn from activity and cost	
Geologic Mapping	Look for surface expression of young faults (alteration, fluid leaks, etc.) to complete 3D model of MSHSZ. Use Weyerhaeuser LiDAR	
Mapping Total	\$14,000	
Passive Seismic Survey	Image details of shear zone including permeability anomalies, magma chamber	
Seismic Survey Total	\$100,000	
Magnetotelluric Survey	Further confirmation of 3D fault structure, hydrothermal alteration, fluid conduit, in order to recommend slimhole sites.	
MT Survey Total	\$28,500	
Electrical Resistivity Survey	Check LiDAR lineaments and mapped faults for resistivity anomalies indicative of leaky structures	
Electrical Resistivity Survey Total	\$2,500	
MSHSZ Low-Cost Estimate (not including staff time)	\$145,500	

WRV		
Logistical Site Advantages	Site Favorables	Site Uncertainties

Washington Division of Geology and Earth Resources

Phase 1 Technical Report

Close proximity to transmission lines, road access, highest data quality and quantity	Very high gradient. Clear geomorphic expression of faulting.	Depth and extent of heat source, extent and geometry of faults.
Activity	What we hope to learn from activity and cost	
Geochronology of Buck Mountain diorite	Is Buck Mountain a heat source?	
Age Analysis Total	\$5,000	
WRV Low-Cost Estimate (not including staff time)	\$5,000	

MB		
Logistical Site Advantages	Site Favorables	Site Uncertainties
Cyrq and SnoPUD as potential partners, close proximity to transmission lines, road access, existing geothermal leases	Very high shallow gradient, Quaternary stratovolcano	Fault locations, are LiDAR lineaments active structures?, what are the fluid pathways, deep structures
Activity	What we hope to learn from activity and cost	
Geologic Field Survey	New LiDAR recently flown. Check LiDAR lineaments, if faults are found, then trench faults to determine timing of deformation	
Geologic Field Survey Total	\$14,000	
Electrical Resistivity Survey	Check LiDAR lineaments and mapped faults for resistivity anomaly indicative of leaky structures	
Resistivity Survey Total	\$2,500	
Magnetotelluric Survey	Further confirmation of 3D fault structure, hydrothermal alteration, fluid conduit, in order to recommend slimhole sites.	
MT Survey Total	\$28,500	
MB Low-Cost Estimate (not including staff time)	\$45,000	

Staffing Costs	
Activity: staff salary, indirect, supplies, travel, software	Cost
WADGER total: Staff time, indirect costs, travel (per diem, driving, hotel), supplies	\$233,188
AltaRock	\$70,000
Temple University	\$20,000
USGS: Indirect (~25%), meetings, workshops, supplies, and software	\$55,879
Staff Cost Total	\$379,067
Low-Cost Budget Total	\$564,067

Table 11: Low-cost estimate proposal for Phase 2.

Anticipated Permitting Requirements and Barriers to Address

We have been in contact with the BLM and USFS for information, applications, and permitting requirements for our proposed activities for Phase 2. The geophysical surveys we are proposing have minimal surface disturbance (digging shallow holes to place equipment) and therefore require only forest service authorization and a temporary special-use permit (FS2700-25). We have started working with the USFS and BLM to obtain these permits for MB. The areas in MSHSZ we are interested in is exempt from permitting because the land and mineral rights are owned and operated by Weyerhaeuser and AltaRock (project partners), and permission to conduct exploration in the AOI has been granted. The WRV AOI is located on private land.

Catalog of Supporting Files Used in the Analysis

Heat and Permeability Input data			
Description of input data	MSHSZ	WRV	MB
Spring and fumarole locations	X	X	X
Spring and fumarole geothermometry	X	X	X
Quaternary Intrusives	X		X
Quaternary volcanic vents	X	X	X
Temperature-gradient wells and water wells with bottomhole temperature	X	X	X
Mapped faults	X	X	X
Seismic catalog with focal mechanisms where available	X	X	X
Strain rate tensors from GPS velocity data	X	X	X
Maximum shear strain rate data from GPS velocity data	X	X	X
Dilational strain rate data from GPS velocity data	X	X	X
Block boundaries	X	X	X

Supplemental data			
Description of input data	MSHSZ	WRV	MB
Study area boundary	X	X	X
Restricted land use	X	X	X
Geothermal lease lands	X		X
Areas of Interest	X	X	X

Scripts, files, and processes used to prepare input data for permeability modeling			
Description of data	MSHSZ	WRV	MB
Scripts to construct fault geometry from mapped faults and seismicity	X	X	
Scripts to construct fault geometry from mapped faults	X	X	X
Seismic catalogs used to construct individual faults	X	X	
Equally spaced points on mapped faults to construct individual faults	X	X	X
Scripts to build observation grids	X	X	X
2D strain rate tensors components	X	X	X
Scripts to convert 2D strain rates to 3D stress tensors	X	X	X

Scripts, files, and processes used to run Poly3D and process permeability layers			
Description of data	MSHSZ	WRV	MB
3D fault geometries as nodes, triangulated nodes and normal vectors	X	X	X
3D magma chamber geometries as nodes, triangulated nodes and normal vectors	X		X

Washington Division of Geology and Earth Resources

Phase 1 Technical Report

3D stress tensors at 200m and 3km	X	X	X
Functions to write Poly3D input files	X	X	X
Scripts to run Poly3D from directory of C++ compiled code	X	X	X
Functions to read Poly3D output files	X	X	X
Scripts to process Poly3D output data into permeability layers at 200m and 3km	X	X	X
Scripts to process Poly3D output data into sensitivity layers at 200m and 3km	X	X	X

Scripts, files, and processes used for permeability data quality/uncertainty mapping			
Description of data	MSHSZ	WRV	MB
Script to map permeability uncertainty	X	X	X
Function to calculate seismic density	X	X	
Function to calculate error envelope	X	X	X
Function to assign fault quality	X	X	X
Seismic catalogs used to construct individual faults	X	X	
Residual 3D fault geometries at 200m and 3km	X	X	X

Fault models and observation grids at 200m and 3km			
Description of data	MSHSZ	WRV	MB
Fault geometry at 200m and 3km	X	X	X
Observation grids at 200m and 3km	X	X	X

Heat potential maps			
Description of data	MSHSZ	WRV	MB
Temperature gradient	X	X	X
Volcanic vent proximity	X	X	X
Intrusive rock proximity	X	X	X
Hot spring and fumarole proximity	X	X	X
Geothermometry proximity	X	X	X
Combined heat potential map	X	X	X

Permeability potential maps			
Description of data	MSHSZ	WRV	MB
Slip tendency at 200m and 3km	X	X	X
Dilation tendency at 200m and 3km	X	X	X
Displacement at 200m and 3km	X	X	X
Displacement gradient at 200m and 3km	X	X	X
Maximum Coulomb shear stress at 200m and 3km	X	X	X
Sigma 3 at 200m and 3km	X	X	X
Maximum shear strain rate at 200m and 3km	X	X	X
Dilational strain rate at 200m and 3km	X	X	X

Washington Division of Geology and Earth Resources

Phase 1 Technical Report

Combined permeability potential map at 200m and 3km	X	X	X
Heat and permeability potential combined maps			
Description of data	MSHSZ	WRV	MB
Combined heat and permeability potential maps at 200m and 3km	X	X	X
Heat uncertainty maps			
Description of data	MSHSZ	WRV	MB
Temperature gradient	X	X	X
Volcanic vent proximity	X	X	X
Intrusive rock proximity	X	X	X
Hot spring and fumarole proximity	X	X	X
Geothermometry proximity	X	X	X
Combined heat uncertainty map	X	X	X
Permeability uncertainty maps			
Description of data	MSHSZ	WRV	MB
Fault geometry uncertainty at 200m and 3km	X	X	X
Permeability model sensitivity maps			
Description of data	MSHSZ	WRV	MB
Fault geometry sensitivity at 200m and 3km	X	X	X
Heat and permeability uncertainty combined maps			
Description of data	MSHSZ	WRV	MB
Combined heat and permeability uncertainty maps at 200m and 3km	X	X	X
Risk maps			
Description of data	MSHSZ	WRV	MB
Combined favorability and uncertainty maps at 200m and 3km	X	X	X

Table 12: Catalog of supporting files that will be submitted to the GDR.

Technology Transfer Activities

Publications resulting from the Phase 1 activities include:

Forson, C., M.W. Swyer, G.M. Schmalzle, J.L. Czajkowski, T.T. Cladouhos, N. Davatzes, D.K. Norman, and R.A. Cole, 2015, “ Geothermal Play-Fairway Analysis of Washington State prospects”, Geothermal Resources Council Transactions, In Press.*

*The presentation that accompanied this paper won ‘Best Presentation Award’ for the Play Fairways 2 Session at the Geothermal Resources Council 2015 conference.

Also a poster at the GRC:

www.dnr.wa.gov/publications/ger_presentations_grc_2015_forson.pdf

Website featuring some of the input data used in this report:

<https://fortress.wa.gov/dnr/geology/?Theme=geothermal>

References Cited

- Anderson E. M., 1951. "The Dynamics of Faulting and Dyke Formation with Applications to Britain" Oliver and Boyd, Edinburgh p. 206.
- Barker, S. E. and S.D. Malone, 1991. "Magmatic system geometry at Mount St. Helens modeled from the stress field associated with post-eruptive earthquakes" *Journal of Geophysical Research*, v. 96, no. B7, p. 11,883-11,894.
- Barton, C.A., Zoback, M.D., Moos, D. 1995. "Fluid flow along potentially active faults in crystalline rock" *Geology*, v. 23, no. 8, p. 683-686.
- Berri, D. A. and M.A. Korosec, 1983. "Geological and geothermal investigation of the lower Wind River valley, southwestern Washington Cascade Range" Washington Division of Geology and Earth Resources Open File Report 83-5, 48 p., 2 plates.
- Blackwell, D. D., 2010. "Updated and combined Regional Heat Flow and Western Geothermal Area databases" Washington State: Southern Methodist University. 1 Excel spreadsheet. accessed Sept. 25, 2010 at <http://smu.edu/geothermal/georesou/washingt.htm>.
- Boschmann, D. E., J. L. Czajkowski, and J.D. Bowman, 2014. "Geothermal favorability model of Washington State" Washington Division of Geology and Earth Resources Open File Report 2014-02, 1 plate, scale 1:900,000, 20 p. http://www.dnr.wa.gov/publications/ger_ofr2014-02_geothermal_favorability.pdf.
- Bowman, J. D. and J. L. Czajkowski, 2013. "Washington State seismogenic features database [GIS data]" Washington Division of Geology and Earth Resources Digital Data Series DS-1. version 3.0. http://www.dnr.wa.gov/publications/ger_portal_seismogenic_features.zip.
- Bourne, S.J., Brauckmann, F., Rijkels, L., Stephenson, B.J., Weber, A., Willemsse, E.J.M. 2000. "Predictive Modeling of Naturally Fractured Reservoirs using Geomechanics and Flow Simulation" 9th Abu Dhabi International Petroleum Exhibition and Conference, October 15 – 18, 2000.
- Bourne, S. J., Willemsse, E. J. M., 2001. "Elastic Stress Control on the Pattern of Tensile Fracturing Around a Small Fault Network at Nash Point UK" *Journal of Structural Geology*, v. 23 p. 1753-1770.
- Burkey, J., 2008. "LOWESS- Locally Weighted Scatterplot Smoothing that does not require the statistical toolbox in matlab" MATLAB release, MATLAB 7.7 (R2008b).
- Caine, J. S., J. P. Evans, and C. B. Forster, 1996. "Fault zone architecture and permeability structure" *Geology*, v. 18, issue 11, p. 1025-1028.
- Childs, C., J. Watterson, and J. J. Walsh, 1995. "Fault Overlap Zones within Developing Normal Fault Systems" *Journal of the Geological Society, London*, v.152, p. 535-549.
- Chou, P. C. and N. J. Pagano, 1967. "Elasticity; Tensor, Dyadic, and Engineering Approaches" D. Van Nostrand Company, Inc. Princeton, NJ.
- Crider, J. G., Frank, D., Malone, S.D., Poland, M.P., Werner, C., Caplan-Auerbach, J., 2011. "Magma at depth: A retrospective analysis of the 1975 unrest at Mount Baker, Washington, USA" *Bulletin of Volcanology*, v. 73, no. 2, p. 175-189.
- Curewitz, D., Karson, J. A., 1997. "Structural Settings of Hydrothermal Outflow: Fracture Permeability Maintained by Fault Propagation and Interaction" *Journal of Volcanology and Geothermal Research*, v. 79 p. 149-168.
- Czajkowski, J. L. and J. D. Bowman. 2014. "Volcanic vents database for Washington State [GIS data]" Washington Division of Geology and Earth Resources Digital Data Series DS-3. version 1.0, http://www.dnr.wa.gov/publications/ger_portal_volcanic_vents.zip.
- Czajkowski, J. L., J. D. Bowman, L. A. Fusso, and D.E. Boschmann, 2014a. "Geologic mapping and geothermal assessment of the Wind River valley, Skamania County, Washington" Washington Division of Geology and Earth Resources Open File Report 2014-01, 30 p., 1 plate, scale 1:24,000.
- Czajkowski, J. L., J. D. Bowman, L. A. Fusso, and D.E. Boschmann, 2014b. "Thermal and mineral springs database for Washington State [GIS data]" Washington Division of Geology and Earth Resources Digital Data Series DS-7, version 1.0, http://www.dnr.wa.gov/publications/ger_portal_thermal_mineral_springs.zip.

Washington Division of Geology and Earth Resources

Phase 1 Technical Report

- Czajkowski, J. L., J. D. Bowman, L. A. Fusso, and D.E. Boschmann, 2014c. "Washington State geothermal well database [GIS data]" Washington Division of Geology and Earth Resources Digital Data Series DS-8, version 2.0, http://www.dnr.wa.gov/publications/ger_portal_geothermal_wells.zip.
- Davatzes, N. C., Eichhubl, P., Aydin, A., 2005. "Structural Evolution of Fault Zones in Sandstone by Multiple Deformation Mechanisms: Moab Fault, Southeast Utah" *Geologic Society of America Bulletin*; January/February 2005; v. 117 p. 135-148.
- Davatzes, N.C., Hickman, S.H. 2009. "Fractures, stress and fluid flow prior to stimulation of well 27-15, Desert Peak, Nevada, EGS Project" *PROCEEDINGS: Thirty-Fourth Workshop on Geothermal Reservoir Engineering*, Stanford University, Stanford, California, February 9-11, 2009.
- Evarts, R. C., R.P. Ashley, J.G. Smith, 1987. "Geology of the Mount St. Helens area—Record of discontinuous volcanic and plutonic activity in the Cascade arc of southern Washington" *Journal of Geophysical Research*, v. 92, no. B10, p. 10,155-10,169.
- Faulds, J.E., Coolbaugh, M., Blewitt, G., and Henry, C.D., 2004. "Why is Nevada in hot water? Structural controls and tectonic model of geothermal systems in the northwestern Great Basin" *Geothermal Resources Council Transactions*, p. 649-654.
- Faulds, J.E., Garside, L.J., 2003. "Preliminary geologic map of the Desert Peak – Brady Geothermal Fields, Churchill County, Nevada" *Nevada Bureau of Mines and Geology Open-File Report 03-27*.
- Faulkner, D. R., T.M. Mitchell, E. Jensen, and J. Cembrano, 2011. "Scaling of fault damage zones with displacement and the implications for fault growth processes" *Journal of Geophysical Research*, v. 116, no. B05403, 11 p.
- Ferrill, D.A., J. Winterle, G. Wittmeyer, D. Sims, S. Colton, and A. Armstrong, 1999. "Stressed rock strains groundwater at Yucca Mountain, Nevada", *GSA Today*, p. 1-7.
- Gass, T.E., 1982. "Geothermal heat pumps" *Geothermal Resources Council Bulletin*, v. 11, no. 11, p. 3-8.
- Goenel, K.D., 2013. "Implementing the Analytic Hierarchy Process as a standard method for multi-criteria decision making in corporate enterprises—A New AHP Excel Template with Multiple Inputs" *Proceedings of the International Symposium on the Analytic Hierarchy Process 2013*.
- Hackl, M., R. Malservisi, and S. Wdowinski, 2009. "Strain rate patterns from dense GPS networks" *Natural Hazards and Earth Systems Sciences*, v. 9, p. 1177-1187.
- Heffer, K., 2002. "Geomechanical Influences in Water Injection Projects: an Overview" *Oil and Gas Science and Technology – Rev. IFP*, v. 57, no., 5, p. 415-422.
- Hickman, S.H., Zoback, M.D., Barton, C.A., Benoit, R., Svitek, J., Summers, R., 2000. "Stress and Permeability Heterogeneity within the Dixie Valley Geothermal Reservoir: Recent Results From Well 82-5" *PROCEEDINGS: Twenty-Fifth Workshop on Geothermal Reservoir Engineering*, Stanford University, Stanford, California, January 24-26, 2000.
- Hickman, S.H., Davatzes, N.C. 2010. "In-situ stress and fracture characterization for planning of an EGS stimulation in the Desert Peak Geothermal Field, Nevada" *PROCEEDINGS: Thirty-Fifth Workshop on geothermal reservoir engineering*, Stanford University, Stanford California, February 1-3, 2010.
- Hodge, B.E., Crider, J.G., 2010. "Investigating mechanisms of edifice deflation, 1981-2007, at Mount Baker volcano, Washington, United States" *Journal of Geophysical Research*, v. 115, B04401, doi:10.1029/2009JB006730.
- Huang, S.; and H.N. Pollack, 1998. "Global borehole temperature database for climate reconstruction" *National Oceanic and Atmospheric Administration/National Climatic Data Center Paleoclimatology Program Data Contribution Series #1998-044*, v. 2001. <http://www.ncdc.noaa.gov/paleo/borehole/intro.html>.
- Jessop, A.M., V.S. Allen, W. Bentkowski, M. Burgess, M. Drury, A.S. Judge, T. Lewis, J. Majorowicz, J.C. Mareschal, and A.E. Tavlör. 2005. "The Canadian geothermal data compilation" *Geological Survey of Canada Open File 4887*. doi:10.4095/220364, http://ftp2.cits.rncan.gc.ca/pub/geott/ess_pubs/220/220364/of_4887.zip.
- Karingithi, C.W., 2009. "Chemical geothermometers for geothermal exploration" *Short course IV on Exploration for Geothermal Resources*, Kenya, Nov., 2009, accessed on 3/6/2015 at: <http://www.os.is/gogn/unu-gtp-sc/UNU-GTP-SC-10-0603.pdf>
- Kattenhorn, S.A., Pollard, D.D., 2001. "Integrating 3-D seismic data, field analogs, and mechanical models in the analysis of segmented normal faults in the Wytch Farm oil field, southern England, United Kingdom" *American Association of Petroleum Geologists Bulletin*, v. 85, no. 7, p. 1183-1210.
- Keith, T.E. C., T.J. Casadevall, and D.A. Johnston, 1981. "Fumarole encrustations—occurrence, mineralogy, and chemistry" *IN* Lipman, P.W. and D.R. Mullineaux, editors, "The 1980 eruptions of Mount St. Helens, Washington" *U.S. Geological Survey Professional Paper 1250*, p. 239-250.

Washington Division of Geology and Earth Resources

Phase 1 Technical Report

- Korosec, M.A., 1983. "Geothermal resource targets—progress and proposals" *IN* Korosec, M.A., W.M. Phillips, J.E. Schuster, and others, "The 1980-1982 geothermal resource assessment program in Washington" National Technical Information Service DOE/ET/27014-T6, p. 268-293.
- Korosec, M.A., 1984. "Summary of geothermal exploration activity in the State of Washington from 1978 to 1983—Final program report to the U.S. Department of Energy" Washington Division of Geology and Earth Resources Open File Report 84-2, 42 p.
- Maerten, L., Pollard, D.D., Marten, F., 2001. "Digital mapping of three-dimensional structures of the Chimney Rock fault system, central Utah" *Journal of Structural Geology*, v. 23, no. 4, p. 585-592.
- Maerten, L., P. Gillespie, and D.D. Pollard, 2002. "Effects of Local Stress Perturbation on Secondary Fault Development" *Journal of Structural Geology*, v. 24, p. 145-153.
- McCaffrey, R., M.D. Long, C. Goldfinger, P.C. Zwick, J.L. Nabelek, C.K. Johnson, and C. Smith, 2000. "Rotation and plate locking at the southern Cascadia subduction zone" *Geophysical Research Letters*, v. 27, no. 19, p. 3117-3120.
- McCaffrey, R., A.I. Qamar, R.W. King, R. Wells, G. Khazaradze, C.A. Williams, C.W. Stevens, J.J. Vollick, and P.C. Zwick, 2007. "Fault locking, block rotation and crustal deformation in the Pacific Northwest" *Geophysical Journal International*, v. 169, no. 3, p. 1315-1340.
- Micklethwaite, S., Cox, S.F., 2004. "Fault-segment rupture, aftershock-zone fluid flow, and mineralization". *Geology*, v. 32, no. 9, p. 813-816.
- Morris, A., Ferrill, D.A., Henderson, D.B., 1996. "Slip-tendency analysis and fault reactivation" *Geology*, v. 24, no. 3, p. 275-278.
- Muffler, L.J.P., 1993. "Tectonic and hydrologic control of the nature and distribution of geothermal resources" *Geo-Heat Center Quarterly Bulletin*, v. 15 no. 2, p. 1-10.
- Noorollahi, Y., Itoi, R., Fujii, H., Tanaka, T., 2007. GIS model for geothermal resource exploration in Akita and Iwate prefectures, northern Japan. *Computers & Geosciences*, v. 33, no. 8, p. 1008-1021.
- Noorollahi, Y., Itoi, R., Fujii, H., Tanaka, T., 2008. GIS integration model for geothermal exploration and well siting. *Geothermics*, v. 37, no. 2, p. 107-131.
- Poux, B., Suemnicht, G., 2012. Use of GIS geoprocessing to select the most favorable sites for geothermal exploration in Oregon. *Geothermal Resources Council Transactions*, v. 37, p. 745-750.
- Powell, T. and W. Cumming, 2012. "Spreadsheets for geothermal water and gas geochemistry; 3rd ed." *Proceedings, Thirty-fifth Workshop on Geothermal Reservoir Engineering*. SGP-TR-188. 10 p..
<http://repositor.v.stategeothermaldata.org/metadata/record/9e15e1a59b768b330d029e86dc023a37/file/geochemistryspreadsheets-powell-cumming-standford-2010.pdf>.
- Saaty, T.L., 2008. "Decision making with the analytical hierarchy process" *International Journal of Service Sciences*, v. 1, no. 1, p. 83-98.
- Sherrod, D.R., W.E. Scott, and P.H. Stauffer, editors, 2008. "A Volcano rekindled—the renewed eruption of Mount St. Helens, 2004–2006" U.S. Geological Survey Professional Paper 1750, 856 p. and DVD-ROM, <http://pubs.usgs.gov/pp/1750/>.
- Shevenell, L., and F. Goff, 1995. "Evolution of hydrothermal waters at Mount St. Helens, Washington, USA" *Journal of Volcanology and Geothermal Research*, v. 69, p. 73-94.
- Smith, R.L. and H.R. Shaw, 1973. "Volcanic rocks as geologic guides to geothermal exploration and evaluation [abstract]" *Eos (American Geophysical Union Transactions)*, v. 54, no. 11, p. 1213.
- Swyer, M.S., Davatzes, N.C., 2013. Evaluating the role of the rhyolite ridge fault system in the Desert Peak geothermal field with robust sensitivity testing through boundary element modeling and likelihood analysis. *PROCEEDINGS, Thirty-Eighth Workshop on Geothermal Reservoir Engineering*, Stanford University, Stanford, California, February 11-13, 2013.
- Tamagawa, T., Pollard, D.D., 2008. "Fracture permeability created by perturbed stress fields around active faults in a fractured basement reservoir" *American Association of Petroleum Geologists*, v. 92, no. 6, p. 743-764.
- Thomas, A.L., 1993. "*Poly3D*—a three-dimensional, polygonal-element, displacement discontinuity boundary element computer program with applications to fractures, faults, and cavities in the Earth's crust" M.S. thesis, Stanford University, California.

Washington Division of Geology and Earth Resources

Phase 1 Technical Report

- USFS, 2014. Decision Notice and Finding of No Significant Impact, Mt. Baker Geothermal Consent to Lease, USDA Forest Service, Mt. Baker-Snoqualmie National Forest, Whatcom and Skagit Counties, WA. Retrieved 10/15/2015 from http://a123.g.akamai.net/7/123/11558/abc123/forestservic_download.akamai.com/11558/www/nepa/100231_FSPLT3_2571128.pdf
- USGS, 2008. Assessment of Moderate- and High-Temperature Geothermal Resources of the United States, Fact Sheet 2008-3082. Retrieved 10/15/2015 from <http://pubs.usgs.gov/fs/2008/3082/>
- Washington Division of Geology and Earth Resources. 2010a. "Surface geology. 1:100,000-scale GIS data, June 2010" Washington Division of Geology and Earth Resources. 60.1 M B. http://www.dnr.wa.gov/ResearchScience/Topics/GeosciencesData/Pages/gis_data.aspx.
- Washington Division of Geology and Earth Resources. 2010b. "Surface geology. 1:500,000-scale GIS data, June 2010" Washington Division of Geology and Earth Resources. 12.2MB. http://www.dnr.wa.gov/ResearchScience/Topics/GeosciencesData/Pages/gis_data.aspx.
- Weaver, C.S. and S.W. Smith, 1983. "Regional tectonic and earthquake hazard implications of a crustal fault zone in southwestern Washington" *Journal of Geophysical Research*, v. 88, no. B12, p. 10,371-10,383.
- Weaver, C.S., W.C. Grant, and J.E. Shemeta, 1987. "Local crustal extension of Mount St. Helens, Washington" *Journal of Geophysical Research*, v. 92, no. B10, p. 10,170-10,178.
- Wells, R. E., C.S. Weaver, and R.J. Blakely, 1998. "Fore-arc migration in Cascadia and its neotectonic significance" *Geology*, v. 26, no. 8, p. 759-762.
- Wessel, P., and D. Bercovici, 1998. "Interpolation with splines in tension: a Green's function approach" *Mathematical Geology*, vol. 30, no. 1, p. 77-93.
- Willemse, E.J., D.D. Pollard, and A. Aydin, 1996. "Three-Dimensional analysis of Slip Distributions on Normal Fault Arrays with Consequences for Fault Scaling" *Journal of Structural Geology*, v. 18 no.2/3, p. 295-309.
- Zoback, M.D., 2007. "Reservoir Geomechanics". Cambridge University Press, Cambridge U.K., p. 130-139.

Appendix A

Data Processing and Intermediate Rasters for the Heat Potential Models

The multi-criteria heat potential model for each of the three plays is composed of the weighted sum of five intermediate rasters: (1) temperature gradient, (2) Quaternary volcanic vents, (3) Quaternary intrusive rocks, (4) hot spring and fumaroles, and (5) spring and fumarole geothermometry (Figs. 2–4).

Volcanic Vent Proximity: Buffering for volcanic vents by vent type is as follows: stratovolcanoes = 5 mi, calderas = 3 mi, and minor vents = 1.5 miles (see Fig. A1 below). Individual buffer polygons for stratovolcanoes, calderas, and minor vents were separately converted to weighted rasters with the raster value equal to the product of age weight and rock type weight (Table A1). Separately, Euclidean distance analyses were performed on individual minor vents, stratovolcanoes, and calderas, and the resultant distance rasters were reclassified using fuzzy linear transformations with ROIs equal to the respective buffer distances, a cell size of 500 feet, and no hedge. The minor vents, stratovolcano and caldera weighted rasters were multiplied by their respective reclassified distance rasters. Finally, the caldera, stratovolcano, and minor vent group rasters were combined using the fuzzy ‘OR’ overlay tool (See Figures A1–A3 for the volcanic vent proximity rasters for each of the three play areas).

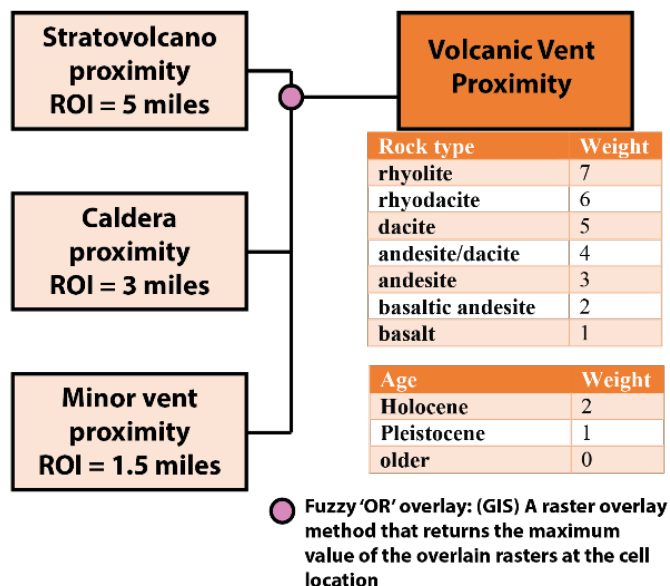


Figure A1: Volcanic vent proximity workflow showing the weights assigned to different rock types and the ROI used for the different vent types.

Intrusive Rock Proximity: The intrusive rock proximity raster used late Pliocene to Holocene intrusive rhyodacitic to andesitic polygons from the source data. Euclidean distance analysis was performed on these polygons, and the resultant proximity raster was normalized to a 0 to 1 scale using a fuzzy linear transformation function with an ROI of 3 mi, a cell size of 500 ft, and no

hedge (See Figures A1–A3 for the intrusive rock proximity rasters for each of the three play areas).

Spring Proximity: *Notes on Data Processing and caveats:* All springs (cold and warm) were used in this analysis, because while thermal springs tell us where we have geothermal upwelling, the cold springs are data points that provide evidence as to where there is no thermal upwelling. Data selection for the MSHSZ was based on the following criteria:

- The hot springs on the pumice plain to the north of MSH are warm springs that are heated by the cooling pyroclastic flow and are not tapped in to the source (as evidenced by geochemistry and rapidly cooling spring temperatures, as measured over decades). Since these springs are not tapping into the heat source and are a result of groundwater interacting with cooling volcanics these springs (the “Pumice Plain springs”) were excluded from the heat potential model for MSH.
- The fumarole on MSH was excluded from the heat potential model. The reason for this removal is that with a maximum recorded temperature of 800 °C (as well as many other recorded temperatures in the same range) this temperature skews the data and makes normalizing the temperature proximity raster less meaningful. Additionally the fumarole temperatures were taken in 1980 and 1981 and have not been taken since. These temperatures are recording active volcanic outgassing and are not necessarily indicative of the current state of the geothermal system.
- The most recent temperature recordings were used for all of the springs in the MSH area instead of using the maximum temperature for this play, which would skew the data because so many temperatures were taken in 1980 and 1981 immediately following the eruption, and these values are typically much higher than the current temperature.

Data processing for springs: Individual springs were buffered to a distance of 0.5 mi. Non-overlapping groups of buffered polygons were then individually converted to weighted rasters with the raster value equal to the most recent spring temperature. Separately, Euclidean distance analyses were performed on each spring, and the resultant distance rasters were reclassified using fuzzy linear transformations with an ROI of 0.5 mi, a 100-ft cell size and no hedge. The individual weighted rasters were then multiplied by the reclassified distance rasters. The individual multiplied distance and temperature rasters were then combined using the mosaic to new raster tool in ArcGIS with a 100-ft cell size, 32-bit float, 1 band, and maximum mosaic operator. The combined spring raster was then normalized using the raster calculator tool in ArcGIS (See Figs. A1–A3 for the spring proximity rasters for each of the three play areas).

Geothermometry proximity: *Notes on Data Processing and caveats:* Geothermometer temperatures were found by inputting measured spring chemistry data into Powell and

Cumming's (2010) geothermometer spreadsheet. Na-K-Ca Mg-corrected geothermometer temperatures were used for all springs in MSH with the exception of acidic springs (SO₄) where Quartz geothermometer temperatures were used as suggested in the book *Chemistry and Geothermal Systems* (Ellis and Mahon, 1977). If the charge balance is over 5% or under -5% then the geothermometry is flagged as invalid and no geothermometer was used, the value is null and that spring was not used in the geothermometry model. It should be noted that the Mount St. Helens geothermometry is weighted much less here than in other areas because the water chemistry in the region suggested that the spring waters were immature and therefore not in equilibrium with the host rocks (Shevenell and Goff, 1995).

Data processing for spring geothermometry: Individual springs were buffered to a distance of 0.5 mi. Non-overlapping groups of buffered polygons were then individually converted to weighted rasters with the raster value equal to the geothermometer derived temperature. Separately, Euclidean distance analyses were performed on each spring, and the resultant distance rasters were reclassified using fuzzy linear transformations with an ROI of 0.5 mi, a 100 foot cell size and no hedge. The individual weighted rasters were then multiplied by the reclassified distance rasters. The individual multiplied distance and temperature rasters were then combined using the mosaic to new raster tool in ArcGIS with a 100-ft cell size, 32-bit float, 1 band, and maximum mosaic operator. The combined spring geothermometry raster was then normalized using the raster calculator tool in ArcGIS (See Figs. A1, A2, and A3 for the spring geothermometry proximity rasters for each of the three play areas).

Temperature gradient: Temperature gradient values from temperature gradient wells (gradient type A) and water wells with a bottom-hole temperature measurement (gradient type B) from across the state were used in the temperature gradient analysis. Weights were assigned to the various wells in order to give higher rank to deep temperature-gradient wells with more temperature measurements, which are more representative of the temperature at depth, and lower weight to water wells with only a bottom-hole temperature.

Then sum the weights for each individual temperature-gradient well from the table above (values will range from 2–8), and then normalize the weight by multiplying by 0.1 and add 1 so that a weight of 8 becomes 1.8, etc. Water wells with a bottomhole temperature are assigned a weight of 1 (as shown in the far left column in Table A1 below).

TG Well Depth (m)	Weight	No. of temp. measurements	Weight	Gradient Type (A/B)	Weight
0–60	1	1–15	1	A	2
60–250	2	16–30	2	B	1
> 250	3	> 30	3		

Table A1: Weighting schema for temperature-gradient and water wells for use in favorability modeling.

Interpolation between wells: In order to get a regional picture of the temperature gradient at each of the three play-fairway areas interpolation between gradient well locations was conducted in ArcGIS. Two different methods of interpolation were employed for this study. Kriging interpolation was used where the data points were more evenly distributed (MSHSZ) and inverse Distance weighting (IDW) interpolation was used where data points were clustered (WRV) or sparse (MB). Originally Kriging interpolation was done for all three sites, but we realized that a kriging interpolation didn't accurately model the measured gradients at WRV or MB like it did at MSH. For this reason we tried various interpolation methods and the IDW technique most accurately modeled the temperature-gradient based on the existing data points at WRV and MB.

MSHSZ: A Kriging interpolation was used with a simple type Kriging, a prediction output type and a normal score transformation. A direct approximation method with 27 bins was used. Interpolation was performed at a 500-ft grid resolution. The resulting temperature-gradient raster was clipped to the study area and normalized to a 0 to 1 scale using the raster calculator (Fig. A1).

WRV and MB: Inverse Distance Weighting (IDW) tool was used for interpolation between wells. A smooth search neighborhood with an optimized power and one sector with 0° angle was used in modeling. The resulting temperature-gradient raster was clipped to the study area(s) and normalized to a 0 to 1 scale using the raster calculator (Figs. A2–A4).

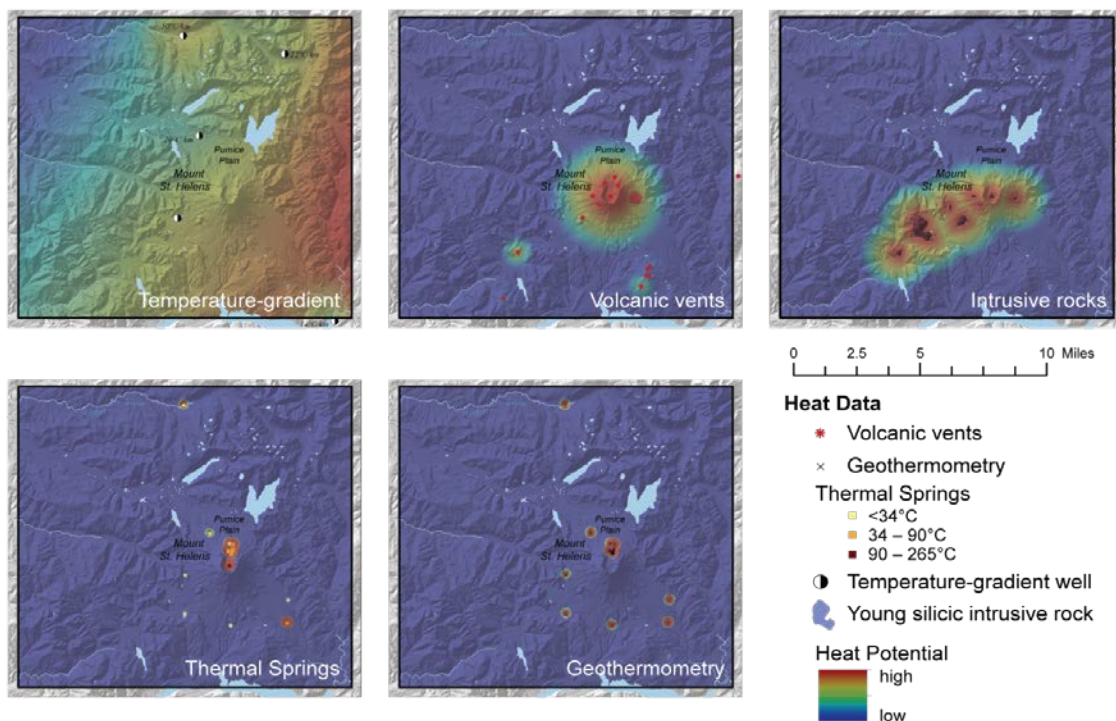


Figure A2: Individual heat potential favorability input rasters for MSHSZ. These input rasters were combined and weighted with weights from the AHP (Appendix C) to generate the heat potential model for MSHSZ seen in Figure 7A in the text of this report.

Washington Division of Geology and Earth Resources
Phase 1 Technical Report

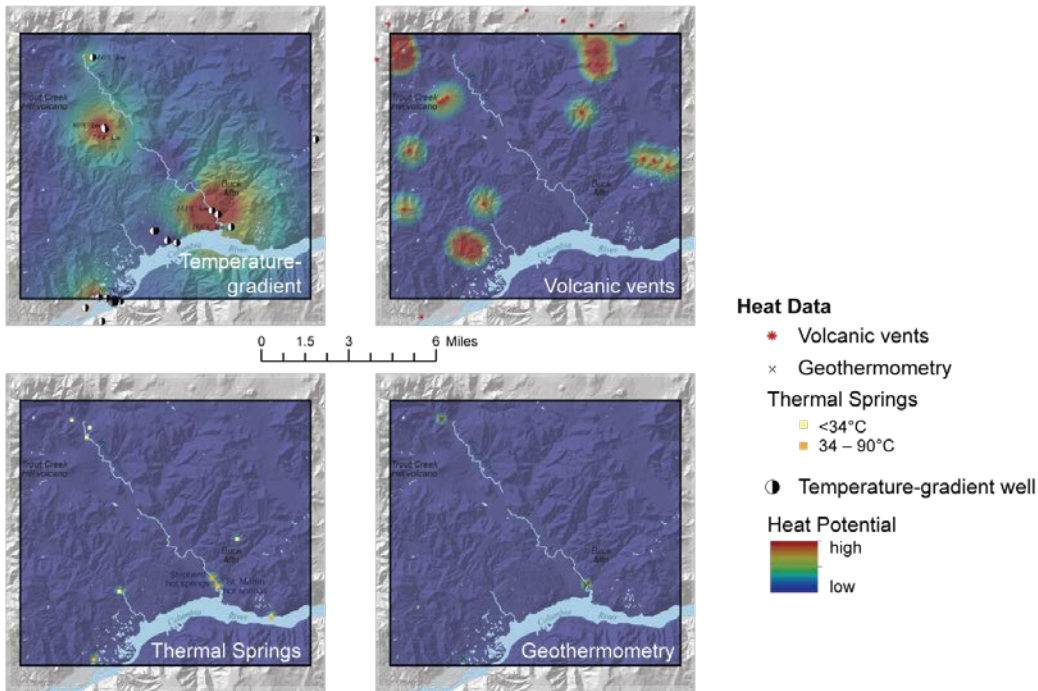


Figure A3: Individual heat potential favorability input rasters for WRV. These input rasters were combined and weighted with weights from the AHP (Appendix C) to generate the heat potential model for WRV seen in Fig. 7B in the text of this report.

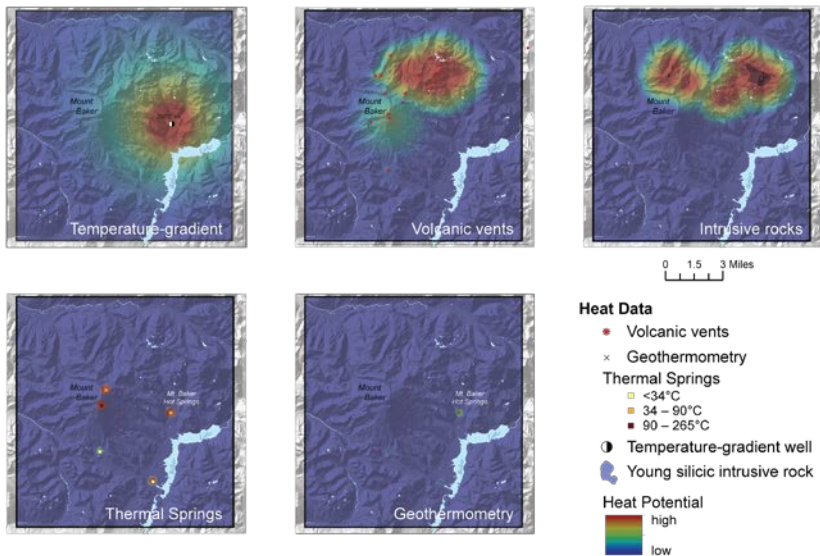


Figure A4: Individual heat potential favorability input rasters for MB. These input rasters were combined and weighted with weights from the AHP (Appendix C) to generate the heat potential model for MB seen in Fig. 7C in the text of this report.

Appendix B

Data Processing and Intermediate Rasters for the Permeability Potential Models

Detailed Permeability Potential Modeling Methodology

The innovative modeling technique use in this study relies on the assumption that geothermal resources are strongly dependent on faults. A global survey of 822 faults at 25 different sites by Curwitz and Karson, 1997, indicated that the majority of hot springs and hydrothermal upflow are dependent faults, fault tiplines, and the mechanical interaction between multiple faults that dynamically maintain permeable fracture networks necessary for geothermal upwelling, with only 22% of hot springs being unrelated to faults (Fig. B1).

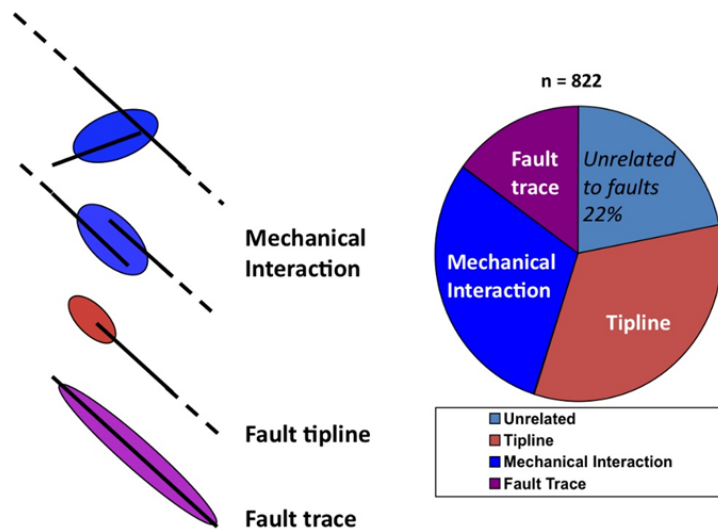


Figure B1: Conceptualized depiction of various types of fault geometry that localize hot springs and hydrothermal deposits. The percentage data of hot springs and their association to faults was taken from a global survey of 822 faults located at 25 different sites, which found that only 22% of hot springs are unrelated to faulting. The stress concentrations that occur at faults have a complex relationship with fault geometry, which can potentially cause a decrease rather than an increase in fracture potential (Curewitz & Karson, 1997).

Modeling fault slip in an elastic half-space can indicate where stress/strain favorable to fracture formation is localized in proximity to faults that can be useful to geothermal exploration. By idealizing faults as discontinuities within a homogeneous and isotropic medium it is possible to calculate using linear elastic theory and the Coulomb-Griffith failure criterion where tensile and shear fractures should form in the adjacent volume due to stresses induced by slip on a fault driven by a remote stress tensor (Bourne & Willemsse, 2001; Maerten and others, 2002; Davatzes and others, 2005).

This method was applied to the fault system at the Desert Peak geothermal field, and showed favorable stresses at the location of the most successful injection and production wells at that facility (Fig. B2)(Swyer and Davatzes, 2013).

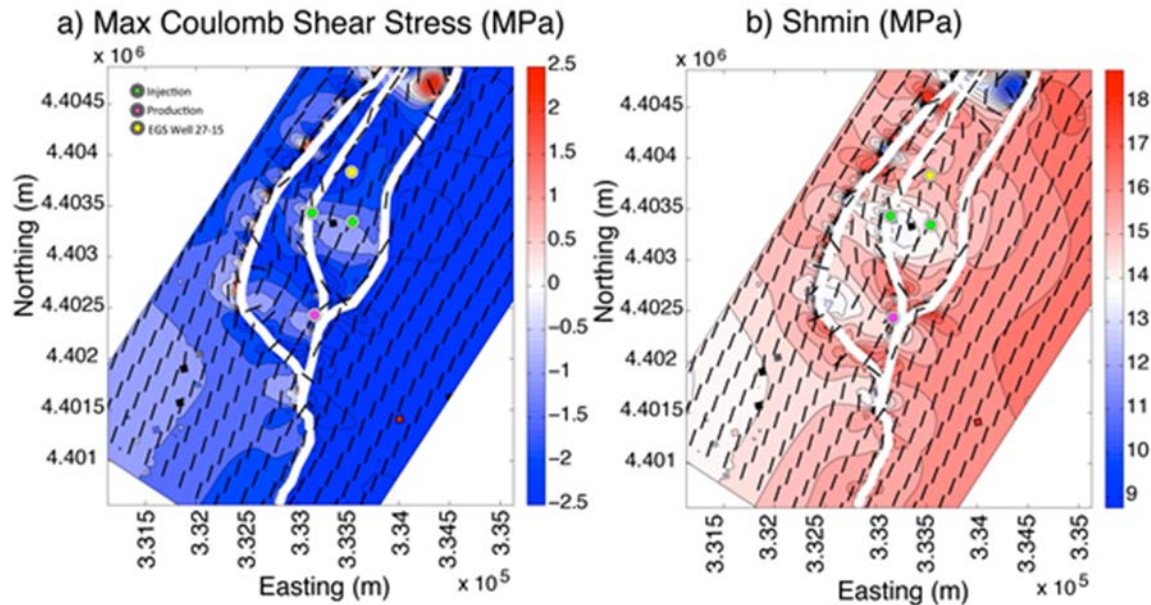


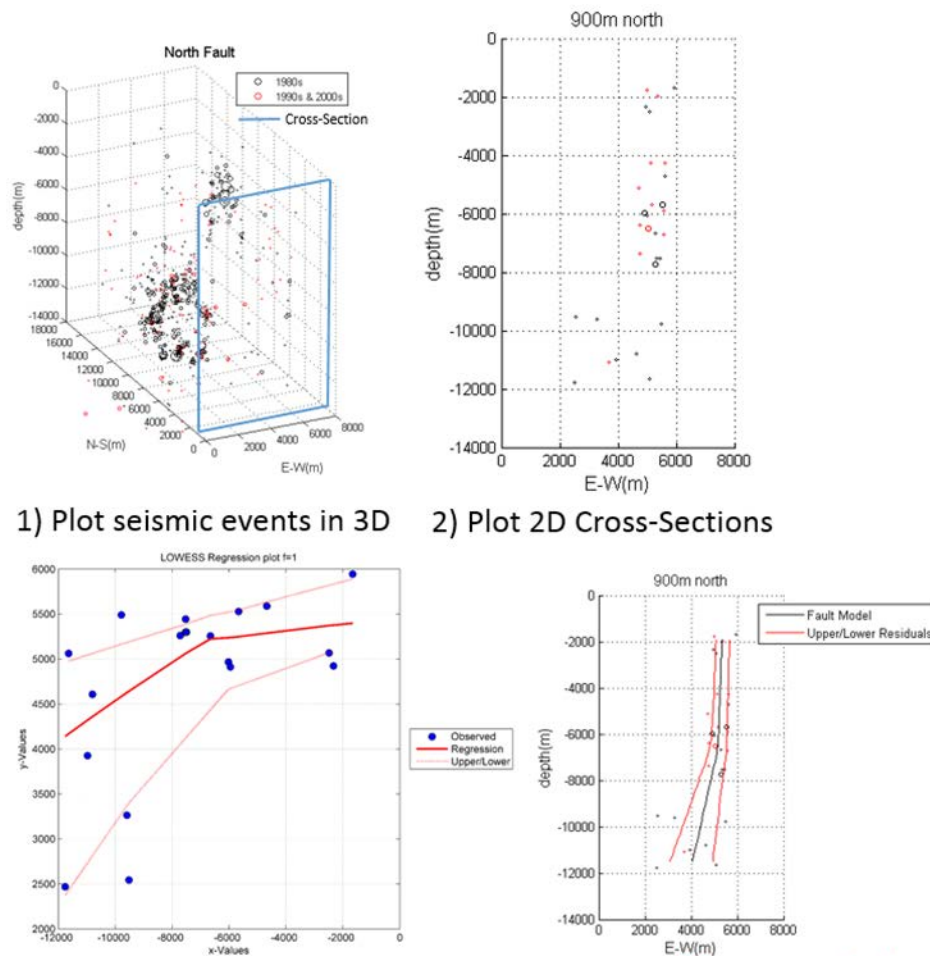
Figure B2: a) modeled maximum Coulomb shear stress in the Desert Peak geothermal field as a proxy for shear failure potential, b) modeled S_{hmin} as a proxy for tensile failure potential (Swyer and Davatzes, 2013).

The multi-criteria permeability potential model for each of the three plays is composed of the weighted sum of eight intermediate rasters: (1) slip and (2) dilation tendency on mapped and seismically inferred faults (3) maximum shear strain rate, and (4) dilational strain rate at the surface, (5) fault displacement distribution, and (6) displacement gradient, (7) maximum Coulomb shear stress, and (8) tensile fracture density (Σ_3). Parameters 1–6 are modeled from faults mapped at the surface, seismicity, and GPS derived strain rate data; parameters 7&8 are derived from GPS velocity data. The underlying assumptions in the permeability potential modeling are that geothermal fluids travel along faults and in the damage zone surrounding the fault, that high fracture density promotes a percolating fracture network with porosity to store fluids and a heat exchange area, and active deformation provides the potential to restore permeability and porosity lost to mineral alteration and precipitation.

Fault data were compiled from the DGER 1:100,000-scale digital surface geology, 1:24,000-scale digital surface geology, and active faults data within the digital seismogenic features database (WADGER, 2010a,b; Bowman and Czajkowski, 2014). Earthquake hypocenter locations were taken from the DGER seismogenic features database (Bowman and Czajkowski, 2014), originally obtained from the Pacific Northwest Seismic Network (PNSN), along with available earthquake focal mechanisms.

Model Configuration: Modeling of the permeability potential requires (1) the geometry of the faults (and for MSHSZ and MB, the geometry of the magma chamber), (2) specified tractions, or burgers vector (displacement discontinuity) on their respective surfaces, and (3) remote stress or strain/strain rate boundary conditions. In this study, the faults are modeled as surfaces of zero residual shear traction and zero normal displacement. The magma chamber models have normal tractions derived in previous modeling studies and have zero shear traction if the geometry is known, and zero displacement boundary if the geometry is not known. In addition, the Earth's surface is treated as traction free, and in these initial models is constrained to be flat. The 3D remote strain rate is constrained by GPS station velocities; here our focus is to use the strain rate to infer the anisotropy of the elastic strain tensor.

3D Fault geometry: Seismic catalogs for the region from the Pacific Northwest Seismic Network (PNSN) were used to constrain fault geometry at depth in the absence of clear surface indicators from field mapping and available LiDAR data. In some cases, the seismic catalog is robust enough to show clear planar alignment that can be used to construct a very well constrained fault geometry. Areas with a robust seismic catalog were used to develop the methodology that employs the regression function LOWESS (Locally Weighted Scatterplot Smoothing, Burkey, 2008) for defining fault planes that is very useful in areas with less data, such as the WRV to the southeast of MSH. The regression function also defines the residuals of the fault geometry fit to seismicity which were used to quantify uncertainty (Fig. B3).



1) Plot seismic events in 3D 2) Plot 2D Cross-Sections

3) LOWESS regression to cross-sections w/ upper/lower residuals

Figure B3: Workflow for constructing fault geometry using LOWESS. Upper and lower residuals from regression are also used to model fault geometry uncertainty.

At WRV, larger faults with micro-seismicity and focal mechanisms were used along with mapped fault traces to constrain fault geometry at both the surface and at depth. At MB, the seismicity was not used to constrain fault geometry at depth. This is because the available seismic catalog only contains events created by glacier fracturing at or near the surface and Deep Long Period (DLP) events associated with deep magma movement (Nichols and others, 2011). Only the 100k mapped faults were used to model faults at MB. The dip of the normal/strike-slip faults was assumed to be 80° .

Remote stress tensor: The remote stress tensor used in the model was derived from the publically available Global Positioning System (GPS) time series from the National Science Foundation (NSF) Earthscope's Plate Boundary Observatory (PBO) and Central Washington University's Pacific Northwest Geodetic Array (PANGA) at every 0.04° longitude and 0.10° latitude. The GPS station velocities were used to infer strain rates using the 'splines in tension' method (Wessel and Bercovici, 1998) using a spline tension of 0.3 for all modeling.

The strain rate tensors modeled from GPS velocities were used to calculate the dilatational strain rate and the maximum shear strain rate (Appendix C) which are useful for modeling permeability potential on a regional scale, and were both used as layers in the permeability potential model of the three areas (Fig. B4).

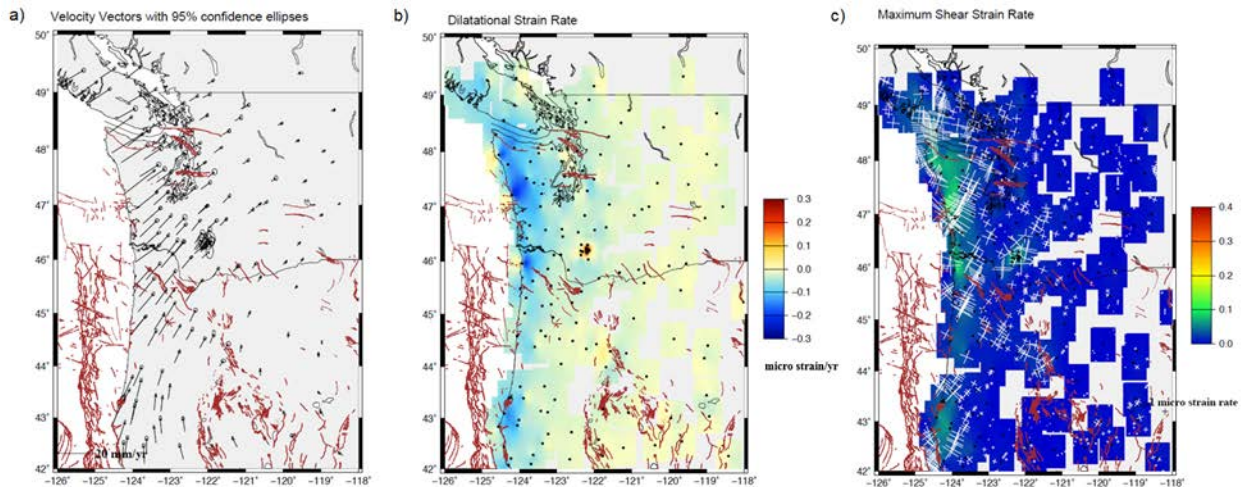


Figure B4: a) GPS station velocity vectors with 95% confidence ellipses, b) dilatational strain rate and c) maximum shear strain rate with $\theta_{1,2}$ or the two potential directions of the maximum shear strain as white crosses that represent two potential directions of active faults (Appendix C). Quaternary faults shown in red.

A major lesson learned from this study is that modeled strain rate tensors are very useful for deriving remote stress for the Poly3D modeling at each site, but should be used with great caution. Initial model runs that used strain rate tensors derived from the raw GPS velocities (Fig. B4) caused faults in the model to have opposite senses of slip than what is observed in the field and evidenced from seismic focal mechanisms, particularly within the MSHSZ (Weaver and others, 1987) and the WRV, which are both known to have right-lateral strike-slip motion on northwest-striking faults. Therefore, the strain rates were derived separately for subduction zone locking at depth and block rotation near the surface (Appendix C) within crustal block boundaries modeled from GPS velocities, as well known or suspected mapped faults, seismicity, and paleomagnetic rotations (McCaffrey and others, 2007)(Fig. B5).

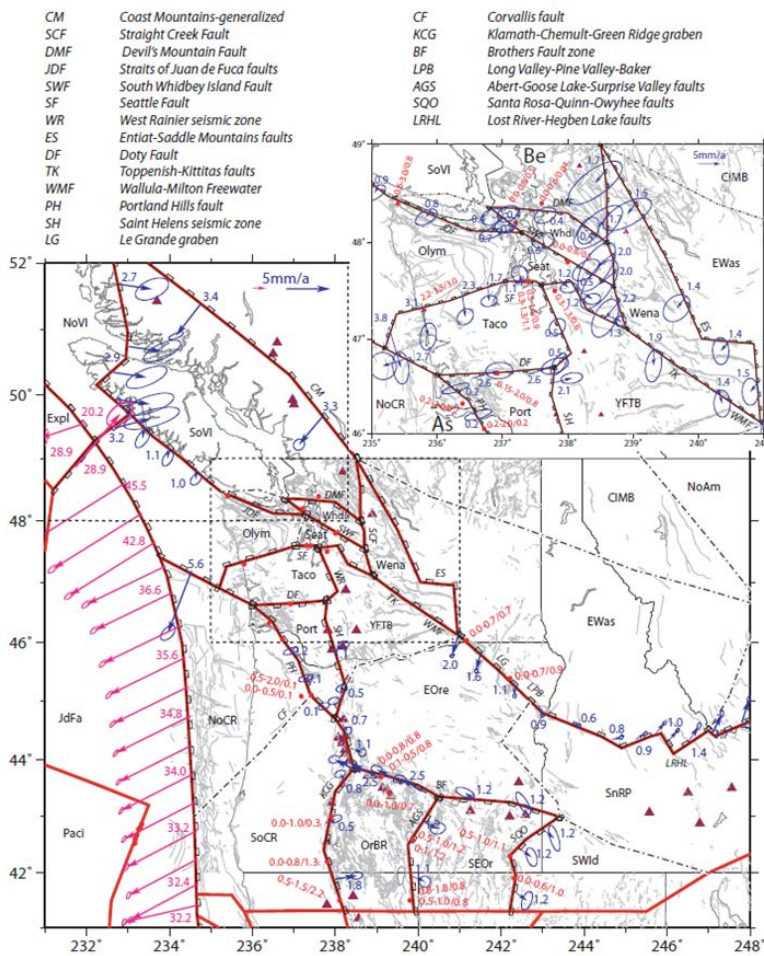


Figure B5: Crustal block boundaries modeled by McCaffrey and others (2007). Block-bounding faults are shown as red lines with small rectangles on hanging wall side. Blue vectors show motion of hanging wall relative to footwall with 70% confidence ellipses. Red dots along faults show positions of geologic fault slip estimates. Fault name abbreviations listed at the top.

The strain rate tensors derived for crustal block rotation were used as the remote stress boundary condition (Fig. B6).

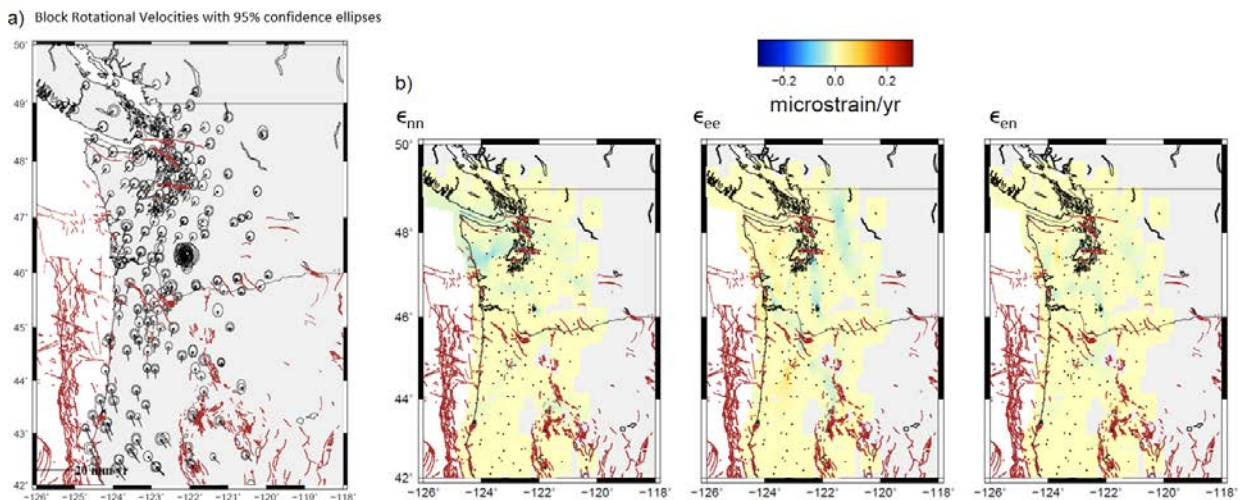


Figure B6: a) Block rotational velocities with 95% confidence ellipses and b) modeled strain tensor components used for the remote boundary conditions at the three areas.

In addition, higher magnitudes of strain near the crustal block boundaries and volcanic centers were removed from the strain field used to calculate the homogeneous remote strain tensor at each site. This is because the Poly3D modeling is meant to simulate stress/strain near these structures, so using strain from the same areas as a boundary condition causes circular logic within the model. Taking these steps to correct the strain rate data at each site produced adequate boundary conditions for the Poly3D models (Fig. B7).

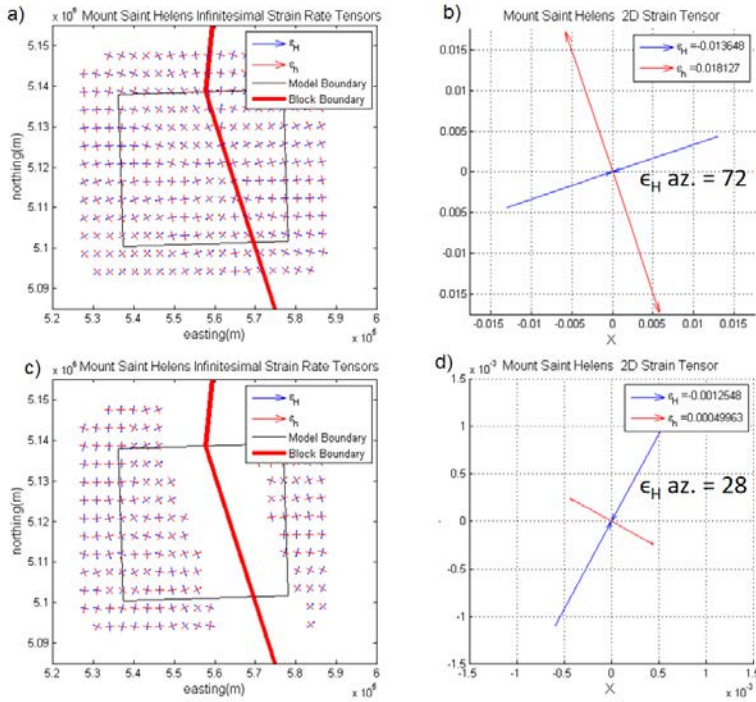


Figure B7: a) Strain rate tensors not removed near the crustal block boundary representing the shear zone and volcanic center and b) resulting average strain tensor. c) Strain rate tensors removed from block boundary and d) resulting average strain tensor.

The components of the Infinitesimal strain rate tensors within and outside the model area were averaged, and the two eigenvalues were used as the two principal horizontal strains (ϵ_H and ϵ_h). The 3D strain tensor is assumed to be Andersonian (one of the principal strains oriented vertically, Anderson, 1951), with the vertical strain (ϵ_V) calculated using Hooke’s Law (Chou and Pagano, 1967):

$$\epsilon_V = -\nu(\epsilon_H + \epsilon_h) \quad \text{Eq. 1}$$

Where ν is a Poisson’s ratio of 0.25. Using the two eigenvalues of the strain rate tensor and the vertical strain found using Eq. 1, the three relative magnitudes of strain are known, and therefore can be used to estimate the relative magnitudes of the three principal stresses. All the strain rates in units of microstrain/year were multiplied by a Young’s Modulus E of 30 GPa to get stress. The vertical stress was made equivalent to the litho-static stress at 3 km, and the minimum and maximum horizontal stresses (S_{hmin} and S_{Hmax}) were adjusted by the same amount as the vertical stress. The stress magnitudes at 3 km were then divided by 15 to get stress magnitudes at 200 m.

Fig. B8 shows the location of the modeled strain rate tensors used to derive the remote stress at Mount St. Helens. The relative magnitudes of strain are shown in Figs. B8b and c for the 2D and 3D strain tensors respectively. The stress profile used at Mount St. Helens is shown in

Fig. B9d). The stress gradient of S_{Hmax} is 41.2 MPa/km, the stress gradient of S_{hmin} is 23.7 MPa/km, and the vertical stress gradient is 26.8 MPa/km.

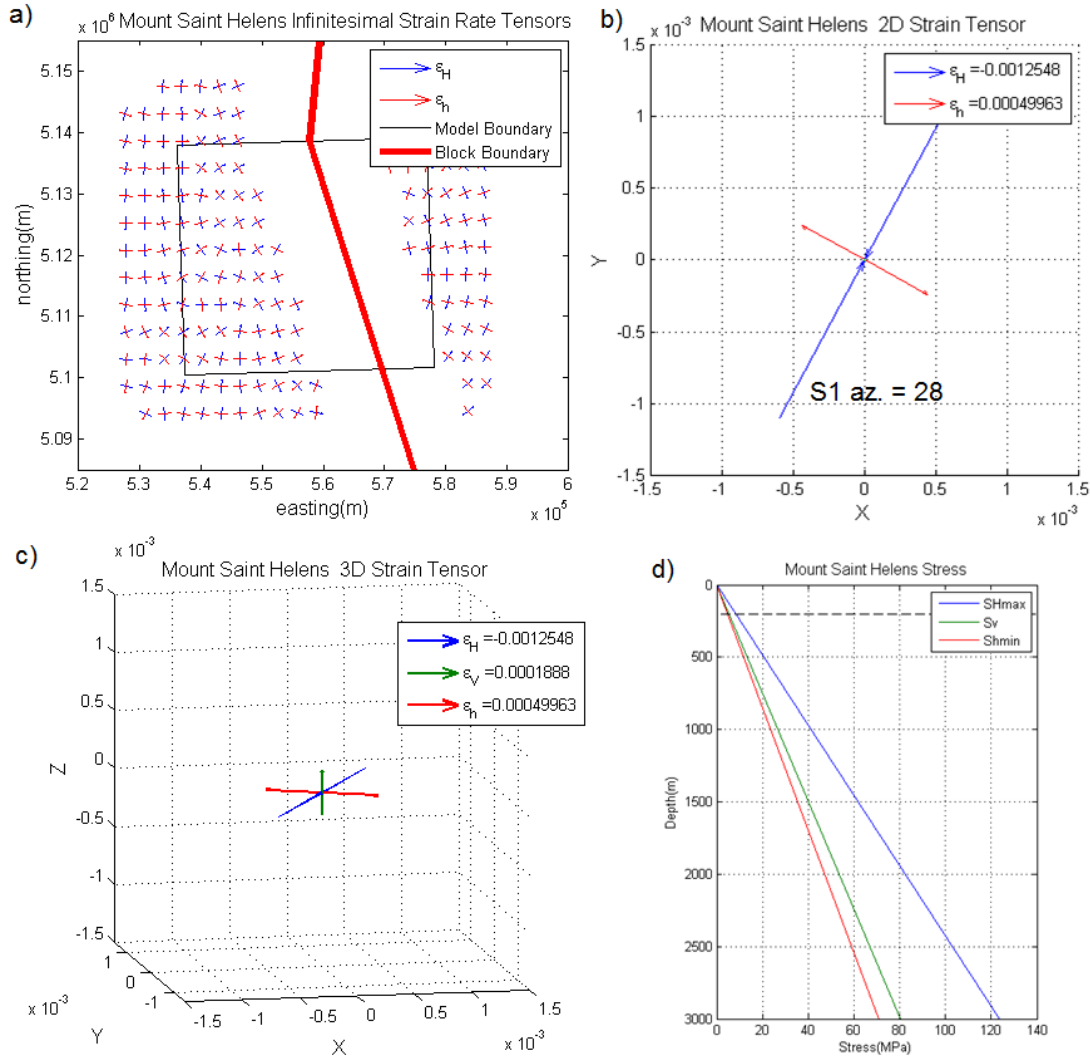


Figure B8: a) modeled strain rates used for Mount St. Helens remote stress with crustal block boundary shown as thick red line, b) average 2D strain tensor from modeled strain rate with a maximum principal strain azimuth of 28, c) 3D strain tensor with vertical strain found using Eq. 2, and d) stress profile for the three principal stresses used at Mount St Helens with dashed line at 200 m depth.

Figure B9 shows the location of the modeled strain rate tensors used to derive the remote stress for Wind River. The relative magnitudes of strain are shown in Figs. B9b and c for the 2D and 3D strain tensors respectively. The stress profile used at Wind River is shown in Fig. B9d. The stress gradient of S_{Hmax} is 50.5 MPa/km, the stress gradient of S_{hmin} is 10.1 MPa/km, and the vertical stress gradient is 26.8 MPa/km.

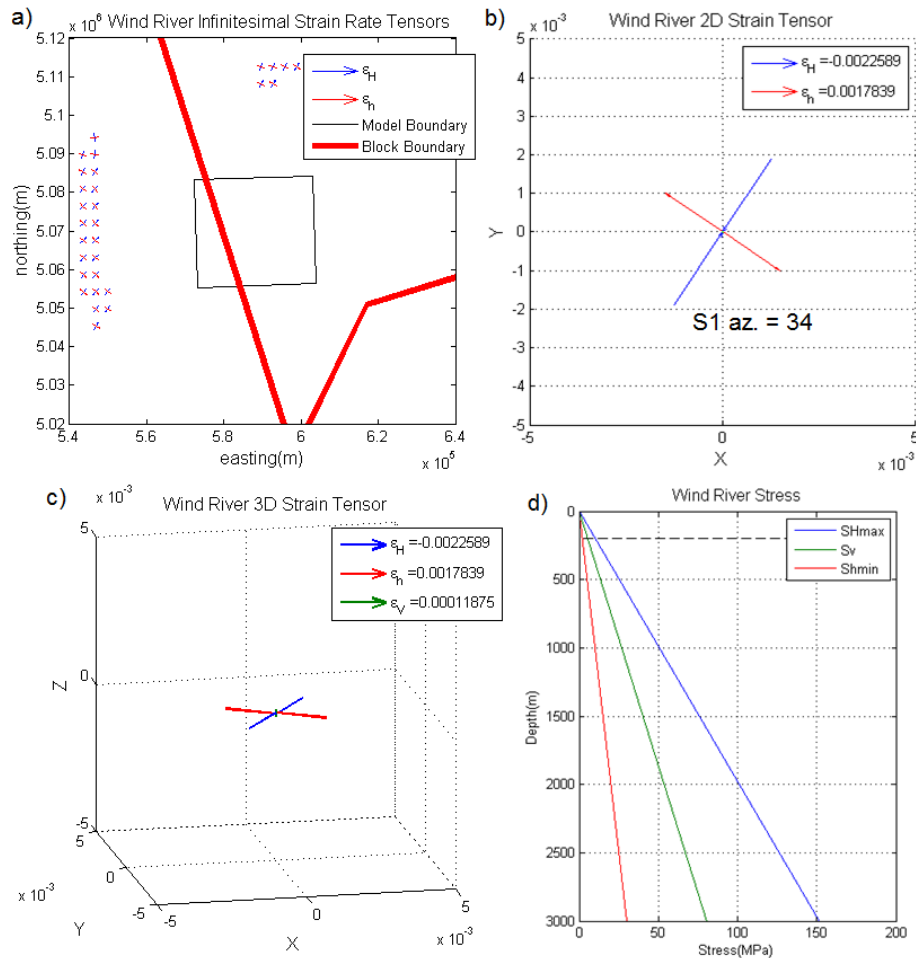


Figure B9: a) modeled strain rates used for Wind River remote stress with crustal block boundaries shown as thick red line, b) average 2D strain tensor from modeled strain rate with a maximum principal strain azimuth of 34, c) 3D strain tensor with vertical strain found using Eq. 2, and d) stress profile for the three principal stresses used at Mount St. Helens.

Figure B10 shows the location of the modeled strain rate tensors used to derive the remote stress for Wind River. The relative magnitudes of strain are shown in Figs. B10b and c for the 2D and 3D strain tensors respectively. The stress profile used at Wind River is shown in Figs. B10 d. The stress gradient of S_{Hmax} is 55.0 MPa/km, the stress gradient of S_{Hmin} is 26.6 MPa/km, and the vertical stress gradient is 26.8 MPa/km.

Fault element boundary conditions: For the fault elements, the shear traction was set to zero which simulates slip on a frictionless fault, and the normal displacement was set to zero, which prevents the fault from opening or the fault walls from interpenetrating. These boundary conditions provide an end-member case for the stress change induced by fault slip which provides a clearer map of stress perturbation than if the faults were modeled with a friction solver.

Washington Division of Geology and Earth Resources
Phase 1 Technical Report

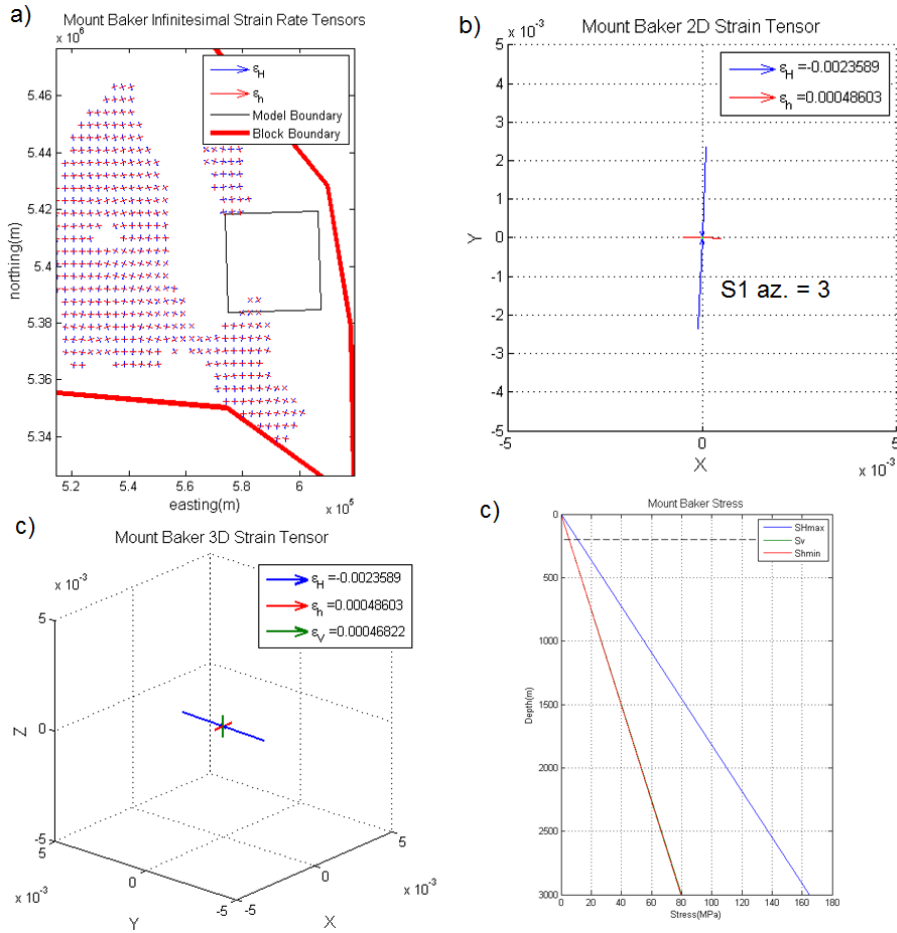


Figure B10: a) modeled strain rates used for Mount Baker remote stress with crustal block boundaries shown as thick red line, b) average 2D strain tensor from modeled strain rate with a maximum principal strain azimuth of 34, c) 3D strain tensor with vertical strain found using Eq. 2, and d) stress profile for the three principal stresses used at Mount St Helens.

Magma chamber boundary conditions: Magma chamber modeling for MSH and MB were modeled in a similar style as Mogi, 1958, who originally derived the theory for modeling deformed or deforming volcanic centers at depth as spheres or ellipsoids. Modeling stress changes around an underground fluid boundary by treating it as a traction free surface is a common practice in the oil and gas industry in the case of salt intrusions (Zoback, 2007) and was adopted similarly for the magma chambers.

The magma chamber at MSH is modeled as a triangulated ellipsoid with dimensions and location following Barker and Malone (1991) which was fit to an aseismic gap under the MSH crater (Fig. B11). Like the faults, the elements of the magma chamber have zero shear traction, but the normal traction is equal to the magma-static stress of the magma chamber at each observation depth, which is less than the litho-static stress due to magma withdrawal during the 1980 explosive eruptions.

$$P_m = \rho_m g h \quad \text{Eq. 2}$$

Where P_m is the magma-static pressure which is used for the normal tractions, ρ_m is the magma density (2.46 g/cm^3), g is acceleration due to gravity, and h is the depth of each observation grid.

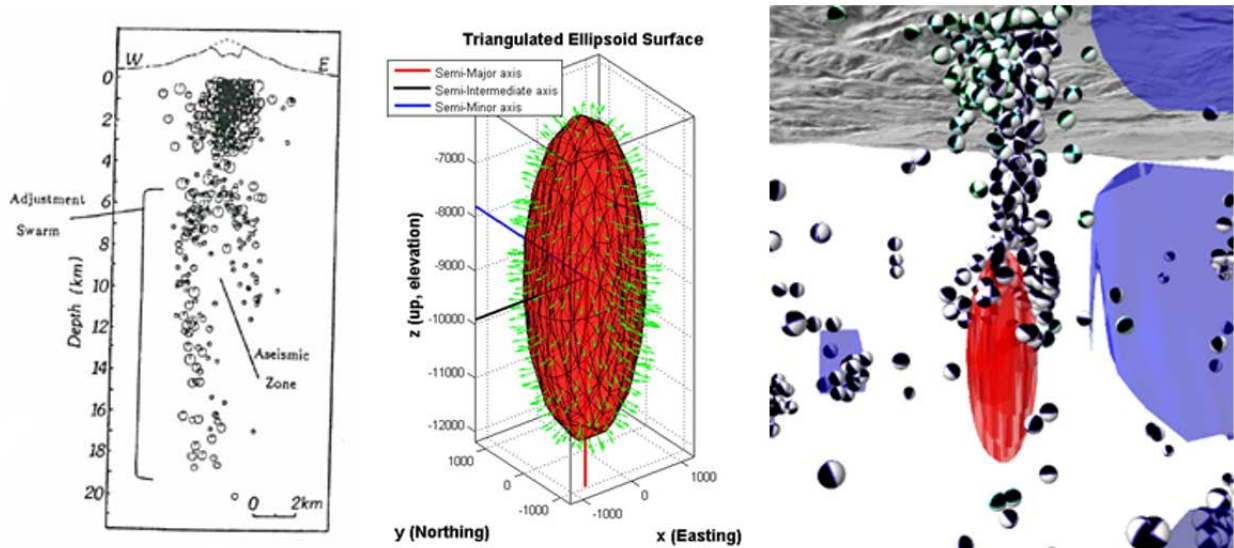


Figure B11: Geometry of MSH magma chamber fit to an aseismic gap under MSH.

The magma chamber at MB is modeled as a triangulated sphere with the dimensions and location best fit to field gathered line length changes between GPS benchmarks placed on the summit following Hodge and Crider, 2010. The study by Hodge and Crider modeled the magma chamber as an inward displacement boundary to simulate elevated levels of degassing and thermal flux, however using the displacement boundary in *Poly3D* created unrealistically high stress concentrations ($\sim 10^{18}$ MPa). Therefore, the average strain rate from the line length changes on MB of -420 nanostrain/yr was used, and was multiplied by E to get a stress, which is the same way the remote tectonic stresses were derived. Using this boundary condition with the remote strains derived from the PBO and PANGA benchmarks is a more accurate physical representation of the fact that the strain caused by MB is two orders of magnitude higher than surrounding tectonic strain (Crider and others, 2011). Because the magma chamber model for MB was calibrated to surface data, the ‘best fit’ model is a non-unique solution and therefore does not represent the true geometry of the underground traction free surface. Therefore, the magma chamber was modeled with a zero shear displacement boundary rather than a zero shear traction boundary.

Model results: The faults, magma chamber, and corresponding local and remote boundary conditions are implemented in *Poly3D* to derive constraints on permeability potential both along the modeled faults and in the surrounding volume. On the fault itself these include the static slip and dilation tendency as well as the modeled displacement discontinuity and gradient of displacement. In the surrounding volume, these include the maximum Coulomb shear stress and least compressive principal stress. In addition, the dilatation and maximum shear strain rate are modeled from GPS velocities and strain rates for all of Washington and Oregon and are interpolated to a higher resolution across the entirety of each study area. These parameters are

assessed on observation planes at 200 m and 3 km depth, where they are the basis of weighted rasters used for the favorability maps. The relationship of each of these parameters to permeability potential is described below.

Fault-related outputs:

Displacement is the magnitude of fault parallel (shear) displacement discontinuity across the fault surface in meters (Fig. B12). Higher levels are typically associated with development of a low permeability fault core and a surrounding damage zone of potentially higher permeability (for example, Caine and others, 1996) This allows the fault to act as a barrier to cross-fault flow, but to possibly conduct fluids parallel to the fault plane.

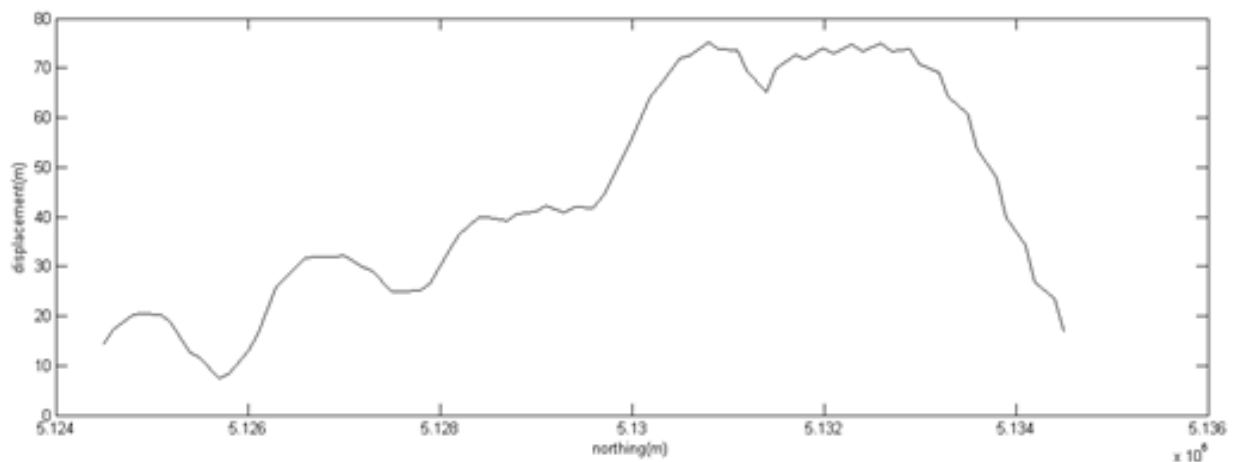


Figure B12: Displacement on fault surface north of Mount St Helens calculated from strike-slip and dip-slip components of displacement.

Displacement gradient is the change in slip along the fault surface divided by distance along fault surface between fault elements (Fig. B13). High displacement gradients occur at the fault tips or where mechanical interaction with other, nearby slipping fault segments is strong. Higher slip gradients reveal strain and a corresponding concentration of stress that is likely to correlate with damage in or adjacent to the fault. If this damage takes the form of dilating shear or tensile fractures this should promote permeability along the fault (Childs and others, 1995; Willemse and others, 1996).

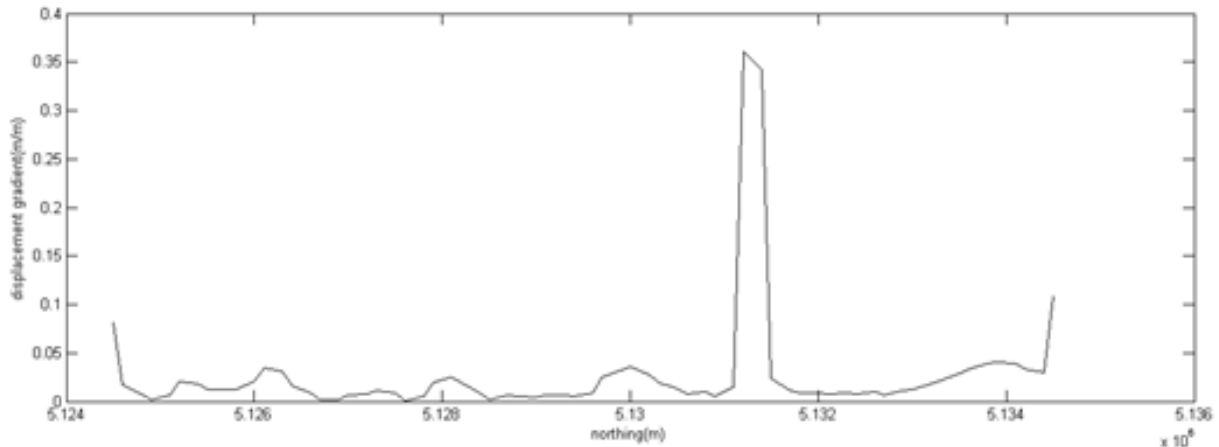


Figure B13: Displacement gradient on fault surface north of Mt. St. Helens calculated from fault displacement shown in Figure B12 above.

Slip tendency (T_s) is the ratio of static shear to normal traction resolved on a fault surface by the remote stress/strain (Morris and others, 1996).

$$T_s = \tau/\sigma_n \quad \text{Eq. 3}$$

The shear (τ) and normal (σ_n) tractions are highly dependent on the local fault attitude relative to the remote stress tensor. They are calculated using Cauchy's law.

$$[\sigma_{ij}]\{n_j\} = \{T_i\} \quad i, j = x, y, z \quad \text{Eq. 4}$$

Where σ_{ij} is the stress tensor, n_j is the fault normal vector, and T_i is the traction vector. σ_n and τ are the normal and shear components relative to the normal vector. A higher slip tendency means the fault has a higher potential for slip as a result of the homogeneous remote stress, although the effect of stress change from nearby faults and magma chambers is neglected. An advantage of this method is that it primarily depends on the fault geometry and anisotropy of the remote stress tensor, rather than the magnitude of the principal stresses which are more difficult to constrain in detail. If the slip tendency exceeds the coefficient of static friction on the fault surface, then the fault will slip. Faults with higher slip tendencies tend to act as fluid conduits, whereas faults with low slip tendencies can potentially block groundwater flow, or compartmentalize the reservoir.

Dilation tendency (T_d) is the ratio of the difference between the most compressive principal stress (σ_1) and the normal traction, and the difference between the most compressive principal stress and the least compressive principal stress (σ_3) (Ferrill and others, 1999).

$$T_d = (\sigma_1 - \sigma_n)/(\sigma_1 - \sigma_3) \quad \text{Eq. 5}$$

Similar to slip tendency, this ratio is based on the static stress tensor. When dilation tendency is at its maximum value of 1, then the fault surface is perpendicular to σ_3 . In a strike-slip fault

setting, this also generally corresponds to a near vertical fault. Open faults and fractures can host large amounts of fluid flow, and fractures increase their flowrate as a cubic function of fault aperture according to the cubic law for fractures (Zoback, 2007).

Stress/Strain-related outputs:

Maximum Coulomb shear stress (S_c) is the potential for shear fracture failure in a volume of rock based on a Mohr-Coulomb failure criterion.

$$S_c = \left(\frac{(\sigma_1 - \sigma_3)}{2} \sqrt{\mu_i^2 + 1} \right) - \mu \left(\frac{(\sigma_1 + \sigma_3)}{2} \right) \quad \text{Eq. 6}$$

Where μ_i is the coefficient of internal friction assumed to be 0.6. S_c is used as a proxy for fault/fracture density (Childs and others, 1995; Maerten and others, 2002). As S_c increases, more orientations of potential shear fracture reach their strength threshold, which has the potential to both increase the density of fractures as well as promote connectivity. This in turn implies potential for a more convoluted flow path and therefore greater heat exchange between the reservoir rock and circulating fluids (Fig. B14).

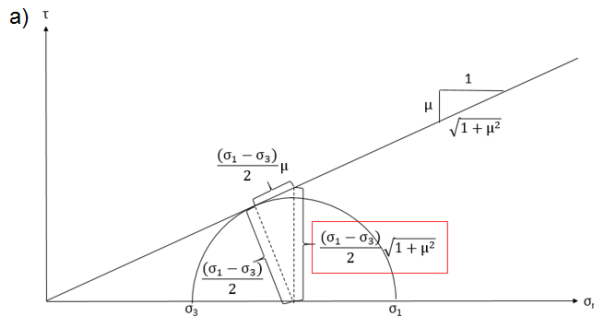
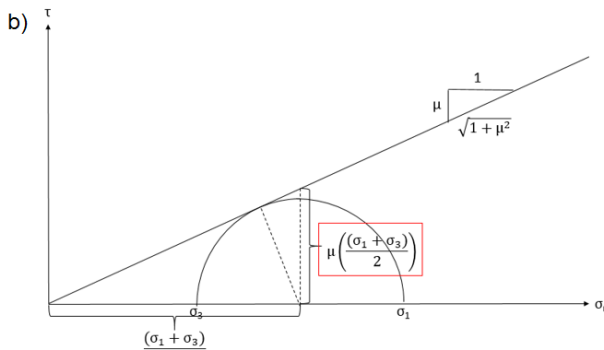


Figure B14: a) The first term of S_c defining the contribution of differential stress and **b)** the second term defining the contribution of the mean stress.

$$S_c = \left(\frac{(\sigma_1 - \sigma_3)}{2} \sqrt{1 + \mu^2} \right) - \mu \left(\frac{(\sigma_1 + \sigma_3)}{2} \right)$$



$$S_c = \left(\frac{(\sigma_1 - \sigma_3)}{2} \sqrt{1 + \mu^2} \right) - \mu \left(\frac{(\sigma_1 + \sigma_3)}{2} \right)$$

Sigma 3 (σ_3) is the least compressive principal stress (i.e., confining pressure). A lower σ_3 both promotes dilation during slip of fractures and a higher potential for tensile failure. A negative σ_3 indicates tension and fracture opening.

Dilatational strain rate (δ) is derived from GPS and reveals areas that are contracting or extending, and can be used to identify areas of active thrust or normal faulting (Hackl and others, 2009) (Appendix C)(Fig. B4b).

Maximum shear strain rate derived from GPS indicates active strike-slip faults, as motion along faults is related to shear on that structure (Hackl and others, 2009) (Appendix C)(Fig. B4c).

Data processing for the permeability potential layers:

The outputs from MATLAB and Poly3D (fault data: displacement, displacement gradient, slip tendency, and dilation tendency; and the area surrounding the faults: maximum Coulomb shear stress and sigma 3) at both depth slices 200 m and 3 km, are all point data with values representing the various input layers at a grid space of 2,000 ft. The stress layers were normalized to ± 3 standard deviations above and below the mean. The fault displacement and displacement gradient were normalized to their maximum values, and slip and dilation tendency were left alone because they already range from 0–1. The points were then interpolated using an inverse distance weighting (IDW) process, with a power of 2, and a standard neighborhood type. The resultant map was exported to a raster with a 500-ft cell size, clipped to the study area, and re-normalized using a fuzzy membership with a bilinear resampling method and no hedge. Data from the maximum shear and the dilatational strain rate was converted from a .grd file to an .asc file via Generic Mapping Tools software. The strain rate maps were clipped to the extent of the study area, projected and resampled using the ‘project raster’ tool with a bilinear resampling method, and a 500-ft cell size. The dilatational strain rate map was then normalized using the raster calculator tool by adding the maximum value to the raster, then dividing everything by twice the maximum value. This normalization reassigns the negative values associated with compression in the dilatational strain raster to a lower positive value; the raster is then re-normalized using a fuzzy membership with a bilinear resampling method and no hedge. The maximum shear strain rate values were normalized by dividing the raster by the maximum value of the maximum shear strain rate. The individual permeability potential rasters for each of the three plays are shown below in Figures B15–B17.

Combining permeability potential layers:

The permeability inputs were then combined using the weighted sum tool. The weights assigned to each heat input raster were based on the individual input from experienced geothermal professionals and the weights were combined using the Analytical Hierarchy Process (AHP) of Saaty (2008)(Goepel, 2013). The weights of each individual permeability input are shown in Table C1. The weighted sum raster was then normalized using the fuzzy membership tool with a linear transformation.

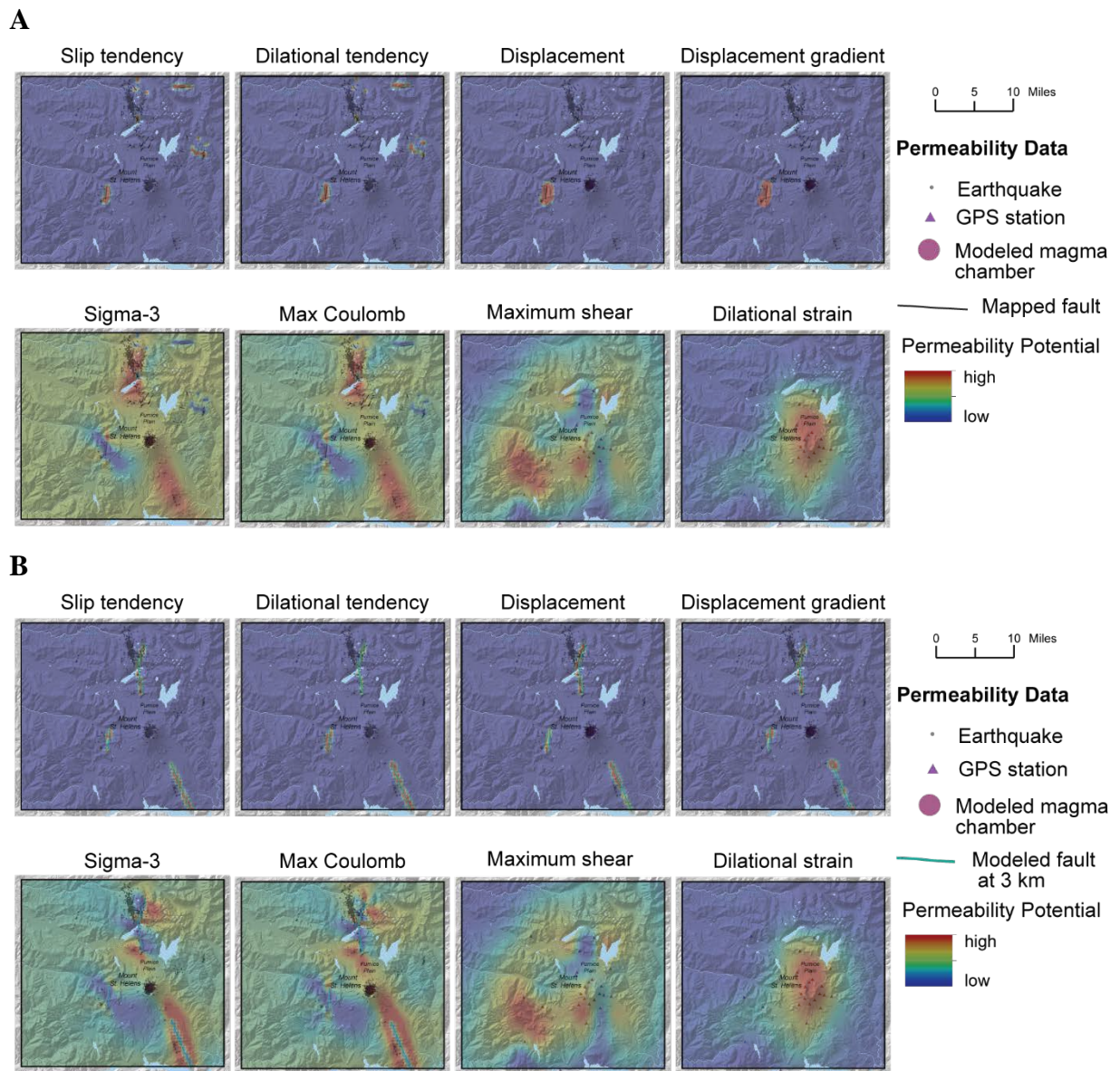


Figure B15: Individual permeability potential rasters for MSHSZ at **A)** 200 m, and **B)** 3 km depth slices.

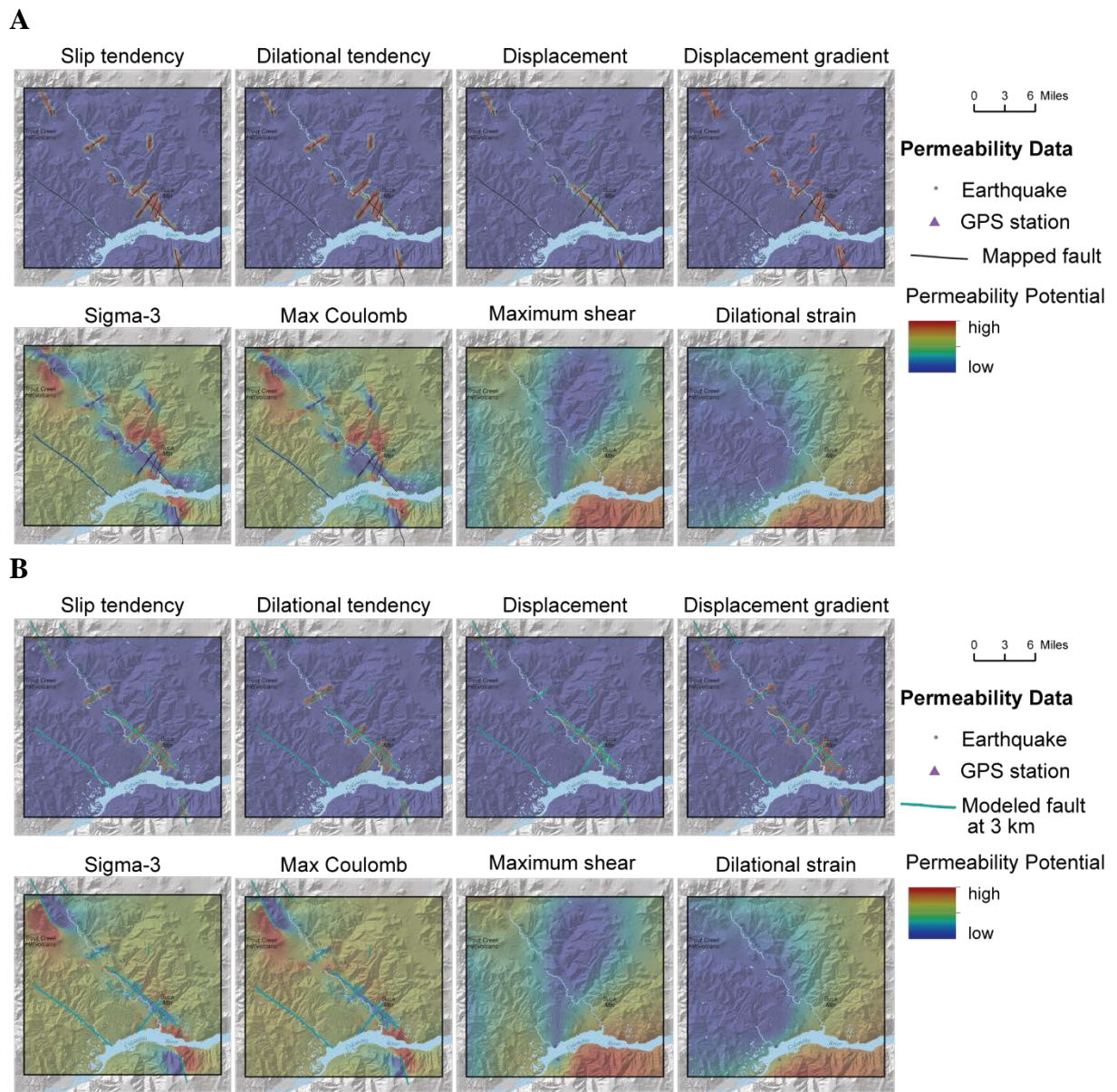


Figure B16: Individual permeability potential rasters for WRV at **A)** 200 m, and **B)** 3 km depth slices.

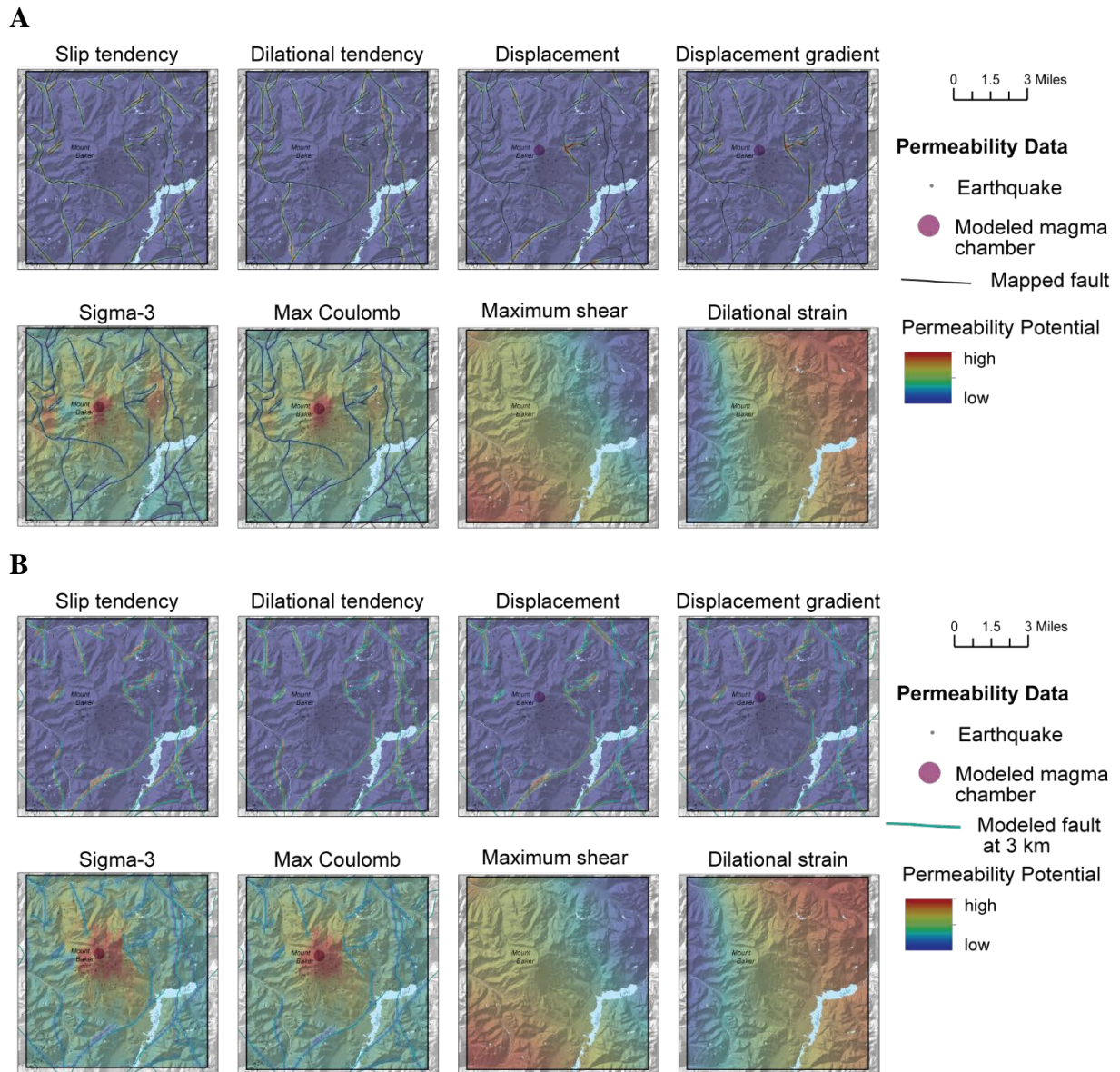


Figure B17: Individual permeability potential rasters with input data for MB at **A)** 200 m, and **B)** 3 km depth slices.

Appendix C: Analytical Hierarchy Process (AHP)

AHP worksheet example

A

Participant 1		1	α: 0.1 CR: 5%	
Name	Weight	Date	Consistency Ratio	
i	j	Criteria	more important?	Scale (1-9)
1	2	Displacement	Displacement	A 1
1	3		Sigma 3	B 3
1	4		max Coulomb	B 3
1	5		Slip tendency	B 6
1	6		Dilation tendency	B 7
1	7		max Shear Strain	B 3
1	8		Dilational strain	B 3
2	3		Displacement gradient	Sigma 3
2	4	max Coulomb		B 3
2	5	Slip tendency		B 6
2	6	Dilation tendency		B 6
2	7	max Shear Strain	B 3	
2	8	Dilational strain	B 3	
3	4	Sigma 3	max Coulomb	A 2
3	5		Slip tendency	B 4
3	6		Dilation tendency	B 5
3	7		max Shear Strain	A 1
3	8	Dilational strain	B 3	
4	5	max Coulomb	Slip tendency	B 5
4	6		Dilation tendency	B 6
4	7		max Shear Strain	A 2
4	8		Dilational strain	B 2
5	6	Slip tendency	Dilation tendency	B 2
5	7		max Shear Strain	A 5
5	8		Dilational strain	A 3
6	7	Dilation tendency	max Shear Strain	A 6
6	8		Dilational strain	A 6
7	8	max Shear Strain	Dilational strain	B 4

B

AHP Analytic Hierarchy Process (EVM multiple inputs)
 K. D. Goepel Version 26.07.2014 | Free web based AHP software on: <http://bomsq.com>

Only input data in the light green fields and worksheets!

n= 8 Number of criteria (3 to 10) Scale: 1 Linear
 N= 5 Number of Participants (1 to 20) α: 0.1 Consensus: 70.1%
 p= 0 selected Participant (0=consol.) 2 7 Consolidated

Objective: weight each permeability layer based on how you think it influences the overall permeability of the region

Author: Corina Forson
 Date: 11-Aug-15 Thresh: 1E-07 Iterations: 3 EVMcheck: 7.4E-08

Table	Criterion	Comment	Weights	Rk
1	Displacement	Amount of shear displacement on fault surface in n	5.2%	8
2	Displacement gra	Shear displacement on fault surface divided by dis	6.8%	7
3	Sigma 3	least compressive principal stress. A lower σ3 mea	9.4%	5
4	max Coulomb	potential for shear fracture failure in the rock volum	13.8%	3
5	Slip tendency	A higher slip tendency means the fault has a higher	21.7%	2
6	Dilation tendency	A higher dilation tendency means the fault has a hig	24.4%	1
7	max Shear Strain	Identifies areas that may have active faults	7.4%	6
8	Dilational strain	Defines areas that are extending/compressing	11.3%	4
9		for 9&10 unprotect the input sheets and expand the	0.0%	
#		question section ("+" in row 66)	0.0%	

Result: Eigenvalue lambda: 8.132
 Consistency Ratio 0.37 GCI: 0.05 CR: 1.3%

Figure C1: A) One example of the pairwise comparison of the permeability input parameters. B) An example of the combined opinions of 5 participants for permeability parameter weighting.

AHP-Derived weights for the three study areas

Analytical Hierarchy Process (AHP) Derived Weights for Heat and Permeability Input Parameters							
Heat Parameters			Permeability Parameters				
Study Area	Parameter		Study Area	Parameter			
MSHSZ	Temperature Gradient—51.9%		MSHSZ	Displacement—3%			
	Quaternary Volcanic Vent—16.4%			Displacement Gradient—17.1%			
	Quaternary Intrusive—13.5%			Slip Tendency—14.9%			
	Hot Spring or Fumarole—12.4%			Dilation Tendency—14.6%			
	Geothermometry from Hot Spring or Fumarole—5.7%			Max Coulomb Shear Stress—20.6%			
WRV	Temperature Gradient—66.6%			WRV		Sigma 3—6.5%	
	Quaternary Volcanic Vent—12.9%					Displacement Gradient—11.7%	
	Quaternary Intrusive—NA					Slip Tendency—13.8%	
	Hot Spring or Fumarole—13.5%					Dilation Tendency—23%	
	Geothermometry from Hot Spring or Fumarole—7%					Max Coulomb Shear Stress—24.6%	
MB	Temperature Gradient—53.9%		MB	Max Shear Strain Rate—5.3%			
	Quaternary Volcanic Vent—16.8%			Displacement Gradient—6.8%			
	Quaternary Intrusive—8.7%			Slip Tendency—21.7%			
	Hot Spring or Fumarole—11.2%			Dilation Tendency—24.4%			
	Geothermometry from Hot Spring or Fumarole—9.3%			Max Coulomb Shear Stress—13.8%			
	Sigma 3—9.4%						
	Max Shear Strain Rate—7.4%						
	Dilational Strain Rate—11.3%						

Table C1: AHP-derived weights for the three study areas.

Appendix D

Analysis of High-Precision GPS Time Series and Strain Rates

http://file.dnr.wa.gov/publications/ger_bos_altarock_GPS_strain_rates_2015_report.pdf

Appendix E

Data Processing for the Uncertainty and Risk Models

The details of the data quality and spatial certainty ranking parameters for the heat uncertainty model are outlined below.

Spring and Geothermometry Uncertainty:

1. Crop the feature class to only include the springs and geothermometry derived springs within the three plays
2. Add dummy points to the corners of each play area
3. Individually buffer all the points (using model builder) to a 2640-ft buffer
4. Convert buffer polygons to rasters using model builder and assigning the value of the polygon to be the data quality value (one set of rasters) and the spatial quality value (a second set of rasters)
5. Run 'Euclidean Distance' tool on each of the springs and dummy points using model builder with a ROI of 2640 ft using the iterate feature selection function
6. Invert the Euclidean distance rasters and normalize them (so the center is 1 and it radially decreases to 0 within the ROI) by using the 'fuzzy membership' tool in model builder with the iterate raster function
7. Multiply the spatial quality polygons and the fuzzified Euclidean distance polygons (multiplying the same point (Spring ID) for each) using model builder
8. Multiply the data quality polygons and the fuzzified Euclidean distance polygons (multiplying the same point (Spring ID) for each) using model builder
9. Then multiply the two spatial and data quality Euclidean distance rasters for each unique Spring ID (the outputs of steps 7 and 8) to get the certainty raster for each unique spring ID
10. Use Mosaic to raster to combine the outputs from step 9 for the springs and the respective dummy points for each play area individually. The parameters used in mosaicking were:
11. 32-bit float, cell size of 500, 1 band, maximum mosaic operator (takes the maximum of the overlapping cells), and a match color map mode.

Parameter	Value	Description
Spring proximity data certainty	5	Sampled in 2012/2013 complete water chemistry analysis
	4	Sampled in 2012–2013, mostly complete water chemistry analysis
	3	Sampled only once, and mostly complete water chemistry analysis
	2	Sampled only once and poor water chemistry analysis
	1	Sampled but the date isn't known no chemistry

Parameter	Value	Description
Spring proximity location accuracy	1	Spring with GPS measurement
	0.5	Spring without GPS measurement= TRS
	0	Decreases to 0 within the radius of influence (0.5 mi)

Table E1: Spring data quality and spatial accuracy weights

Parameter	Value	Description
Geothermometer proximity data quality	5	Charge balance +/-3 %, spring sampled in 2012/2013 and sampled previously, multiple geothermometers give similar (within 30 degrees) temperature result,
	4	Charge balance +/-4 %, spring sampled in 2012/2013, multiple geothermometers give mostly similar (within 50 degrees) temperature result
	3	Charge balance +/-5 %, spring sampled after 2000, multiple geothermometers give varying results (~100 degrees)
	2	Charge balance +/-5 %, spring sampled before 2000, geothermometers give mostly similar results (within 50 degrees)
	1	Charge balance +/-5 %, spring sampled before 2000, geothermometers give varying temperatures (within 100 degrees)

Parameter	Value	Description
Geothermometer proximity spatial quality	1	Spring with GPS measurement
	0.5	Spring without GPS measurement
	0	Decreases to 0 within the radius of influence (0.5 mi)

Table E2: Geothermometry data quality and spatial accuracy weights

Volcanic Vent Uncertainty:

Vent uncertainty was very difficult to assign values to because in some instances the presence of a volcano is pretty self-evident (Mount St. Helens for example) whereas other smaller vents are less obvious. The data quality parameters were based on how many sources (maps) referenced or mapped each vent and if the rocks at the vent have an age date. Spatial certainty was included in the quality certainty and so the spatial certainty analysis assigns a value of 1 to each vent and has the value decrease within the assigned ROI of each vent (Table E3).

Parameter	Value	Description
Volcanic vent proximity data quality	5	Vent cited by 3 or more sources, and has an age date
	4	Vent cited by 2 or more sources, and has an age date
	3	Vent cited by 1 source, and has an age date
	2	Vent cited by 2 or more sources, without an age date
	1	Vent cited by 1 source, without an age date

Table E3: Volcanic vent data quality weights

1. Crop the vent feature class to only include the vents within the three plays
2. Add dummy points to the corners of each play area
3. Individually buffer all the vent points (using model builder) to their respective buffer distances (based on ROIs in table above)
4. Convert buffered polygons to rasters using model builder and assigning the value of the polygon to be the data quality value
5. Run 'Euclidean Distance' tool on each of the vents and dummy points using model builder with the respective ROIs using the iterate feature selection function
6. Invert the Euclidean distance rasters and normalize them (so the center is 1 and it radially decreases to 0 within the ROI) by using the 'fuzzy membership' tool in model builder with the iterate raster function
7. Multiply the data quality polygons and the fuzzified Euclidean distance polygons (multiplying the same point (Spring ID) for each) using model builder
Use Mosaic to raster to combine the outputs from step 7 for the vents and the respective dummy points for each play area individually. The parameters used in mosaicking were: 32-bit float, cell size of 500, 1 band, match color map mode, Maximum mosaic operator (uses the maximum value in areas where cells overlap)

Intrusive rock uncertainty:

Parameter	Value	Description
Intrusive rock proximity	5	Historic intrusive mapped by 3 or more sources
	4	Holocene intrusive mapped by 3 or more sources, and has an age date
	3	Pleistocene intrusive mapped by 3 or more sources, and has an age date
	2	Late Pliocene intrusive mapped by 3 or more sources, and has an age date
	1	Intrusive mapped by 2 or more sources no age date

Table E4: Intrusive rock data quality weights

Spatial certainty was included in the quality certainty and so the spatial certainty analysis assigns a value of 1 to each intrusive and has the value decrease within the assigned ROI of each vent.

1. Crop the feature class to only include the intrusives within the three plays
2. Add dummy polygons to the corners of each play area
3. Individually buffer all the intrusive polygons (using model builder) to a 3-mile buffer
4. Convert buffered polygons to rasters using model builder and assigning the value of the polygon to be the data quality value
5. Run 'Euclidean Distance' tool on each of the intrusives and dummy points using model builder with the respective ROIs using the iterate feature selection function
6. Invert the Euclidean distance rasters and normalize them (so the center is 1 and it radially decreases to 0 within the ROI) by using the 'fuzzy membership' tool in model builder with the iterate raster function
7. Multiply the data quality polygons and the fuzzified Euclidean distance polygons (multiplying the same polygon (intrusive_ID) for each) using model builder
8. Use Mosaic to raster to combine the outputs from step 7 for the intrusives and the respective dummy polygons for each play area individually. The parameters used in mosaicking were: 32-bit float, cell size of 500, 1 band, match color map mode, Maximum mosaic operator (uses the maximum value in areas where cells overlap), and color match mode.

Temperature-gradient uncertainty:

The data quality for temperature-gradient wells is based on the information we have from well logs. The R^2 value is the fit of the regression line (that determines the TG used) to the data points— gradient method “A” means that it was a temperature gradient well and not a water well where gradients are inferred from bottomhole temperatures (method “B”). The number of sample points is the number of times the temperature was measured downhole.

Heat Parameters	Data Quality Ranking	Description
Temperature gradient	5	R^2 Value > 0.90; gradient method A; number of sample points > 30
	4	R^2 Value > 0.80; gradient method A; number of sample points > 20
	3	R^2 Value > 0.50; gradient method A; number of sample points > 10
	2	Depth > 50 m; gradient method A
	1	Water well with inferred TG from bottomhole temp and surface temp = Method B

Table E5: Temperature gradient data quality weights

The radius of influence assigned to each temperature gradient well was dependent on the depth of the well. Radii were assigned the following buffers:

TG depth buffer/ ROI (mi)	TG depth
5	> 400 m
4	300–399 m
3	200–299 m
2	100–199 m
1	0–99 m

Table E6: Radii of influence for temperature-gradient wells

1. Crop the feature class to only include the TG and water wells within the three plays
2. Add dummy points to the corners of each play area
3. Individually buffer all the wells (using model builder) their respective buffers based on the table above
4. Convert buffered polygons to rasters using model builder and assigning the value of the polygon to be the data quality value
5. Run 'Euclidean Distance' tool on each of the TG wells and dummy points using model builder with the respective ROIs using the iterate feature selection function
6. Invert the Euclidean distance rasters and normalize them (so the center is 1 and it radially decreases to 0 within the ROI) by using the 'fuzzy membership' tool in model builder with the iterate raster function
7. Multiply the data quality polygons and the fuzzified Euclidean distance polygons (multiplying the same point (Spring ID) for each) using model builder
8. Use Mosaic to raster to combine the outputs from step 7 for the wells and the respective dummy points for each play area individually. The parameters used in mosaicking were: 32-bit float, cell size of 500, 1 band, match color map mode, and a maximum mosaic operator (uses the maximum value in areas where cells overlap, which uses the values associated with the highest certainty).

Combining the heat uncertainty parameters:

1. Use the mosaic to new raster tool in ArcGIS to combine each of the heat parameter uncertainty layers (described above) using a 100' cell size, and a mean mosaic operator.
 2. Clip each raster to the study area.
 3. Use the raster calculator to normalize the combined heat potential model by dividing the model by 5.
-

Appendix F

Preliminary USGS work plan and budget for proposed Phase II collaboration

The USGS work plan and budget estimates have been incorporated into our Phase 1 high and low-cost proposals. The details of our discussions with them about potential for collaboration and budget estimates are provided below.

Preliminary USGS Work Plan:

The proposed work will provide 1) regional geophysical characterization and 2) detailed potential field and MT modeling. Potential field and MT data studies will be coordinated and combined to yield an integrated assessment of the subsurface. Where present, existing data (e.g., from geology, seismic, borehole logs and cores, electrical studies, etc.) will be considered in our analyses.

Potential field studies:

Potential field (gravity and magnetic) methods are sensitive to lateral variations in rock properties (density and magnetization) and are critical for characterization of subsurface geology and structure. The geometry, depth, and physical properties of crustal sources determine the character of the observed gravity or magnetic field. Thus, we use observed gravity and magnetic fields to resolve the geometry and lithology of crustal sources. We routinely apply a broad-based approach, drawing on multiple methods of data acquisition, analysis, and interpretation, incorporating geologic, geophysical, and subsurface information wherever possible.

Potential field products include both map-based interpretations and modeling that involve: filtering and derivative techniques that enhance map-based information, forward modeling to determine crustal sources, and inverse approaches to estimate depth, thickness, and geometry of concealed lithologies. These methods can be useful in geothermal studies by modeling basin geometry, and mapping structures such as contacts, faults, and fractures that may facilitate the circulation of geothermal fluids.

Our approach will involve several steps: 1) compile and reprocess existing potential field data, 2) collect, process, and interpret new potential field data, 3) collect and process hand samples for rock property measurements, and 4) synthesize and interpret all of the data in the area.

In addition, as part of the data collection process, an aeromagnetic survey covering the MSHSZ and WRV study areas will be contracted by a commercial operator. The USGS will design the airborne geophysical survey and develop the contract. If the survey is contracted directly through the DNR (as opposed to through the USGS) then the USGS will help assist in writing the contract and will provide the primary scientific oversight of the survey.

Depending on the study area, we plan to acquire combinations of gravity and ground-magnetic data either across a grid or along select transects, in order to facilitate potential field mapping and detailed modeling. In addition, regional gravity data will be collected over a

broader area, focusing on areas of sparse coverage that will help to constrain the regional field and interpret regional structure within the study area. Representative rock samples will be collected concurrently with the gravity and magnetic data collection, and their physical properties (density, magnetic susceptibility, and magnetic remanence) will be determined in the laboratory to aid in quantitative modeling of measured geophysical anomalies. Finally, we will develop two-dimensional geophysical models of the subsurface geology and structure that will provide critical information for understanding fluid flow conduits and constraints.

Magnetotelluric studies:

Unlike potential field data, the Magnetotelluric (MT) method is sensitive to the presence of fluids in the subsurface and can be utilized in geothermal studies to image magmatic heat sources, hydrothermal fluids, and major fracture networks that provide pathways for subsurface fluid flow. In addition, MT measurements provide information about the subsurface as a function of depth and direction, complementing the potential field data.

Our approach will be to collect MT data along selected profiles for 2D and/or 3D modeling. Data collection will be targeted for investigating the top 10 km, or deeper if desired. In areas such as Mount St. Helens, where multiple MT surveys have been previously collected, we will try to use existing data and fill in areas of interest. MT data will be inverted in 2D and 3D, if needed, to produce resistivity models as a function of depth. The resistivity models will be jointly interpreted with the gravity and magnetic models to help characterize heat sources, fracture networks and fluid pathways.

Work plan:

- * Design and develop an aeromagnetic contract for a survey of the MSHSZ and WRV study areas.
- * Compile existing geophysical data. This requires reprocessing and editing of existing data.
- * Collect new regional gravity data.
- * Collect detailed gravity data along selected profiles.
- * Collect rock-property samples.
- * Collect detailed ground magnetic profiles.
- * Collect MT data.
- * Perform rock-property measurements.
- * Process gravity and magnetic data.
- * Perform MT data processing.
- * Perform potential field mapping and modeling. This involves the application of various filtering and transformation techniques to produce a suite of maps for interpretation, as well as both forward and inverse modeling.
- * Perform MT modeling and integrate with potential field interpretations.
- * Provide summary report of results.

Budget

The proposed budget is based on the lowest cost estimate of performing the proposed research that minimizes salaries and emphasizes costs necessary to achieve the science objectives. Wherever possible, research costs are shared by existing USGS projects that have overlapping research objectives. Travel costs are estimated using standard average rates based on destination and duration of each trip. Travel costs include roundtrip transportation, lodging, meals, and incidentals.

The bulk of the requested funding is for the aeromagnetic survey, field and lab efforts, and data processing and analysis. Miscellaneous other direct costs include materials, equipment, supplies, and software. Additional partial support is requested for project meetings, workshops, and conferences.

In order to minimize field deployment costs, the proposed budget assumes that the DNR will provide personnel (students, interns or staff) to assist in field efforts and will cover their field expenses (external to the proposed budget).

The budget includes the fringe and indirect rates to the USGS. The USGS indirect costs are based on the FY2016 rate of 53.042% (though rates for out-years will change—typically ~1% increase/yr). Indirect costs have been applied, in the accompanying draft budget, to the entire budget except the aeromagnetic survey contract (Note that this assumes that our Science Center administration will not charge overhead on this subcontract. If overhead cannot be waived, the survey would be contracted directly through the DNR).

Draft budget for USGS activities on WA State PFA project

Potential field studies (roughly assumes >500 stations total)

Aeromagnetic survey of MSHSZ and WRV study areas	
Aeromagnetic contract	120000
Salary/benefits to manage the contract (1 person, 2 weeks)	6000
Gravity survey of the MSHSZ study area	
Fieldwork (1 USGS person, 2 weeks, assisted by 1 DNR staff)	10500
Processing of gravity data (1 person, 2 weeks)	6000
Modeling, synthesis & interpretation (1 person, 4 weeks)	12000
Gravity survey of the WRV study area	
Fieldwork (1 USGS person, 2 weeks, assisted by 1 DNR staff)	10500
Processing of gravity data (1 person, 2 weeks)	6000
Modeling, synthesis & interpretation (1 person, 4 weeks)	12000
Gravity survey of MB study area	
Fieldwork (1 USGS person, 2 weeks, assisted by 1 DNR staff)	10500
Processing of gravity data (1 person, 2 weeks)	6000
Ground magnetic survey of MB study area	
Fieldwork (1 USGS person, 2 weeks, assisted by 1 DNR staff)	10500

Washington Division of Geology and Earth Resources

Phase 1 Technical Report

Processing of magnetic data (1 person, 1 week)	3000
Modeling, synthesis & interpretation (1 person, 4 weeks)	12000
subtotal on Potential field studies	225000
MT studies (roughly assumes >50 stations total)	
MT survey of the MSHSZ study area	
Fieldwork (1 USGS person, 2 weeks, assisted by 2-3 DNR staff)	10500
Processing of MT data (1 person, 2 weeks)	6000
Modeling, synthesis & interpretation (1 person, 4 weeks)	12000
MT survey of the WRV study area	
Fieldwork (1 USGS person, 2 weeks, assisted by 2-3 DNR staff)	10500
Processing of MT data (1 person, 2 weeks)	6000
Modeling, synthesis & interpretation (1 person, 4 weeks)	12000
MT survey of MB study area	
Fieldwork (1 USGS person, 2 weeks, assisted by 2-3 DNR staff)	10500
Processing of MT data (1 person, 2 weeks)	6000
Modeling, synthesis & interpretation (1 person, 4 weeks)	12000
sub-total on MT studies	85500
Other	
Meetings & workshops	\$3,000
Equipment servicing and maintenance	\$2,000
Supplies and software	\$2,000
subtotal on Other	\$7,000
Sub-total on all	\$317,500
Indirect Costs (applied to everything except aeromag contract)	\$104,758
Total	\$422,258